Universitat de Girona

# ANALYSIS OF TIME-DEPENDENT FLEXURAL BEHAVIOUR OF CONCRETE MEMBERS REINFORCED WITH FIBRE REINFORCED POLYMER BAR

**Cristina MIÀS i OLLER**

**Dipòsit legal: GI. 1891-2012**
http://hdl.handle.net/10803/96914

*Analysis of time-dependent flexural behaviour of concrete members reinforced with fibre reinforced polymer bar* està subjecte a una llicència de Reconeixement 3.0 No adaptada de Creative Commons

© 2012, Cristina Miàs i Oller

Universitat de Girona

# Analysis of time-dependent flexural behaviour of concrete members reinforced with fibre reinforced polymer bars

Thesis submitted for the degree of Doctor of Philosophy

by

Cristina Miàs i Oller

2012

Escola Politècnica Superior
Departament d'Enginyeria Mecànica i de la Construcció Industrial

**DOCTORAL PROGRAMME IN TECHNOLOGY**

# Analysis of time-dependent flexural behaviour of concrete members reinforced with fibre reinforced polymer bars

Cristina Miàs i Oller
2012

*Thesis Supervisors:*

Dr. Lluís Torres Llinàs
*Universitat de Girona, Spain*

Dr. Albert Turon Travesa
*Universitat de Girona, Spain*

Thesis submitted for the degree of Doctor of Philosophy by the University of Girona

To whom it might concern,

Dr. Lluís Torres Llinàs and Dr. Albert Turon Travesa, Professors at the Universitat de Girona of the Department of Enginyeria Mecànica i de la Construcció Industrial,

CERTIFY that the study entitled *Analysis of time-dependent flexural behaviour of concrete members reinforced with fibre reinforced polymer bars* has been carried out under their supervision by *Cristina Miàs Oller* to apply the doctoral degree with the International Mention,

Girona, September 2012

| Dr. Lluís Torres Llinàs | Dr. Albert Turon Travesa |
|---|---|
| *Universitat de Girona, Spain* | *Universitat de Girona, Spain* |

*Al meu avi*

*i a tots els que brillen,*

The present work has been funded by the Spanish Government (Ministerio de Ciencia e Innovación) under research grant BES-2008-005740. Also, it has been partially funded by the Spanish Government under research projects BIA2007-60222 and BIA2010-20234-C03-02.

The research stay of the author at the University of Sheffield at United Kingdom has been funded by the Spanish Government (Ministerio de Ciencia e Innovación) under grant SEST1000I000920XV0.

This Ph.D. thesis has been prepared as a compendium of papers, according to the regulations of the University of Girona (*Normativa d'ordenació dels ensenyaments universitaris de doctorat de la Universitat de Girona Aprovada pel Consell de Govern en la sessió 3/12, de 26 d'abril de 2012*). The thesis includes four original papers: two papers that have already been published in peer-reviewed journals; one additional paper accepted, and another one that has already been submitted, which is under revision at the moment of preparing this document.

The complete references of the papers comprised in this thesis, the impact factors, quartile, and category of the journals are:

- C. Miàs, Ll. Torres, A. Turon, M. Baena, C. Barris. *A simplified method to obtain time-dependent curvatures and deflections of concrete members reinforced with FRP bars,* Composite Structures 2010; 92(8): 1833-38.

**doi:** 10.1016/j.compstruct.2010.01.016

(Impact Factor: 2.24, journal 4 of 24, *Quartile 1*, Category: *Materials Science, Composites*)

- Ll. Torres, C. Miàs, A. Turon, M. Baena. *A rational method to predict long-term deflections of FRP reinforced concrete members,* Engineering Structures 2012; 40:230-39.

**doi**: 10.1016/j.engstruct.2012.02.021

(Impact Factor: 1.351, journal 22 of 118, *Quartile 1*, Category: E*ngineering, Civil*)

- C. Miàs, Ll. Torres, A. Turon, C. Barris. *Experimental study of immediate and time-dependent deflections of GFRP Reinforced concrete beams*, Composite Structures, 2012 (in Press, Accepted Manuscript).

**doi**: 10.1016/j.engstruct. 2012.08.052

(Impact Factor: 2.24, journal 4 of 24, *Quartile 1*, Category: *Materials Science, Composites*)

- C. Miàs, Ll. Torres, A. Turon, I. A. Sharaky. *Effect of material properties on long-term deflections of GFRP reinforced concrete beams*. Submitted to Construction and Building Materials Journal.

(Impact Factor: 1.834, journal 8 of 56, *Quartile 1*, Category: *Construction and Building Technology*)

*The four papers have been published in (or submitted to) journals with impact factors within the first quartile, according to the 2011 Journal Citation Reports.*

# Acknowledgements - Agraïments

First and foremost I would like to thank my supervisors, Dr. Lluís Torres and Dr. Albert Turon, for giving me the opportunity to begin this trip together. Thanks for your guidance and your time during these last four years. *Moltes gràcies per tot.*

I would like to acknowledge the Department of Mechanical Engineering and Industrial Construction of the University of Girona, and particularity to the research group Analysis of Advanced Materials for Structural Design (AMADE) for the opportunity given.

I would also like to thank Dr. Kypros Pilakoutas, Dr. Maurizio Guadagnini and Dr. Kyriakos Neocleous for their support during my research stay at the University of Sheffield.

*M'agradaria també donar les gràcies a aquells que han col·laborat en la realització dels assajos experimentals, especialment a la Marta Baena, Irene Vilanova i Cristina Barris; tot i la tensió dels assajos, juntes hem rigut i compartit bons moments! Jordi Vicens i Sergi Saus, sense la vostra "força bruta" i la vostra inventiva aquests assajos no haurien estat possible, mil gràcies.*

*Gràcies a la gent d'AMADE per l'ajuda i els bons moments que hem compartit. Gràcies a tots, als que encara avui en formeu part i als que heu marxat a buscar nous horitzons, E.V. González, J. Bonilla, P. Vicens, E. Pajares, D. Sans, P. Badalló, M. Gascons, J. Bofill, N. Hereu, D. Piedrafita, C. Sarrado, L. Zubillaga, J. Vives, L. Marín, X. Cahís, M. Llorens , N. Gascons, S. Ortiz... i aquells qui un temps enrere van fer que el projecte AMADE fos possible: J. Costa, J.A. Mayugo, A. Turon, D. Trias, P. Maimí, N. Blanco, J. Renart.*

*A la Dolors i la Montse per fer que els migdies també siguin moments especials.*

*Al meus amics, a tots, per fer-me sentir sempre a prop vostre, gràcies Anna, Susagna, Maria, Sergi, Josep i Maria, Albert, Tere i a tota la colla al complet!*

*A la meva família. A la Judith, per ser com és. A la meva àvia, per estar sempre al meu costat. Als meus pares, gràcies mare per aquest suport incondicional que sempre m'has donat (entre tu i jo, t'estimo molt); gràcies Rafael pels valors que m'has transmès.*

*Per últim gràcies a tu, si Joan, a tu, per tot el que hem compartit i espero continuar compartint (quilòmetres per recórrer...).*

# Summary

In the past two decades, a large number of research programmes focussed on short-term flexural behaviour of fibre reinforced polymer (FRP) reinforced concrete (RC) members has been carried out. However the number of studies on the long-term behaviour of FRP reinforced concrete members is still scarce.

In this work, long-term behaviour of FRP RC beams has been investigated both analytically and experimentally to further extend the knowledge in this particular research domain. In this respect, a new methodology to determine the long-term deflections due to creep and shrinkage is presented. Based on multiplicative coefficients, the methodology is straightforward and simple, and therefore suitable to be used in design. In addition, an experimental campaign on two series of GFRP RC beams subject to long-term loading has been performed. Different reinforcement ratios, concrete strengths and sustained load levels have been considered. For comparison purposes steel reinforcement has also been used. The experimental long-term results have been reported and discussed. Furthermore they have been compared to predictions using the most representative procedures, as well as, the proposed methodology presented in this work.

# Resum

En les últimes dues dècades, han aparegut nombrosos estudis centrats en el comportament instantani a flexió de bigues de formigó armades amb materials compostos. No obstant això, els estudis referents al comportament a llarg termini encara són escassos.

En aquest treball, s'investiga el comportament a llarg termini de bigues armades amb barres de material compost, tant des del punt de vista analític com experimental, amb l'objecte d'ampliar així aquest camp d'estudi.

En aquest sentit es presenta una nova metodologia per a la determinació de fletxes diferides degudes als efectes de la fluència i la retracció del formigó. La metodologia presentada es basa en coeficients multiplicadors, essent així un mètode directe i simple, apte per ser utilitzar en el disseny.

Addicionalment, l'estudi presenta els resultats d'una campanya experimental realitzada en dues etapes, on bigues armades amb barres de material compost amb fibra de vidre (GFRP) han estat sotmeses a càrregues a llarg termini. S'han considerat diferents quanties de reforç, resistències de formigó i nivells de càrrega. Per tal de comparar-ne els resultats, també s'han assajat bigues armades amb barres d'acer. Els resultats experimentals han estat analitzats i comparats amb els models de predicció més significatius, així com amb la metodologia desenvolupada i presentada en aquest estudi.

# List of Figures

Figure 2.1. Instantaneous and long-term strains and curvatures in a cracked section ............ 17

Figure 2.2. (a) Multiplicative coefficient kcreep and (b) relative error between analytical procedure, Eq.(13), and proposed method, Eq.(18). ............................................................. 21

Figure 2.3. Comparison of the proposed coefficient $k_{creep}$ and the coefficient obtained using the CEB [17], $\varphi(t,t_0)\kappa_{\varphi,2}$. ..................................................................................... 23

Figure 2.4. Relationship between $M_s/M_{cr}$ and $n\rho$ for FRP reinforced concrete beams. ......... 27

Figure 2.5. Error made using the proposed method to calculate the total deflection for different levels of concrete shrinkage. .................................................................... 28

Figure 2.6. Comparison of the predicted total mid-span deflection using different methods.. 30

Figure 3.1. Ratio between total curvatures predicted using (Eq. 18) and Eurocode 2, $\frac{\psi_T(t,t_0)_{proposed}}{\psi_T(t,t_0)_{EC-2}}$, ......................................................................................................... 50

Figure 3.2. Comparison of experimental data with the predicted total mid-span ................... 59

Figure 3.3 Effect of applied moment on the total-to-initial deflection prediction ratio, $\frac{\delta_T}{\delta(t_0)}$. ........................................................................................................................... 60

Figure 3.4. Effect of the free shrinkage strain and creep coefficient on the total-to-initial deflection prediction ratio $\frac{\delta_T}{\delta(t_0)}$. Applied moments: (a) M=1.5Mcr , (b) M=3Mcr. ............. 62

Figure 4.1. Geometric details of the tested beams. ................................................................ 83

Figure 4.2. Experimental set-up (a) instantaneous loading tests (b) sustained loading test..... 85

Figure 4.3. Load mid-span deflection curves for beams N_G12. .......................................... 87

Figure 4.4. Load mid-span deflection curves for beams N_G16. .......................................... 87

Figure 4.5. Total deflections for (a) beams reinforced with 2Ø12 GFRP bars ........................ 95

Figure 4.6.Total deflections for beams: (a) N_L1_G12a (b) N_L2_G12a. ............................ 99

Figure 4.7. Total deflections for beams: (a) N_L1_G16a (b) N_L2_G16a. ......................... 100

Figure 5.1. Geometric details of the tested beams ............................................................... 114

Figure 5.2. (a) Cylindrical moulds (b) cylindrical mould for the creep coefficient determining with embedded strain gauge (c) set-up for creep tests on cylinders...................................... 117

Figure 5.3. Set-up for long-term tests ..................................................................................... 119

Figure 5.4. Temperature and relative humidity registered in the laboratory during N_beams tests........................................................................................................................................ 121

Figure 5.5. Temperature and relative humidity registered in the laboratory during H_beams tests........................................................................................................................................ 121

Figure 5.6. Experimental free shrinkage strain – Concrete of N_beams series ..................... 122

Figure 5.7. Experimental free shrinkage strain – Concrete of H_beams series ..................... 123

Figure 5.8. Experimental creep coefficient – Concrete of N_beams series ........................... 124

Figure 5.9. Experimental creep coefficient – Concrete of H_beams series ........................... 125

Figure 5.10. Total deflections for N_beams reinforced with (a) 2Ø12 GFRP, (b) 2Ø16 GFRP, (c) 2Ø10 steel bars.................................................................................................................. 129

Figure 5.11. Total deflections for H_beams reinforced with (a) 2Ø12 GFRP, (b) 2Ø16 GFRP, (c) 2Ø10 steel bars.................................................................................................................. 130

Figure 5.12. Total deflections versus time since loading for beams (a) N_L1_G12 (b) N_L2_G12.......................................................................................................................... 135

Figure 5.13. Total deflections versus time since loading for beams (a) H_L1_G12 beams and (b) H_L2_G12 beams (c) H_L1_G16 beams and (d) H_L2_G16 beams............................ 138

# List of Tables

Table 2.1. Predicted/Experimental deflections ........ 32

Table 3.1. Ratio between total curvatures predicted using Eq. (18) and Eurocode 2, $\frac{\psi_T(t,t_0)_{proposed}}{\psi_T(t,t_0)_{EC-2}}$, for different environmental conditions ($f_c$=30MPa). ........ 51

Table 3.2. Comparison of the total-to-initial deflection prediction ratio, $\frac{\delta_T}{\delta(t_0)}$, for $M$=1.5$M_{\mathrm{cr}}$. Constant parameters: $f_c$=30MPa, d/h=0.9, $\xi$ =2. ........ 64

Table 3.3. Comparison of the total-to-initial deflection prediction ratio, $\frac{\delta_T}{\delta(t_0)}$, for $M$=3$M_{\mathrm{cr}}$. Constant parameters: $f_c$=30MPa, d/h=0.9, $\xi$ =2. ........ 65

Table 4.1. Geometric properties of beams. ........ 83

Table 4.2. Mechanical properties of GFRP rebars. ........ 84

Table 4.3. Applied sustained load, $P_{sus}$. ........ 86

Table 4.4. Experimental deflections at load $P_{sus}$. ........ 89

Table 4.5. Comparison of deflections corresponding to load $P$. ........ 91

Table 4.6. Instantaneous deflections corresponding to load $P_{sus}$ ........ 92

Table 4.7. Immediate deflection corresponding to load $P_{sus}$ after cycling. ........ 93

Table 4.8. Ratio between total deflection and immediate deflection. ........ 96

Table 4.9. Comparison between total deflections and analytical predictions using CSA-S806-02 approach (Eq. (8)). Time since loading: 180 days. ........ 101

Table 4.10. Comparison between total deflections and analytical predictions using ACI 440.1R-06 approach (Eq. (7)). Time since loading: 180 days. ........ 101

Table 5.1. Beams designation ..................................................................................... 115

Table 5.2. Composition of concrete .......................................................................... 116

Table 5.3. Concrete mechanical properties ................................................................ 117

Table 5.4. Mechanical properties of GFRP rebars. Values provided by manufacturer in brackets ....................................................................................................... 118

Table 5.5. – Maximum instantaneous loads, *P*, and sustained loads, $P_{sus}$, applied on N_beams series ..................................................................................................... 120

Table 5.6. Maximum instantaneous loads, *P*, and sustained loads, $P_{sus}$, applied on H_beams ........................................................................................................ 120

Table 5.7. Experimental time-dependent concrete properties (average values). ................... 126

Table 5.8. Ratio between the total and immediate deflection for N_beams .......................... 131

Table 5.9. Ratio between the total and immediate deflection for H_beams .......................... 131

Table 5.10. Ratio between theoretical and experimental total deflection at 250 days since loading (N_beams). .......................................................................................... 136

Table 5.11. Ratio between theoretical and experimental total deflection at 700 days since loading (H_beams). .......................................................................................... 139

# Contents

**Summary/Resum** ........ xi

**List of Figures** ........ xiii

**List of Tables** ........ xv

**1. Introduction and objectives** ........ 1

1.1 Introduction ........ 3
1.2 Objectives ........ 5
1.3 Outline of the thesis ........ 6

**2. A simplified method to obtain time-dependent curvatures and deflections of concrete members reinforced with FRP bars** ........ 9

2.1 Introduction ........ 13
2.2 Prediction of time-dependent curvatures based on ........ 15
Eurocode 2 ........ 15
2.3 Prediction of time-dependent curvature due to creep ........ 16
2.3.1 Time-dependent curvature due to creep in cracked sections ........ 16
2.3.2 Derivation of a simplified method to obtain long-term curvature due to creep ........ 19
2.3.3 Comparison with other methods ........ 22
2.4 Prediction of total deflections ........ 24
2.4.1 Simplified method to obtain total deflections ........ 24
2.4.2 Application range of the simplified method to obtain total deflections ........ 26
2.5 Comparison with experimental data ........ 29
2.6 Conclusions ........ 31
2.7 Acknowledgements ........ 33
2.8 References ........ 34

**3. A rational method to predict long-term deflections of FRP reinforced concrete members ..... 37**

3.1 Introduction ..... 41
3.2 Time-dependent coefficients for FRP RC beams ..... 43
3.2.1 Long-term curvature due to creep ..... 44
3.2.2 Long-term curvature due to shrinkage ..... 46
3.2.3 Comparison of the proposed coefficients and the reference analytical procedure ..... 49
3.2.4 Long-term deflection due to creep and shrinkage ..... 52
3.3 Evaluation of total deflections of FRP RC members ..... 54
3.3.1 Prediction models ..... 54
3.3.2 Proposed method ..... 57
3.3.3 Comparison with experimental data ..... 57
3.3.4 Comparison of methodologies for deflection prediction ..... 59
3.4 Conclusions ..... 66
3.5 Acknowledgements ..... 67
3.6 Appendix. Generalized coefficient for long-term curvatures due to creep ..... 68
3.7 References ..... 73

**4. Experimental study of immediate and time-dependent deflections of GFRP reinforced concrete beams ..... 77**

4.1 Introduction ..... 81
4.2 Test specimens and materials ..... 82
4.2.1 Beams specifications ..... 82
4.2.2 Material properties ..... 84
4.2.3 Test set-up ..... 84
4.3 Test results and discussion ..... 86
4.3.1 Short-term deflections ..... 86

4.3.2 Short-term deflection prediction ........ 89
4.3.3 Time-dependent deflections ........ 94
4.3.4 Prediction of time-dependent deflections ........ 96
4.4 Conclusions ........ 102
4.5 Acknowledgements ........ 103
4.6 References ........ 104
**5. Experimental long-term deflections of GFRP reinforced concrete beams under sustained loading ........ 107**
5.1 Introduction ........ 111
5.2 Experimental test program ........ 114
5.2.1 Beams specifications ........ 114
5.2.2 Material properties ........ 116
5.2.3 Experimental set-up ........ 118
5.3 Experimental results ........ 122
5.3.1 Time-dependent effects of concrete ........ 122
5.3.2 Experimental time-dependent deflections ........ 126
5.4 Comparison with analytical models ........ 132
5.5 Conclusions ........ 139
5.6 Acknowledgements ........ 140
5.7 Appendix ........ 141
5.8 References ........ 145
**6. Design methodology for long-term deflections ........ 149**
6.1 Calculation of long-term deflections ........ 151
6.2 Examples ........ 153
6.3 References ........ 160
**7. Conclusions ........ 161**
7.1 Summary ........ 163

7.2 Concluding Remarks ........................................................................................ 164
7.3 Future Work................................................................................................... 166

# 1. Introduction and objectives

## 1.1 Introduction

Fibre reinforced polymer (FRP) bars have emerged as an alternative to steel reinforcement in concrete structures such as seawalls and other marine structures as well as bridge decks, superstructures and pavements exposed to de-icing salts. FRP materials exhibit properties such as corrosion resistance and high tensile strength that make them suitable for this type of structures. In addition, due to their nonconductive properties, FRP materials are also used in concrete structures supporting magnetic resonance imaging units, railway magnetic levitation systems or other equipment sensitive to electromagnetic fields.

FRP bars are made of continuous fibres impregnated with polymeric matrix (also referred as resin). The most common fibre types used in the construction industry are glass, carbon, and aramid. Recently, basalt fibres have also been commercially available. On the other side, the matrix in a polymeric composite can be regarded as both a structural and a protection component. There are two basic types of polymeric matrices used in FRP composites: thermosetting and thermoplastic resins. Generally, thermosetting resins, such as epoxy and vinyl ester are the most used in the construction industry.

FRP bars are anisotropic with higher modulus in the direction of the reinforcing fibres, and are characterized by linear behaviour up to failure, without yielding. Compared to ductile steel, FRP bars generally have higher tensile capacity, limited strain range and lower modulus of elasticity. Steel reinforced concrete sections are commonly under-reinforced to ensure yielding of steel before the crushing of concrete, thus providing ductility and a warning of failure. The non-ductile behaviour of FRP reinforcement makes the concrete crushing the design driving failure mode for flexural members reinforced with FRP bars. Proposed formulations for the design of FRP reinforced concrete (RC) structures are based on the same principles already established for steel RC structures. Nevertheless, the equations derived for steel RC structures have been adapted to the particular behaviour of FRP RC members. In general, due to the lower elastic modulus of FRP bars, the design of FRP RC members is likely to be governed by the serviceability limit states, where deflection control is usually expected to be a limiting factor. In the past two decades, a large amount of studies focussed on bending, shear and FRP-concrete bond have been carried out. A better understanding of short-term behaviour of FRP RC members is now available and collected in the recent literature. However very little published information is focussed on long-term deflections and further experimental works is necessary, as recognized by some existing guidelines (ACI 440.1R-06).

To address long-term deflections due to creep and shrinkage, available guidelines for FRP RC structures, such as ACI 440.1R-06 and CSA-S-806-02, propose simplified procedures based on empirical multiplicative coefficients. These approaches are simple and straightforward but do not account for variations in mechanical properties of materials and environmental conditions. This fact could be of major importance for FRP RC structures where the mechanical properties of the reinforcement can change when using different types of fibres.

On the other hand, using more general methodologies, such as the *Effective Modulus Metho*d (EMM) and the *Age-Adjusted Effective Modulus Method* (AEMM), allows the mechanical behaviour of materials to be taken into account in a more rational way. These methods take into account some of the main parameters involved in the time-dependent behaviour, such as, member geometry, load characteristics (magnitude and duration of load, age of concrete at the time of loading), and material properties (elastic modulus of concrete and FRP reinforcement, creep and shrinkage of concrete). However, complexity is introduced into the calculation.

Therefore, a deep understanding of the main parameters involved in long-term deflections is needed. In addition, a straightforward methodology to computed long-term deflections accounting for the main influencing parameters should be addressed.

## 1.2 Objectives

The overall objective of this work is to investigate the long-term behaviour of FRP RC beams, both analytically and experimentally.

The first objective of this work is to develop a methodology to predict long-term deflections due to creep and shrinkage. This methodology must be simple, however it must account for mechanical properties of materials and environmental conditions.
In addition, since the number of tests regarding the long-term behaviour of FRP reinforced concrete members is still scarce, the second objective of this work is to further extend the experimental data in this particular research domain.

For this purpose, the specific objectives addressed in this study are:

- To obtain a methodology that could be used in design to determine the long-term curvatures and deflections due to creep and shrinkage phenomena.
- To compare the proposed methodology to available prediction models, varying different parameters that can influence the results: applied loads, reinforcement ratios, concrete strength, elastic modulus of reinforcement, creep coefficient and shrinkage strain.
- To carry out an experimental campaign on FRP RC beams with different concrete strengths, different reinforcement ratios, and under different levels of sustained load to study the long-term behaviour under the serviceability requirements.
- To compare the experimental results to the available models, and to examine the ability for prediction of the different existing approaches.
- To compare the experimental results of long-term deflections to the proposed methodology and check its suitability.
- To provide a convenient design methodology for the assessment of long-term deflections of FRP RC members. .

## 1.3 Outline of the thesis

The body of this dissertation consists on the four aforementioned manuscripts, which are included in the following chapters.

In Chapter 2, a straightforward and simple methodology to compute the long-term curvatures and deflections, due to creep, from initial curvatures and deflections is presented. The procedure is based on the multiplicative coefficient $k_{creep.}$ The coefficient is deduced considering the principles of the *Effective Modulus Method* for a fully-cracked section, and it is reduced by mathematical manipulation to be simple but also able to account for variations in the environmental conditions and mechanical properties of materials. Comparison of predictions using the proposed methodology with existing procedures, as well as with experimental results is done and discussed in terms of serviceability conditions.

In Chapter 3, the proposed multiplicative coefficient to obtain long-term deflections due to creep is generalized to take into account the tension-stiffening effect, expanding its applicability. In addition, a multiplicative coefficient to compute long-term deflections due to shrinkage is deduced from general principles of structural mechanics and using the *Effective Modulus Method*. Predictions obtained using both proposed coefficients are compared to experimental results to show their suitability, and to available procedures to highlight the influence of different parameters in predictions.

Chapter 4 presents the experimental programme and its results concerning GFRP RC beams tested at service load and subsequently subjected to different levels of sustained load for 250 days. The effects of the loading-unloading processes and the reinforcement ratios on immediate and long-term deflections are discussed. Analytical comparisons between the experimental data and some of the most representative prediction models are presented and analysed.

Chapter 5 presents an experimental test programme which complements the results presented in Chapter 4. The influence of concrete strength, as well as that of reinforcement ratio on long-term deflections of GFRP RC beams is analysed. Theoretical predictions using available procedures specific for FRP RC members are calculated and compared to obtained experimental long-term deflections. In addition, the experimental data are compared to the methodology proposed in Chapters 2 and 3.

# 2. A simplified method to obtain time-dependent curvatures and deflections of concrete members reinforced with FRP bars

C. Miàs, Ll. Torres, A. Turon, M. Baena, C. Barris. A simplified method to obtain time-dependent curvatures and deflections of concrete members reinforced with FRP bars, Composite Structures 2010; 92: 1833-38.

**doi:** 10.1016/j.compstruct.2010.01.016

## Summary:

*The design of concrete beams reinforced with fibre reinforced polymer (FRP) bars is often governed by the serviceability limit state, in which deflections play an important role. One of the most straightforward and easiest methods for calculating time-dependent deflections is based on applying multiplicative coefficients to instantaneous deflections. These methods have been adopted by ACI.440.1R-06 and CSA-S806-02 for FRP reinforced concrete structures (RCS), introducing slight modifications with respect to steel reinforced concrete members. However, the influence of different material mechanical properties and environmental conditions are not accounted for properly. In this paper, a new method based on a simplified coefficient for the prediction of time-dependent deflections is presented. The influence of variations in environmental conditions and the mechanical properties of the materials are taken into account. The numerical predictions obtained are compared to other models available in the literature and experimental results to validate the accuracy and suitability of the methodology presented.*

## 2.1 Introduction

Fibre reinforced polymers (FRP) are increasingly used as an alternative to steel reinforcement in corrosive environments or where there is a possible interference from magnetic fields, which can cause problems if conventional reinforced concrete structures are used. Due to the lower stiffness of FRP bars compared to steel, the design of concrete beams reinforced with FRP materials is often governed by the serviceability limit state, in which deflections play an important role.

Several methods have been developed for time-dependent analysis of reinforced concrete structures which have been proved to be able to predict the long-term deflections of steel reinforced concrete members due to creep and shrinkage: the *Effective Modulus Method*, the *Mean Stress Method and* the *Age-Adjusted Effective Modulus Method*, among others (Gilbert [1], Bazant [2], Chiorino [3]). These methods take into account some of the main parameters involved in the time-dependent behaviour of reinforced concrete structures, such as the properties of the materials (reinforcement and concrete) and the influence of environmental conditions by introducing the creep and shrinkage values of concrete. Using these methods, accurate predictions can be obtained and consequently the *Effective Modulus Method* and the *Age-Adjusted Effective Modulus Method* have been adopted in some national and international codes and recommendations, such as Eurocode 2 [4], Model Code 90 [5], and ACI 435 [6]. Nevertheless, the use of even more simplified procedures for practical design based on multiplicative coefficients has been widespread, and due to their straightforwardness they are probably the most popular (ACI 318 [7]). In these simplified procedures, time-dependent deflections of steel reinforced concrete structures (SRCS) are obtained by multiplying the short-term deflection due to sustained loads by an appropriate factor. Although these procedures are practical and easy to use, they do not take into account the influence of different material properties, mainly the creep and shrinkage of concrete, or the influence of using different reinforcing materials such as FRP.

FRP reinforced concrete structures (FRPRCS) develop larger deformations than steel reinforced members under the same conditions (concrete class, dimensions and area of reinforcement). The sectional curvatures and the tensioned area are larger, while the compressed area is smaller. In terms of time-dependent behaviour, the relative curvature increment associated with creep and shrinkage is lower than for conventional SRCS due to the smaller compressed area of concrete, and therefore lower time-dependent deflections are expected in FRPRCS. Hence, ACI 440.1R-06 [8], based on tests carried out by Brown and Bartholomew [9] and Brown [10], proposes multiplying the factor used for SRCS by 0.6, although the code recognizes that further work is necessary to validate the coefficient. However, the Canadian standard CSA S806-02 [11] proposes a more conservative approach, adopting the same coefficients as for steel.

Some other studies reported experimental work and analytical proposals on this topic. Arockiasamy *et al.* [12] proposed a multiplicative factor for long-term deflections based on a modification of the ACI 318 procedure [7]. The values of the coefficient were adjusted to their experiments on CFRP reinforced concrete beams. Hall and Ghali [13] compared their experimental long-term deflections of GFRP reinforced concrete beams with the predicted deflections using the procedures of ACI Committee 209 [14] and the CEB-FIB Model Code 1990 [5] with the equations found in Ghali and Favre [15]. They concluded that while ACI Committee 209 overestimated the experimental deflections, CEB-FIB Model Code 1990 gave reasonable predictions. Also the effect of different environmental conditions on the creep behaviour of concrete beams reinforced with GFRP bars under sustained loads was investigated by Al-Salloum and Almusallam [16]. The experimental results showed a strong significant influence of the environmental conditions.

This article proposes a new multiplicative coefficient to predict time-dependent curvatures in

FRPRCS based on the principles of the *Effective Modulus Method* and Eurocode 2 [4]. The proposed coefficient is intended to be simple but also able to account for variations in the environmental conditions and mechanical properties of materials. Simplified equations for deflection calculation are deduced and verified for the most common case of simply supported FRPRC beams.

## 2.2 Prediction of time-dependent curvatures based on Eurocode 2

Based on Eurocode 2 [4], the curvature, $\psi$, in members subjected to flexure, which are expected to crack but may not be fully cracked, can be calculated by:

$$\psi = (1-\xi)\psi_1 + \xi\psi_2 \tag{1}$$

$$\xi = 1 - \beta\left(\frac{M_{cr}}{M}\right)^2 \tag{2}$$

where the subscripts 1 an 2 refer to the uncracked and fully cracked conditions respectively; $\xi$ is an interpolation coefficient to account for tension stiffening; $M_{cr}$ is the cracking moment; $M$ is the applied moment; and $\beta$ is a coefficient taking account of the influence of the duration of loading (1 for a single short-term load, and 0.5 for sustained or repeated loads).

The long-term curvature will increase due to the effects of creep and shrinkage of concrete. For sustained loads, the total curvature including creep, $\psi^*(t,t_0)$, can be calculated by using an effective modulus of elasticity for concrete according to the following expression:

$$\overline{E_c}(t,t_0) = \frac{E_c(t_0)}{1+\varphi(t,t_0)} \tag{3}$$

where $E_c(t_0)$ is the elastic modulus of concrete at the time $t_0$ and $\varphi(t,t_0)$ is the creep coefficient that depends on time and duration of loading.

The curvature due to shrinkage, $\Delta\psi_{sh}(t,t_0)$, can be obtained by:

$$\Delta\psi_{sh}(t,t_0) = \varepsilon_{sh}(t,t_0)n(t,t_0)\frac{S}{I} \tag{4}$$

where $\varepsilon_{sh}(t,t_0)$ is the free shrinkage strain at the time *t*, $S$ is the first moment of area of the reinforcement about the centroid of the section, *I* is the second moment of area of the section, and $n(t,t_0)$ is the effective modular ratio:

$$n(t,t_0) = \frac{E_s}{\overline{E_c}(t,t_0)} \tag{5}$$

with $E_s$ being the elastic modulus of steel. *S* and *I* should be calculated for an uncracked and a fully cracked condition, and the final curvature should be assessed by using Eq. (1).

The basis of this procedure is general for reinforced concrete structures (SRCS, FRPRCS) because it incorporates the main influencing parameters.

## 2.3 Prediction of time-dependent curvature due to creep

### *2.3.1 Time-dependent curvature due to creep in cracked sections*

A fully cracked FRP reinforced concrete section subjected to a bending moment is analysed. Concrete in tension is not considered. It is not recommended to rely on FRP bars to resist compressive stresses and they should be ignored in design calculations [8], therefore the compressive reinforcement is not taken into account in this study.

According to Eq. (3) the effective concrete elastic modulus, $\overline{E_c}(t,t_0)$, decreases due to creep at a rate of $\left(1+\varphi(t,t_0)\right)$. Therefore, the depth of the compression zone of a cracked section subjected to a constant bending moment increases with time to achieve equilibrium, and so does curvature, as shown in Figure 2.1.

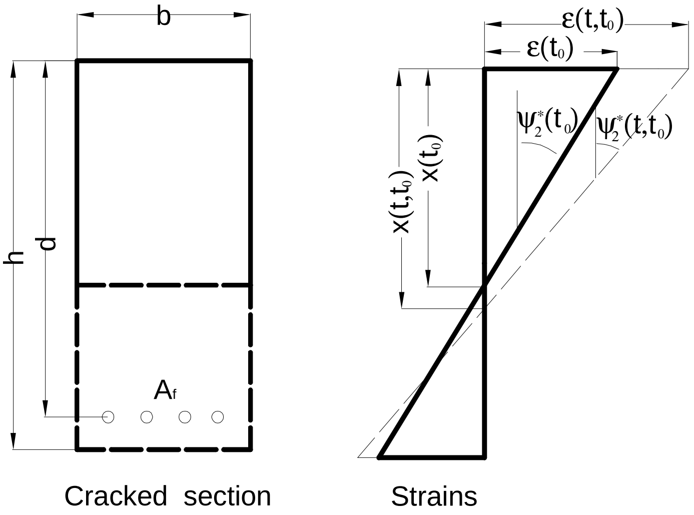
b
h
d
$A_f$
Cracked section
$\varepsilon(t,t_0)$
$\varepsilon(t_0)$
$x(t,t_0)$
$x(t_0)$
$\psi_2^*(t_0)$
$\psi_2^*(t,t_0)$
Strains

Figure 2.1. Instantaneous and long-term strains and curvatures in a cracked section

Assuming that the total curvature in a fully cracked section, including the creep effect, is equal to:

$$\psi_2^*(t,t_0) = \Delta\psi_{2,creep}(t,t_0) + \psi_2(t_0) \tag{6}$$

the relative increment of curvature due to creep can be determined as:

$$\frac{\Delta\psi_{2,creep}(t,t_0)}{\psi_2(t_0)} = \frac{\psi_2^*(t,t_0)}{\psi_2(t_0)} - 1 \tag{7}$$

where $\Delta\psi_{2,creep}(t,t_0)$ is the curvature due to creep, and $\psi_2(t_0)$ the instantaneous curvature.

Assuming that the section is subjected to a constant bending moment, the ratio of curvatures is equal to the ratio between sectional stiffness $k_2(t,t_0)$ and $k_2(t_0)$:

$$\frac{\psi_2^*(t,t_0)}{\psi_2(t_0)}=\frac{\dfrac{M}{k_2(t,t_0)}}{\dfrac{M}{k_2(t_0)}}=\frac{k_2(t_0)}{k_2(t,t_0)} \tag{8}$$

The sectional stiffness of a fully cracked section reads:

$$k_2=E_f A_f(d-x)(d-x/3) \tag{9}$$

where $A_f$ is the area of tensile reinforcement; $d$ is the effective depth; $x$ is the neutral axis depth of the section; and $E_f$ is the elastic modulus of FRP reinforcement. Because of the low level of stress imposed on FRP reinforcement by serviceability conditions [8], the effect of the possible creep deformation of the bar is ignored in front of the greater influence of concrete creep.

Using Eqs. (7), (8), and (9), the relative increment of curvature can be written as:

$$\frac{\Delta\psi_{2,creep}(t,t_0)}{\psi_2(t_0)}=\frac{\left(1-\dfrac{x(t_0)}{d}\right)\left(1-\dfrac{x(t_0)}{3d}\right)}{\left(1-\dfrac{x(t,t_0)}{d}\right)\left(1-\dfrac{x(t,t_0)}{3d}\right)}-1 \tag{10}$$

In the absence of compressive reinforcement, the neutral axis depth for a fully cracked section at the initial time, $x(t_0)$, can be written as:

$$\frac{x(t_0)}{d}=n(t_0)\rho\left(-1+\sqrt{\left(1+\frac{2}{n(t_0)\rho}\right)}\right) \tag{11}$$

where $n(t_0)$ is the ratio between the elastic modulus of reinforcement and concrete, and $\rho$ is the reinforcement ratio.

A similar equation can be written to obtain the neutral axis depth at time *t*, $x(t,t_0)$**,** taking into account the influence of concrete creep with the use of the corresponding coefficient $\varphi(t,t_0)$:

$$\frac{x(t,t_0)}{d} = n(t_0)\left(1+\varphi(t,t_0)\right)\rho\left(-1+\sqrt{\left(1+\frac{2}{n(t_0)\left(1+\varphi(t,t_0)\right)\rho}\right)}\right) \tag{12}$$

Using Eqs. (11) and (12) in Eq. (10), the relative increment of curvature reads:

$$\frac{\Delta\psi_{2,creep}(t,t_0)}{\psi_2(t_0)} = \frac{\left(1-n\rho\left(-1+\sqrt{1+\frac{2}{n\rho}}\right)\right)\left(1-\frac{n\rho}{3}\left(-1+\sqrt{1+\frac{2}{n\rho}}\right)\right)}{\left(1-n\rho(1+\varphi)\left(-1+\sqrt{1+\frac{2}{n\rho(1+\varphi)}}\right)\right)\left(1-\frac{n\rho(1+\varphi)}{3}\left(-1+\sqrt{1+\frac{2}{n\rho(1+\varphi)}}\right)\right)}-1 \tag{13}$$

For the sake of simplicity in Eq.(13), *n* refers the coefficient between the elastic modulus of the reinforcement and the elastic modulus of concrete at the initial time of $n(t_0)$, and $\varphi$ is the creep coefficient $\varphi(t,t_0)$ between *t* and *t*$_0$.

### *2.3.2 Derivation of a simplified method to obtain long-term curvature due to creep*

In this section a multiplicative factor, $k_{creep}$, is deduced to obtain long-term curvature due to creep, $\Delta\psi_{2,creep}(t,t_0)$, from the initial curvature, $\psi_2(t_0)$, so that:

$$\Delta\psi_{2,creep}(t,t_0) = k_{creep}\psi_2(t_0) \tag{14}$$

The coefficient $k_{creep}$ has been deduced using mathematical methods of simplification. In order to mathematically manipulate the expression given in Eq. (13), $\frac{\Delta\psi_{2,creep}(t,t_0)}{\psi_2(t_0)}$ is renamed as $f(r,t)$, *nρ* as $r^2$ and $\varphi$ as *t*. Therefore, Eq. (13) can be rewritten as:

$$f(r,t)=\frac{\left(1-r^2\left(-1+\sqrt{1+\frac{2}{r^2}}\right)\right)\left(1-\frac{r^2}{3}\left(-1+\sqrt{1+\frac{2}{r^2}}\right)\right)}{\left(1-r^2(1+t)\left(-1+\sqrt{1+\frac{2}{r^2(1+t)}}\right)\right)\left(1-\frac{r^2(1+t)}{3}\left(-1+\sqrt{1+\frac{2}{r^2(1+t)}}\right)\right)}-1 \qquad (15)$$

The adimensional parameter *nρ* depends on the elastic moduli of FRP and concrete, and the amount of tensile reinforcement. The elastic modulus of FRP usually ranges between 40 and 120GPa (the lowest values for GFRP, medium values for AFRP and the largest for CFRP). The usual values for concrete strength are between 20 and 80MPa, and for a reinforcement ratio $\rho$ between 0 and 0.04. For concrete beams reinforced with FRP bars, it can therefore be assumed that *nρ* usually ranges between 0 and 0.2.

The creep coefficient, $\varphi$, depends on the loading age, the ambient humidity, element dimensions and the composition of the concrete. Assuming an interval of variation from 1 to 3, a wide range of environmental conditions are taken into account.

Assuming, therefore, that the usual values for *nρ* and *φ* can range from 0 to 0.2 and from 1 to 3 respectively, the Taylor series development of Eq. (15) has been developed about the point (0,2).

$$f(r,t)=-\frac{4}{3}\sqrt{2}r+\frac{22}{27}\sqrt{6}r-\frac{64}{27}\sqrt{3}r^2+\frac{32}{9}r^2+\frac{8}{27}\sqrt{6}rt+.... \qquad (16)$$

Like $\frac{4}{3}\sqrt{2}r+\frac{64}{27}\sqrt{3}r^2\approx\frac{32}{9}r^2+\frac{22}{27}\sqrt{6}r \quad \forall r\in\left(0,\sqrt{0.3}\right)$, Eq. (16) can be approximated as:

$$f(r,\varphi)=\frac{8}{27}t\sqrt{6}r \qquad (17)$$

Therefore, the simplified coefficient $k_{creep}$ can be defined as:

$$k_{creep} = 0.73\varphi\sqrt{n\rho} \qquad (18)$$

It is noteworthy that the proposed coefficient, $k_{creep}$, depends on $n\rho$ and $\varphi$, and so implicitly includes the effects of concrete strength, the environmental conditions and the age of loading. The higher $n\rho$ and $\varphi$ are, the higher the multiplicative coefficient is, due to the increase in the height of the compressive concrete block, which implies an increment of curvature due to concrete creep. This can be observed in Figure 2.2(a).

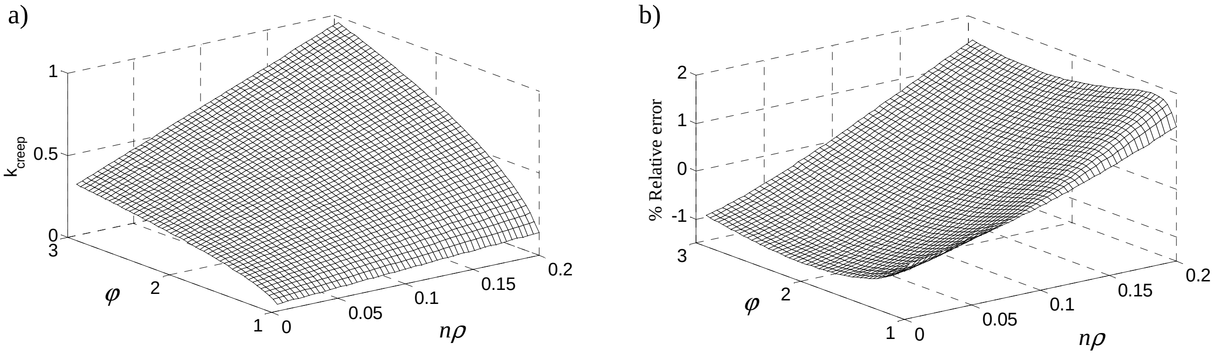

Figure 2.2. (a) Multiplicative coefficient kcreep and (b) relative error between analytical procedure, Eq.(13), and proposed method, Eq.(18).

The proposed simplified coefficient, $k_{creep}$, has been compared with the analytical procedure from Eq. (13) to calculate the prediction of the total curvature, including creep. The difference between the two is reflected in Figure 2.2(b), with the maximum difference being around 1.5%.

### 2.3.3 *Comparison* with other methods

The procedure presented in the CEB Manual on Cracking and Deformations [16], described and illustrated in Ghali and Favre [15], to obtain time-dependent curvatures due to creep is general for SRCS, as is the Eurocode 2 procedure [4]. Moreover it has been proved to be suitable for other reinforcing materials such as FRP [14]. Due to the generality of the method, it seems appropriate to compare it with the method proposed in this work.

Based on [15,17], long-term curvature due to creep can be calculated as:

$$\Delta\psi_{2,creep}(t,t_0)=\varphi(t,t_0)\kappa_{\varphi,i}\ \psi_i(t_0) \qquad (19)$$

where the subscript *i* takes a value of 1 for uncracked transformed sections and 2 for fully cracked transformed sections. $\kappa_\varphi$ is the curvature coefficient related to creep and can be obtained by the following expression:

$$\kappa_{\varphi,i}=\frac{I_c+A_c y_c \Delta y}{\bar{I}} \qquad (20)$$

$I_c$ is the moment of inertia of the concrete area $A_c$ about an axis through the centroid of the age-adjusted transformed section, $y_c$ is the centroid of the $A_c$, $\Delta y$ is the y-coordinate of the centroid of the age-adjusted transformed section, measured downward from the centroid of the transformed section at $t_0$, and $\bar{I}$ is the moment of inertia of the age-adjusted transformed section. The age-adjusted transformed section is calculated from the age-adjusted elastic modulus of concrete, $\overline{E_e}(t,t_0)$:

$$\overline{E_e}(t,t_0)=\frac{E_c(t_0)}{1+\chi(t,t_0)\varphi(t,t_0)} \qquad (21)$$

where $\chi(t,t_0)$ is an ageing coefficient and $\varphi(t,t_0)$ the creep coefficient at age *t*.

As an alternative to using Eq. (20), the coefficient $\kappa_{\varphi,i}$ can be obtained using the charts given by the CEB Design Manual on Cracking and Deformations [17].

Comparing Eq. (14) and (19), the proposed coefficient $k_{creep}$ equals the term $\varphi(t,t_0)\kappa_{\varphi,2}$ for a fully cracked member. Both coefficients are compared in Figure 2.3 for three representative values of the creep coefficient, $\varphi(t,t_0)$ = 1, 2, and 3. A typical value of 0.8 has been taken for the aging coefficient $\chi(t,t_0)$. Both coefficients show the same trend with small differences, as can be observed in Figure 2.3.

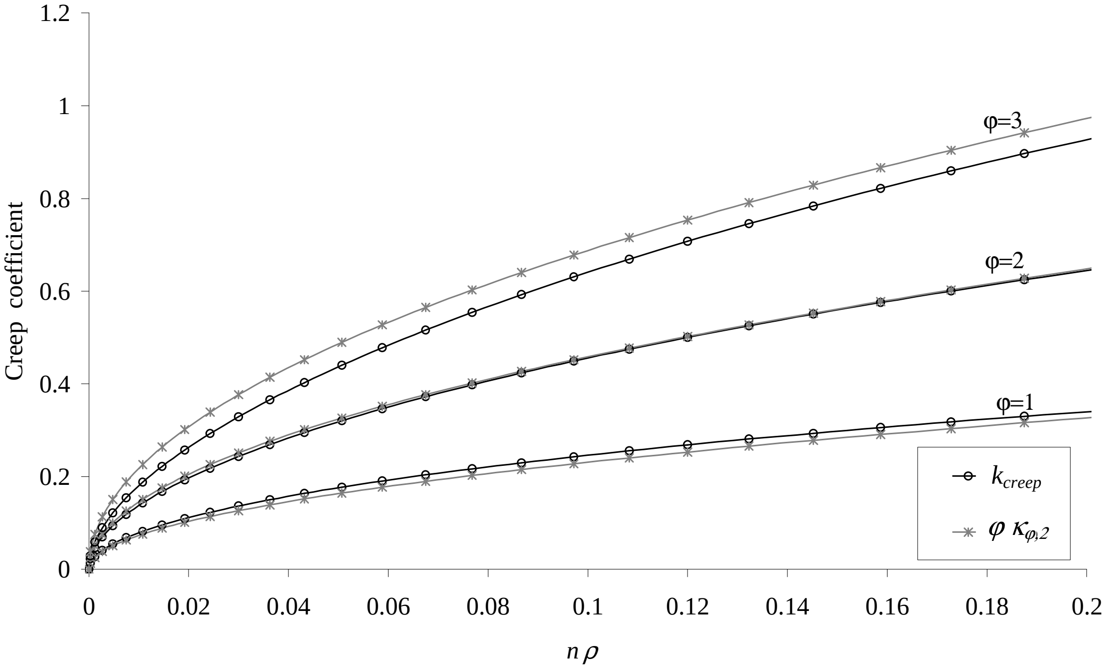

Figure 2.3. Comparison of the proposed coefficient $k_{creep}$ and the coefficient obtained using the CEB [17], $\varphi(t,t_0)\kappa_{\varphi,2}$..

It is worth noting that, for the same level of accuracy, the proposed simplified coefficient, $k_{creep}$, contains implicitly time-dependent parameters, and that its calculus depends only on *nρ* at the initial time of loading and the creep coefficient *φ*. The use of the proposed coefficient is therefore an easy method to obtain total curvatures, including creep, from the initial curvature.

## 2.4 Prediction of total deflections

### 2.4.1 Simplified method to obtain total deflections

In this section a method to obtain total long-term deflection in simply supported beams is presented.

The total long-term deflection, $\delta(t,t_0)$, is given as the sum of instantaneous deflection, $\delta(t_0)$, and time-dependent deflection, $\Delta\delta(t,t_0)$:

$$\delta(t,t_0)=\delta(t_0)+\Delta\delta(t,t_0) \tag{22}$$

where the time-dependent deflection is the sum of creep deflection, $\Delta\delta_{creep}(t,t_0)$, and shrinkage deflection, $\Delta\delta_{sh}(t,t_0)$:

$$\Delta\delta(t,t_0)=\Delta\delta_{creep}(t,t_0)+\Delta\delta_{sh}(t,t_0) \tag{23}$$

For calculation purposes, shrinkage deflection, $\Delta\delta_{sh}(t,t_0)$, caused by uniform curvature along the span, is considered separately from instantaneous and creep deflections, whose curvature varies along the member as a result of load distribution.

Using Mohr's second theorem, the deflection for simply supported beams due to uniform shrinkage, $\Delta\delta_{sh}(t,t_0)$, can be obtained by the following expression:

$$\Delta\delta_{sh}(t,t_0)=\Delta\psi_{sh}(t,t_0)\frac{l^2}{8} \tag{24}$$

where $\Delta\psi_{sh}(t,t_0)$ is the shrinkage curvature calculated using Eq. (4).

Instantaneous and creep deflection can be obtained from double integration of the sectional curvatures. The deflection at the centre of the member strongly depends on the curvature at mid-length. In the usual case of parabolic variation of the curvature over the member's length, the mid-span deflection can be obtained from (Ghali and Favre [17]):

$$\delta(t_0) = \frac{l^2}{96}\left(\psi_{e1} + 10\psi_{centre} + \psi_{e2}\right) \tag{25}$$

where $\psi_{e1}$ and $\psi_{e2}$ are the curvatures at the member's ends, $\psi_{centre}$ is the curvature at mid-length and $l$ is the member's length. When the member is simply supported the end curvatures are zero and consequently

$$\delta(t_0) = \frac{5l^2}{48}\psi_{centre} \tag{26}$$

For calculation purposes a linear relationship between deflections and mid-span curvature can therefore be assumed.

Based on the previous considerations, time-dependent deflection due to creep can be approximated by multiplying the instantaneous deflection by the ratio of curvatures, $\frac{\Delta\psi_{creep}(t,t_0)}{\psi(t_0)}$, as in:

$$\Delta\delta_{creep}(t,t_0) = \delta(t_0)\frac{\Delta\psi_{creep}(t,t_0)}{\psi(t_0)} \tag{27}$$

Therefore, the total long-term deflection can be given as:

$$\delta(t,t_0) = \delta(t_0)\left(1 + \frac{\Delta\psi_{creep}(t,t_0)}{\psi(t_0)}\right) + \Delta\psi_{sh}(t,t_0)\frac{l^2}{8} \tag{28}$$

Long-term curvature due to the effect of creep, $\Delta\psi_{creep}(t,t_0)$, can be determined using Eq. (1), by interpolating between state 1 (corresponding to the uncracked section) and state 2 (corresponding to the fully cracked section):

$$\Delta\psi_{creep}(t,t_0) = 0.5\left(\frac{M_{cr}}{M}\right)^2\Delta\psi_{1,creep}(t,t_0) + \left(1 - 0.5\left(\frac{M_{cr}}{M}\right)^2\right)\Delta\psi_{2,creep}(t,t_0) \tag{29}$$

Under serviceability conditions the uncracked part of the beam is expected to make little contribution to the appearance and growth of cracks, and therefore the time-dependent mean curvature due to creep, $\Delta\psi_{creep}(t,t_0)$, is assumed to be equal to the time-dependent curvature for a fully cracked section, $\Delta\psi_{2,creep}(t,t_0)$ (comparisons are made in the next section):

$$\Delta\psi_{creep}(t,t_0) \approx \Delta\psi_{2,creep}(t,t_0) \tag{30}$$

Using Eqs. (30) and (14) in Eq. (27), the time-dependent deflection due to creep can be rewritten as:

$$\Delta\delta_{creep}(t,t_0) = \delta(t_0)k_{creep} \tag{31}$$

Finally, using Eq. (19) in Eq. (32), the calculation of the total deflection given by Eq. (28) can be approximated by:

$$\delta(t,t_0) = \delta(t_0)\left(1 + 0.73\varphi\sqrt{n\rho}\right) + \Delta\psi_{sh}(t,t_0)\frac{l^2}{8} \tag{32}$$

### 2.4.2 Application range of the simplified method to obtain total deflections

In this section, a parametric study is carried out to determine the application range of the simplified method for simply supported beams under serviceability conditions. The applied moment considered corresponds to the service moment $M_s$, which can be estimated by assuming a recommended maximum bar strain of 2000με [18] to limit crack widths to acceptable values for FRPRCS members [19,20].

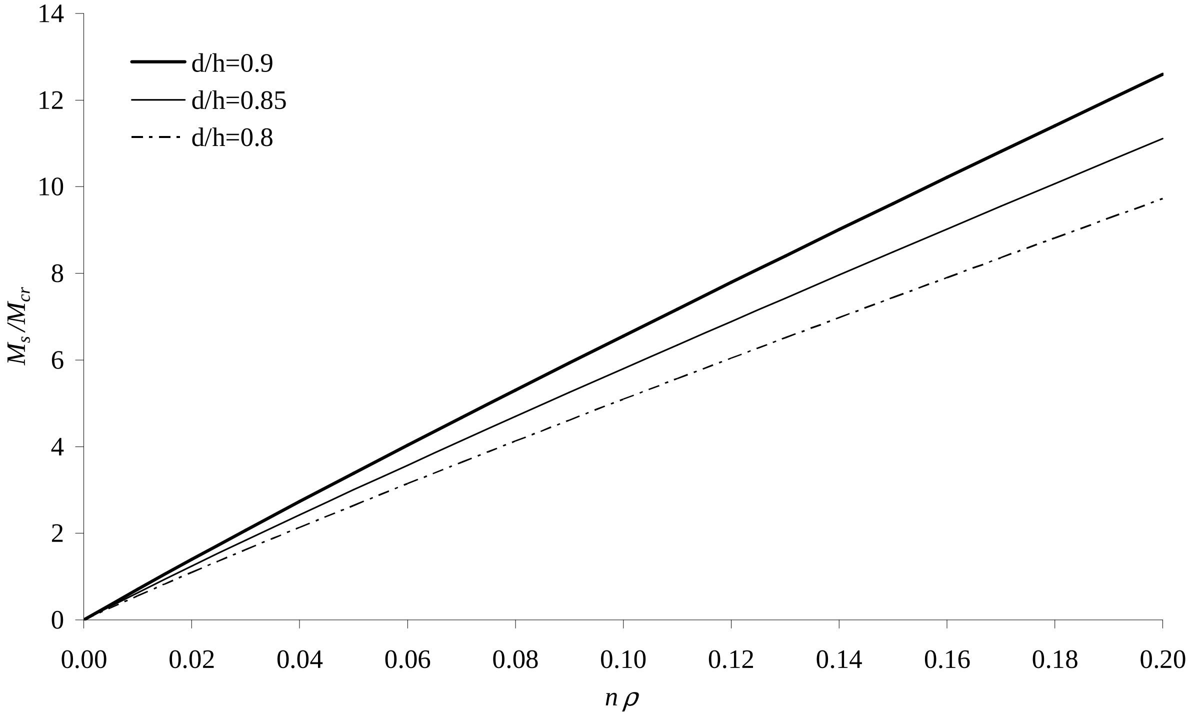

Figure 2.4. Relationship between $M_s/M_{cr}$ and $n\rho$ for FRP reinforced concrete beams.

On this assumption, the ratio $M_s/M_{cr}$ can be represented as a function of $n\rho$ and the ratio $d/h$ between the effective depth, $d$, and the height of the section, $h$, as shown in Figure 2.4.

To examine the error in the long-term deflection prediction when introducing the simplification in Eq. (30), a comparison is made between the direct application of the analytical procedure given by Eq. (28) and the proposed approximate coefficient incorporated in Eq. (32) in terms of the part of the deflection due to creep (first part of the second members in both equations). Usual values of $d/h$=0.9, φ=2 and $E_f$ ranging between 40 and 120GPa and $f_c$ ranging between 20 and 80MPa are considered for the parametric study. Three different values of shrinkage have been taken into account: 0, 200 and 400με.

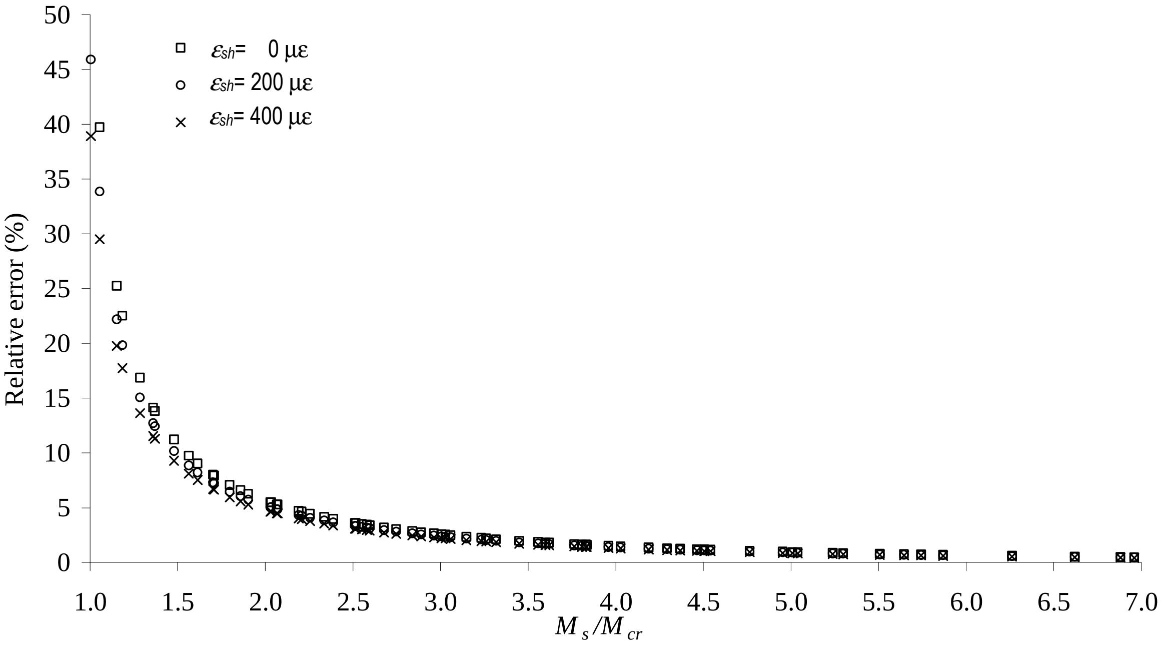

Figure 2.5. Error made using the proposed method to calculate the total deflection for different levels of concrete shrinkage.

The influence of the ratio $M_s/M_{cr}$ on the differences obtained is illustrated in Figure 2.5. The relative error decreases with the increase in the ratio $M_s/M_{cr}$, due to the fact that the proposed coefficient, $k_{creep}$, is developed for a fully cracked section, and therefore the highest errors are found when the value of the service moment is closest to the cracking moment. Assuming an error of less than 10% as an acceptable level of accuracy in deflection calculations, the proposed method is seen to be valid for calculating the total deflection for service loads $M_s/M_{cr}$ greater than 1.5, which in practice includes the majority of cases.

## 2.5 Comparison with experimental data

The procedure proposed here is compared with the experimental results of long-term deflections of concrete beams reinforced with GFRP bars presented by Hall and Ghali [13]. Two levels of sustained loading were considered, with ratios of $M/M_{cr}$ equal to 1.5 and 3.0. The beams were 280mm wide, 180mm high and 3500mm long (3200mm span), and were reinforced with 3Ø15mm GFRP bars ($\rho$=1.29%). The GFRP bars used in these experiments were type 1 C-Bar® with an ultimate tensile strength of 680MPa and a tensile elastic modulus of 42GPa. The values of concrete strength, $f_c$, and the modulus of elasticity of concrete, $E_c$, as determined from cylinder tests, were 31MPa and 21GPa respectively. With these values the modular ratio is $n$=2.

The beams were subjected to short-term cyclical loading to represent service conditions before the application of the pair of concentrated loads. The respective load levels were equal to 11.5 and 5.9kN. The temperature in the laboratory remained constant at 23±2ºC and the average relative humidity over the period of the tests was 24%.

The creep coefficient has been calculated with equations given by the CEB-FIB Model Code 1990 [5], while the free shrinkage has been obtained from the average shrinkage of test cylinders [13].

The experimental total mid-span deflections due to the two loading levels, the theoretical deflections calculated using the ACI 440.1R-06 [8] and CSA-S806-02 [11] direct method, the CEB Manual on Cracking and Deformations [15, 17] and the proposed method with the simplified coefficient $k_{creep}$ are plotted and compared in Figure 2.6. The total deflection includes the instantaneous and the time-dependent deflections due to creep and shrinkage. For the ACI 440.1R-06 and CSA-S806-02 [11] direct method, the total deflection is calculated as:

$$\delta(t,t_0)_{ACI} = \delta(t_0)(1+0.6\xi) \tag{34}$$

$$\delta(t,t_0)_{CSA} = \delta(t_0)(1+S) \tag{35}$$

where $\xi$ and $S$ are the time-dependent coefficients, with values reported in ACI 318-05 [7] and CSA-S806-02 [11].

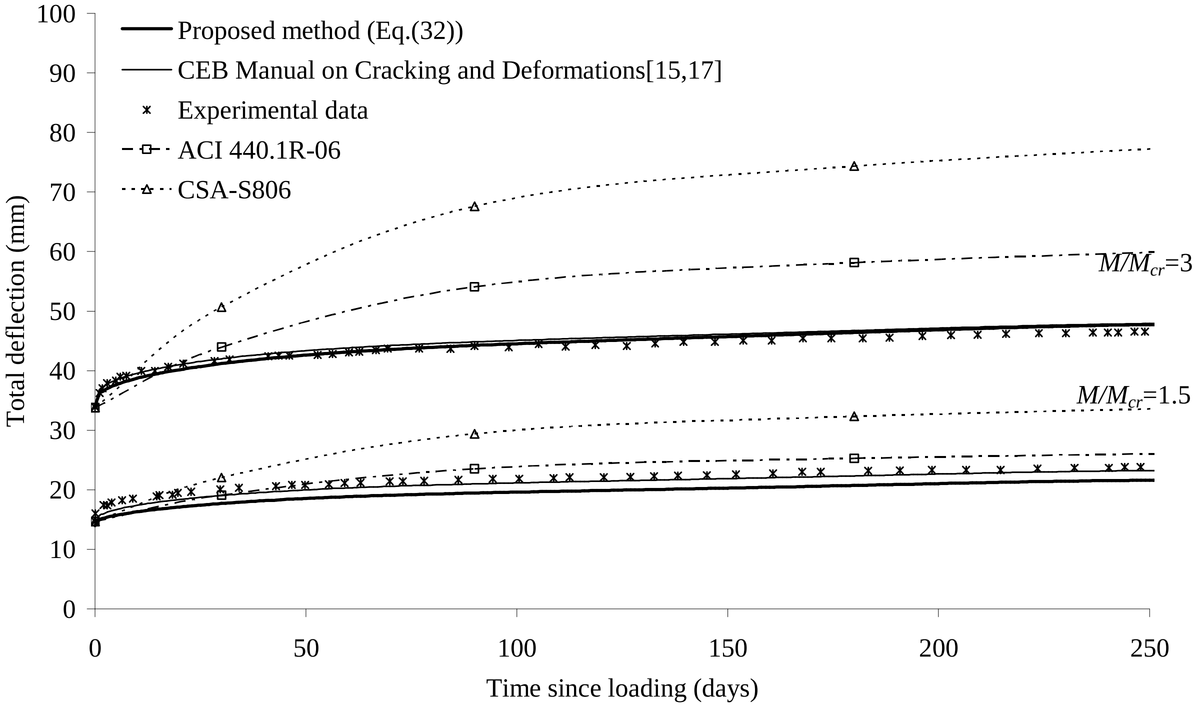

Figure 2.6. Comparison of the predicted total mid-span deflection using different methods.

An overestimation of the mid-span deflections for the two beams tested when using ACI 440.1R-06 and CSA-S806-02 is clearly illustrated in Figure 2.6, mainly for the higher load level. However, the proposed method, Eq. (32), and the CEB Manual on Cracking and

Deformations [15, 17] give similar predictions for both beams, although the latter requires a higher degree of computation. The quantification of the errors for the respective predictions is shown in Table 2.1.

## 2.6 Conclusions

A new simplified method for the evaluation of time-dependent deflections of concrete members reinforced with fibre reinforced polymer bars has been proposed. The method has been deduced from general principles based on the *Effective Modulus Method* and Eurocode 2. From an analytical development of the equations for time-dependent curvature, a new multiplying coefficient to predict time-dependent deflections due to creep of concrete members reinforced with fibre reinforced polymer bars has been proposed. The new coefficient is simple, accurate, and implicitly includes the effects of different materials, mechanical properties, environmental conditions and the age of loading. Based on the aforementioned developments, a simplified method to calculate long-term deflections under serviceability conditions accounting for creep and shrinkage has been presented. A comparison using analytical procedures and the proposed simplification has been made. Good accuracy, with differences of less than 10% for typical cases, has been obtained. Finally, a comparison with experimental results for GFRP reinforced concrete beams reported in the literature has been made, and a good capacity to predict long-term behaviour using the new method has been observed. It has also been shown that using coefficients that do not take into account specific properties can lead to considerable differences in long-term predictions.

| | Pred./Exp. deflections for sustained load: $M/M_{cr}$=1.5 | | | | Pred./Exp. deflections for sustained load: $M/M_{cr}$=3 | | | |
|---|---|---|---|---|---|---|---|---|
| Loading time (days) | CEB Manual | ACI 440.1R-06 | CSA-S806 | Proposed method | CEB Manual | ACI 440.1R-06 | CSA-S806 | Proposed method |
| **30** | 0.94 | 0.93 | 1.08 | 0.88 | 1.00 | 1.04 | 1.20 | 0.98 |
| **90** | 0.97 | 1.09 | 1.36 | 0.90 | 1.03 | 1.24 | 1.55 | 1.01 |
| **180** | 0.97 | 1.09 | 1.40 | 0.90 | 1.03 | 1.28 | 1.64 | 1.02 |
| **250** | 0.97 | 1.09 | 1.41 | 0.90 | 1.04 | 1.29 | 1.67 | 1.03 |

Table 2.1. Predicted/Experimental deflections

## 2.7 Acknowledgements

The authors acknowledge the support provided by the Spanish Government (*Ministerio de Educación y Ciencia*), Project ref. BIA2007-60222. The first author thanks the *Ministerio de Educación y Ciencia* for Grant BES-2008-005740.

## 2.8 References

1. Gilbert R. I, Time effects in concrete Structures. Elsevier, Amsterdam, 1988.

2. Bazant Z.P., Prediction of concrete creep effects using age-adjusted effective modulus method. American Concrete Institute Journal, 69 , 212-217, 1972.

3. Chiorino M., Napoli, P., Mola F.. Koprna M, Structural effects of time-dependent behaviour of concrete. Comité Euro-International du Béton: CEB Design Manual. Bulletin d'Information 136, 1980.

4. CEN 2004, Eurocode 2: Design of Concrete Structures – Part 1-1: General rules and rules for buildings (EN 1992-1-1:2004). Comité Européen de Normalisation, Brussels.

5. CEB- FIP 1990, Model code for concrete structures. Comité Euro-International du Béton. Fédération Internationale de la Précontrainte, Thomas Telford House, London, England, 1990.

6. ACI Committee 435, Control of Deflections in Concrete Structures (ACI 435R-95). American Concrete Institute, Detroit, Michigan, 1995.

7. ACI 318-05, Building Code Requirements for Reinforced Concrete, ACI Committee 318. American Concrete Institute, Detroit, Michigan, 2005.

8. ACI Committee 440, Guide for the Design and Construction of Concrete Reinforced with FRP Bars (ACI 440.1R-06). American Concrete Institute, Farmington Hills, 2006.

9. Brown V. and Bartholomew C., Long-term deflections of GFRP-reinforced concrete beams. First International Conference on Composites in Infrastructure, (ICCI-96), H. Saadatmanesh and M. R. Ehsani, eds., Tucson, Arizona, pp. 389-400, 1996.

10. Brown V., Sustained Load Deflections in GFRP-Reinforced Concrete Beams, Proceedings of the Third Int. Symposium on Non-Metallic (FRP) Reinforcement for Concrete Structures (FRPRCS-3), V. 2, Japan Concrete Institute, Tokyo, Japan, pp. 495-502, 1997.

11. CSA Standard CAN/CSA-S806-02, Design and construction of building components with fibre-reinforced polymers. Canadian Standards Association, Mississauga, Ontario, Canada, 2002.

12. Arockiasamy M., Chidambarama S., Amera A., Shahawy M. Time-dependent deformations of concrete beams reinforced with CFRP bars. Composites Part B: Engineering, 31: 577-592, 2000.

13. Hall T. and Ghali A., Long-term deflection prediction of concrete members reinforced with glass fibre reinforced polymer bars. Canadian Journal of Civil Engineering, 27(5):890–898, 2000.

14. ACI Committee 209, Manual of concrete practice. Prediction of creep, shrinkage and temperature effects in concrete structures (ACI 209R-92). American Concrete Institute, Detroit, Mich., 1992.

15. Ghali A. and Favre R., Concrete Structures: Stresses and Deformations. Ed. Chapman and Hall, London, 1994.

16. Al-Salloum Y.A., Almusallam T.H. Creep effect on the behavior of concrete beams reinforced with GFRP bars subjected to different environments. Construction and Building Materials, 21: 1510-1519, 2007.

17. Comité Euro-International du Béton (CEB), Manual on Cracking and Deformations. Butlletin d’Information nº 158-E, 1985.

18. Newhook J, Ghali A, Tadros G., Concrete flexural members reinforced with fiber reinforced polymer: design for cracking and deformability. Canadian Journal of Civil Engineering; 29: 125-134, 2002.

19. Bischoff P.H., Reevaluation of deflection prediction for concrete beams reinforced with steel and fiber reinforced polymer bars. Journal of Structural Engineering, 131(5); 752-767, 2005.

20. ISIS Canada, Reinforcing concrete structures with fibre reinforced polymers - Design manual No. 3, Manitoba, Canada: ISIS Canada Corporation, 2001.

# 3. A rational method to predict long-term deflections of FRP reinforced concrete members

Ll. Torres, C. Miàs, A. Turon, M. Baena, A rational method to predict long-term deflections of FRP reinforced concrete members, Engineering Structures 2012; 40:230-39.

**doi**: 10.1016/j.engstruct.2012.02.021

## Summary

*Due to the low modulus of elasticity of FRP bars, deflection control is often a limiting factor in the design of FRP reinforced concrete (FRP RC) structures. To address long-term deflections due to creep and shrinkage, available codes and guidelines for FRP RC structures, such as ACI 440.1R-06 and CSA-S806-02, propose simplified procedures based on empirical multiplicative coefficients. Although easy to use, these procedures do not account for the influence of changes in material properties or factors affecting creep and shrinkage of concrete. A straightforward method to predict long-term deflections due to creep and shrinkage based on rational multiplicative coefficients deduced from the principles of the Effective Modulus Method (Eurocode 2) is presented. The proposed method, although simple, accounts for main mechanical properties of materials, variations in environmental conditions or other parameters that can affect creep and shrinkage. The method is compared to CEB-FIP, ACI 440.1R-06 and CSA-S806-02 proposals. A good agreement between the CEB-FIP and the proposed method is obtained. However, the coefficients proposed by ACI and CSA can lead to considerable differences in long-term predictions with respect to the proposed method depending on the characteristics of the structure.*

## 3.1 Introduction

Fibre reinforced polymer (FRP) bars offer an alternative to steel reinforcement in concrete structures where the corrosion in steel or interferences with magnetic fields can be present. However, FRP have lower stiffness than steel reinforcement and, therefore, deflection control can usually be expected to be a limiting factor in the design of FRP reinforced concrete (FRP RC) structures.

Proposed formulations for calculating deflections of FRP RC structures are based on the same principles already established for steel reinforced concrete (SRC) structures. Nevertheless, the equations have been modified to be adapted to the particular behaviour of FRP RC members. A number of studies on flexural behaviour and instantaneous deflections of FRP RC members have been carried out [1-7] and the several proposals that have been made gave acceptable predictions.

Likewise, existing equations for SRC structures have been taken as a reference for long-term deflections of FRP RC structures, the use of multiplicative coefficients on the initial deflection being one of the most widespread methods due to its simplicity [8,9]. Nevertheless it is worth mentioning that these coefficients were empirically calibrated for SRC members under specific conditions (reinforcement and concrete properties, and environmental conditions) [10]. On the other hand, using more general methods based on the calculation of long-term sectional curvatures [11-14] allows the mechanical behaviour of materials to be taken into account in a more rational way, although complexity is introduced into the calculation. As an alternative, to facilitate their use in design practice, multiplicative coefficients which take into account the main mechanical and environmental parameters involved have been derived for creep and shrinkage deformations [12,13]. However, their calculation is not immediate and design charts have been developed for their practical application [12,13].

Due to the lower stiffness of FRP bars, the relative deformation increment associated with creep and shrinkage in FRP RC structures is lower than for conventional SRC elements since there is a smaller concrete area in compression. Based on the results of long-term test of concrete beams reinforced with FRP bars carried out by Brown and Bartholomew [15] and Brown [16], ACI 440.1R-06 [17] proposes to reduce the multiplying factor for SRC structures of ACI 318 [8,10] applying an empirical reduction coefficient of 0.6 to take account of the aforementioned lower effect of creep and shrinkage.  On the other hand CSA-S806-02 [18] proposes a more conservative approach and adopts the same coefficient used for SRC elements. However, available experimental results [19-23] show that ACI and CSA procedures do not always adequately predict long-term deflections of FRP RC members.

Analysis of experimental results on FRP RC beams [19,22] indicate that the CEB-FIP procedure [11,12] together with creep and shrinkage curvature coefficients, as those proposed by Ghali et al. [13], can accurately predict long-term deflections of FRP RC structures. The procedure is based on the Age-Adjusted Effective Modulus Method [24] and it accounts for the effects of member geometry, load characteristics (age of concrete at the time of loading, magnitude and duration of sustained load) and material properties (elastic moduli of concrete and FRP reinforcement, creep and shrinkage of concrete). However, this approach requires a greater degree of computational effort.

A procedure similar to CEB-FIP deduced from the Eurocode 2 [14] approach for long-term deformations, but simple and straightforward, more like ACI 440.1R-06 [17] or CSA-S806-02 [18], was presented in [25] to obtain the long-term deflections due to creep from the initial deflections. A multiplicative coefficient to obtain the long-term deflections due to creep was deduced considering the principles of the Effective Modulus Method [26,27] from Eurocode

2. The coefficient was deduced considering a fully-cracked condition, and comparison with CEB-FIP procedures and experimental results demonstrated its suitability for serviceability conditions.

This paper presents a rational and straightforward method, based on rational multiplicative coefficients, to calculate long-term deflections in FRP RC members due to creep and shrinkage. The previously introduced method for creep deflections of FRP RC structures is generalized to take into account the tension stiffening effect, expanding its applicability. A coefficient for long-term shrinkage deflections is deduced based on general principles of structural mechanics and using the *Effective Modulus Method* [14]. The coefficient is reduced by mathematical manipulation to be simple but also able to account for variations in the environmental conditions and the mechanical properties of materials. The proposed method based on multiplicative coefficients to predict long-term deflections is compared to experimental results to show its suitability, and to CEB-FIP [11-13], ACI440.1R-06 [17], and CSA-S806-02 [18] methodologies to highlight the influence of different parameters in the predictions.

## 3.2 Time-dependent coefficients for FRP RC beams

In this section, time-dependent coefficients to predict long-term curvatures due to creep and shrinkage are presented. Both are deduced from the principles of the Effective Modulus Method [26,27] and Eurocode 2 [14].

A coefficient to compute time-dependent curvatures and deflections due to creep was deduced for a fully-cracked section in [25], showing its suitability for the usual range of loads under serviceability conditions. In this paper, it has been extended and generalized to take into account the unfavourable contribution of the uncracked section, and so the tension stiffening effect, for loads relatively close to the cracking moment. The procedure is completed with the proposal of a coefficient for deformations due to shrinkage effects. As for the coefficient for creep deflections, the deduction is based on general principles of structural mechanics, and it is reduced by mathematical manipulation to be simple but also able to account for variations in the environmental conditions and the mechanical properties of materials. In this case a fully-cracked section is considered to obtain a simpler coefficient, although on the side of safety.

Due to the relationship between curvatures and deflections, the two coefficients can be incorporated into a procedure to predict long-term deflections due to creep and shrinkage.

### *3.2.1 Long-term curvature due to creep*

Sustained stresses applied to concrete will produce a progressive increase in strain due to creep. The environmental conditions, the concrete mixture, the shape of the member, the material properties, as well as the age at loading and the duration of the load influence creep strain.

According to Eurocode 2 [14], the curvature including creep, $\psi(t,t_0)$, in members subjected to flexure, which are expected to crack but may not be fully-cracked, can be calculated by:

$$\psi(t,t_0)=\psi_1(t,t_0)\beta\left(\frac{M_{cr}}{M}\right)^2+\psi_2(t,t_0)\left(1-\beta\left(\frac{M_{cr}}{M}\right)^2\right) \tag{1}$$

where $t$ is the time at which $\psi(t,t_0)$ is to be determined, $t_0$ is the time at the application of the sustained load, $\beta$ is a coefficient taking into account the influence of the duration of the load (1 for a single short-term load, and 0.5 for sustained or repeated loads), $M_{cr}$ is the cracking moment, and $M$ is the applied moment. $\psi_1(t,t_0)$ and $\psi_2(t,t_0)$ are the curvatures including creep at the time $t$ for the uncracked and fully-cracked conditions, respectively, and can be calculated using an effective modulus of elasticity of concrete according to the following expression:

$$E_c(t,t_0) = \frac{E_c}{1+\varphi(t,t_0)} \tag{2}$$

where $E_c$ is the modulus of elasticity of concrete at time $t_0$ and $\varphi(t,t_0)$ is the creep coefficient.

Based on the *Effective Modulus Method* (Eq. 2), the authors presented [25] a simplified method to predict time-dependent curvatures due to creep in flexural members reinforced with FRP bars. According to this method, the increment in long-term curvatures due to creep for a fully-cracked transformed section, $\Delta\psi_{2,creep}(t,t_0)$, can be obtained from the corresponding initial curvature, $\psi_2(t_0)$, using the multiplicative factor $k_{creep}$ :

$$\Delta\psi_{2,creep}(t,t_0) = k_{creep}\psi_2(t_0) \tag{3}$$

$$k_{creep} = 0.73\varphi\sqrt{n\rho} \tag{4}$$

where $\varphi = \varphi(t,t_0)$ is the creep coefficient at time *t; n* is the ratio between the modulus of elasticity of reinforcement, $E_f$, and the modulus of elasticity of concrete, $E_c$; and $\rho$ is the tensile reinforcement ratio. Detailed derivation of Eq. (4) can be found in pp. 1834-1835 of [25].

Although the coefficient $k_{creep}$ was deduced for a fully-cracked section, a parametric study showed its accuracy for calculating the total deflections (initial plus long-term deflections due to creep) under serviceability conditions, when the tension stiffening effect is relatively small [25].

To increase the accuracy of the predictions using the multiplicative coefficient for service moments and moments close to the cracking moment, a new approach is developed to obtain a more general procedure. This approach accounts for the tension-stiffening effect together with the time-dependent loss of flexural stiffness [14], which occurs from cracking under repeated loading or due to sustained loads.

Following this methodology (its full development is presented in the Appendix), the predicted curvature including creep, $\psi(t,t_0)$, can be obtained using the $k_{creep}$ coefficient, given in Eq.(4), and the initial curvature for a sustained load, $\psi(t_0)_{\beta=0.5}$:

$$\psi(t,t_0) = \left(1+k_{creep}\right)\psi(t_0)_{\beta=0.5} \tag{5}$$

where $\psi(t_0)_{\beta=0.5}$ is obtained using $\beta = 0.5$ and Eq. (4-A2) in Eq. (4-A1) from the Appendix:

$$\psi\ (t_0)_{\beta=0.5} = \frac{M}{E_c I_1}\left(0.5\left(\frac{M_{cr}}{M}\right)^2\right) + \frac{M}{E_c I_2}\left(1-0.5\left(\frac{M_{cr}}{M}\right)^2\right) \tag{6}$$

where $I_1$ and $I_2$ are the moments of inertia of uncracked and fully-cracked transformed sections about its centroidal axis, respectively. Calculation of the initial curvature using a factor $\beta$ = 0.5 in the tension-stiffening term according to Eq. (6), is equivalent to the calculation for short-term loading ($\beta$ = 1 in Eq. A1) but using a reduced cracking moment equal to $M'_{cr} = \sqrt{\beta} M_{cr}$, which corresponds to a 30% reduction in the cracking moment as indicated in Scanlon and Bischoff [29].

### *3.2.2 Long-term curvature due to shrinkage*

Concrete shrinkage is a reduction in volume caused principally by the loss of water during the drying process [26]. The environmental, mixture and curing conditions, the material properties and the geometry of the element affect the magnitude of free shrinkage strain of concrete. As the concrete shrinks, the reinforcement is compressed and an equal and opposite tensile force is imposed on the concrete at the level of the reinforcement. If the reinforcement is not symmetrically placed on a section, a shrinkage-induced curvature develops with time.

Shrinkage in an unsymmetrically reinforced concrete beam can produce deflections of significant magnitude, even if the beam is unloaded [28]. This applies also for FRP RC flexural elements, although it is not recommended to rely on FRP bars to resist compressive stresses [17].

Based on general principles of structural mechanics, Eurocode 2 proposes to obtain the long-term curvature due to shrinkage, $\Delta\psi_{sh}(t,t_0)$, by:

$$\Delta\psi_{sh}(t,t_0)=\varepsilon_{sh}(t,t_0)\frac{n(t,t_0)S(t,t_0)}{I(t,t_0)} \tag{7}$$

where $\varepsilon_{sh}(t,t_0)$ is the free shrinkage strain, $S(t,t_0)$ is the first moment of area of the reinforcement about the centroid of the effective transformed section, $I(t,t_0)$ is the moment of inertia of the effective transformed section, and

$$n(t,t_0)=\frac{E_f}{E_c(t,t_0)} \tag{8}$$

is the effective modular ratio, with $E_f$ as the modulus of elasticity of the FRP reinforcement. The first moment of effective transformed area of the reinforcement, $n(t,t_0)S(t,t_0)$, equals the first moment of area of concrete about the centroid of the effective transformed section. The effective transformed section properties are calculated using the effective modulus of elasticity of concrete (Eq. 2). Using of fully-cracked section condition in Eq. (7) greatly simplifies the procedure and gives similar or slightly higher values than interpolating between uncracked and fully-cracked states. Therefore, for a fully-cracked rectangular section, Eq. (7) can be written as:

$$\Delta\psi_{sh}(t,t_0)=\varepsilon_{sh}(t,t_0)\frac{b\cdot x(t,t_0)^2}{2I_2(t,t_0)} \tag{9}$$

where $b$ is the section width and $x(t,t_0)$ is the neutral axis depth of the effective transformed section. Eq. (9) is also valid for T sections if the neutral axis lies within the flange. The moment of inertia of the effective fully-cracked transformed section, $I_2(t,t_0)$, can be obtained by the following expression:

$$I_2(t,t_0) = n(t,t_0)A_f\left(d - x(t,t_0)\right)\left(d - \frac{x(t,t_0)}{3}\right) \tag{10}$$

where $A_f$ is the area of tensile reinforcement ($A_f = \rho bd$) and $d$ is the effective depth.

Using Eqs. (9) and (10), the long-term curvature due to shrinkage reads:

$$\Delta\psi_{sh} = \frac{\varepsilon_{sh}(t,t_0)}{d}\frac{x(t,t_0)^2}{2n\rho(1+\varphi(t,t_0))\left(d - x(t,t_0)\right)\left(d - \frac{x(t,t_0)}{3}\right)} \tag{11}$$

The neutral axis depth of an effective fully-cracked transformed section with no compressive reinforcement can be calculated as:

$$x(t,t_0) = dn\rho(1+\varphi(t,t_0))\left(-1 + \sqrt{1 + \frac{2}{n\rho(1+\varphi(t,t_0))}}\right) \tag{12}$$

If the last term in Eq. (11) is renamed as $k_{sh}$:

$$k_{sh} = \frac{x(t,t_0)^2}{2n\rho(1+\varphi(t,t_0))\left(d - x(t,t_0)\right)\left(d - \frac{x(t,t_0)}{3}\right)} \tag{13}$$

the long-term curvature due to shrinkage reads:

$$\Delta\psi_{sh} = \frac{\varepsilon_{sh}}{d}k_{sh} \tag{14}$$

where $\varepsilon_{sh} = \varepsilon_{sh}(t,t_0)$ is the free shrinkage strain.

Substituting Eq. (12) into Eq. (13), with $\varphi = \varphi(t,t_0)$, $k_{sh}$ can be rewritten as:

$$k_{sh}(n\rho,\varphi) = \frac{1}{2n\rho(1+\varphi)\left(\left(n\rho(1+\varphi)\left(-1+\sqrt{1+\frac{2}{n\rho(1+\varphi)}}\right)\right)-1\right)\left(\left(n\rho(1+\varphi)\left(-1+\sqrt{1+\frac{2}{n\rho(1+\varphi)}}\right)\right)-\frac{1}{3}\right)} \tag{15}$$

The non-dimensional parameter *nρ* depends on the elastic moduli of FRP and concrete, and the reinforcement ratio. Assuming an elastic modulus of FRP between 40 and 120GPa, a concrete strength between 25 and 80MPa, and a reinforcement ratio between 0 and 0.03, *nρ* ranges from 0 to 0.12. Due to variation in environmental conditions, $\varphi$ can be assumed to range from 1 to 3. Accordingly, $k_{sh}$ can be simplified using the Taylor series development of Eq. (15) about point (0,2), obtaining:

$$k_{sh} \approx 1+\frac{1}{18}\sqrt{6n\rho}(4+\varphi) \approx 1+0.14\sqrt{n\rho}(4+\varphi) \tag{16}$$

For practical purposes $\varphi$ can be replaced by a conservative value of 3, and coefficient $k_{sh}$ can be reduced to:

$$k_{sh} = 1+\sqrt{n\rho} \tag{17}$$

### *3.2.3 Comparison of the proposed coefficients and the reference analytical procedure*

Using the deduced multiplicative coefficients to obtain long-term curvatures due to creep and shrinkage (Eqs. 5 and 14), the total curvature reads:

$$\psi(t,t_0)_{T,proposed} = \left(1+k_{creep}\right)\psi(t_0)_{\beta=0.5} + \frac{\varepsilon_{sh}}{d}k_{sh} \tag{18}$$

where $k_{creep}$ and $k_{sh}$ are defined in Eqs. (4) and (17), respectively.

To assess the accuracy of the methodology, a parametric study is carried out comparing the total curvature, including creep and shrinkage, calculated using the proposed simplified coefficients, $k_{creep}$ and $k_{sh}$, and the analytical procedure of Eurocode 2 from which they were derived. To this end, the following typical values have been selected: $d/h$=0.9, $f_c$ ranging between 25 and 80MPa, $\rho$ ranging between 0.002 and 0.03, and $E_f$ ranging between 40 and 120GPa. Creep coefficient and free shrinkage strain have been taken as $\varphi$=2 and $\varepsilon_{sh}$=350με. Additionally, different levels of applied moment have been used: 1.5$M_{cr}$, 2$M_{cr}$, 3$M_{cr}$, and 5$M_{cr}$.

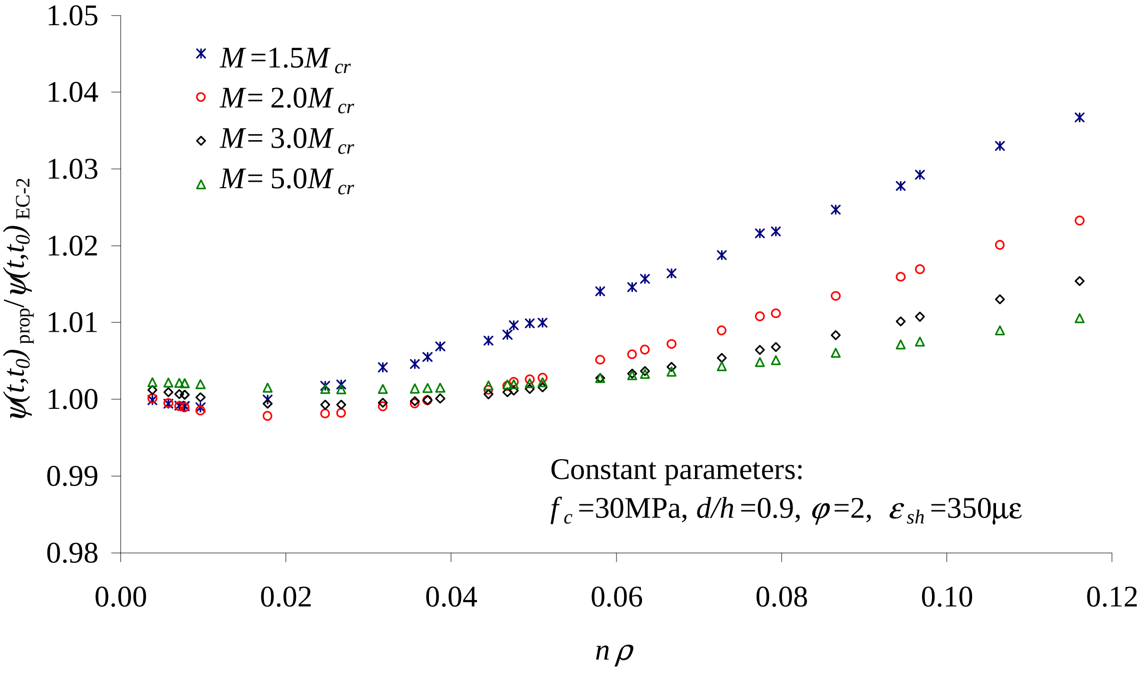

Figure 3.1. Ratio between total curvatures predicted using (Eq. 18) and Eurocode 2, $\dfrac{\psi_T(t,t_0)_{proposed}}{\psi_T(t,t_0)_{EC-2}}$, for different levels of applied moment.

The ratio between the curvatures obtained using the simplified coefficients and the general analytical method $\frac{\psi_T(t,t_0)_{proposed}}{\psi_T(t,t_0)_{EC-2}}$ is illustrated in Table 3.1, for concrete with $f_c$=30MPa. For a concrete strength ranging between 25 and 80MPa, the ratio varies between 0.99 and 1.04, thus showing good accuracy of the simplified procedure.

Additionally, the study has been conducted for different values of creep coefficient, $\varphi$, and free shrinkage strain, $\varepsilon_{sh}$ (keeping $f_c$ = 30MPa). Results for bending moments equal to 1.5$M_{cr}$ and 3$M_{cr}$ are presented in Table 3.1. Again good accuracy is observed.

| | | $M$=1.5$M_{cr}$ | | | $M$=3.0 $M_{cr}$ | | |
|---|---|---|---|---|---|---|---|
| $\varphi$ | $\varepsilon_{sh}$ ($\mu\varepsilon$) | $n\rho$= 0.02 | $n\rho$= 0.08 | $n\rho$= 0.12 | $n\rho$= 0.02 | $n\rho$= 0.08 | $n\rho$= 0.12 |
| 1 | 100 | 0.98 | 0.99 | 0.99 | 0.99 | 0.99 | 0.99 |
| 1 | 200 | 1.00 | 1.02 | 1.04 | 0.99 | 1.00 | 1.01 |
| 2 | 200 | 0.98 | 0.99 | 1.00 | 1.00 | 1.00 | 1.00 |
| 2 | 350 | 1.00 | 1.02 | 1.04 | 1.00 | 1.01 | 1.02 |
| 3 | 350 | 0.99 | 1.00 | 1.01 | 1.01 | 1.01 | 1.02 |
| 3 | 500 | 1.01 | 1.02 | 1.03 | 1.01 | 1.01 | 1.02 |

Table 3.1. Ratio between total curvatures predicted using Eq. (18) and Eurocode 2, $\frac{\psi_T(t,t_0)_{proposed}}{\psi_T(t,t_0)_{EC-2}}$, for different environmental conditions ($f_c$=30MPa).

It can therefore be concluded that the deduced simplified coefficients can be applied for a wide range of values of $n\rho$ including different materials and reinforcement ratios, as well as creep and shrinkage values.

### *3.2.4 Long-term deflection due to creep and shrinkage*

Initial and total deflections including creep can be obtained from the double integration of sectional curvatures. In the usual case of parabolic variation of curvatures over the member's length, the mid-span deflection can be obtained as [13]:

$$\delta_m = \frac{l^2}{96}\left(\psi_{end,l} + 10\psi_m + \psi_{end,r}\right) \tag{19}$$

where $\psi_m$ is the curvature at mid-span, $\psi_{end,l}$ and $\psi_{end,\mathrm{r}}$ are the curvatures at the member's left and right end, respectively, and *l* is the member length. From Eq. (19) it can be seen that the deflection at the centre of the member strongly depends on the curvature at mid-span.

Using Eq. (5) in Eq.(19), the deflection including creep at time *t*, for members with different support conditions (continuous or fixed end members) reads:

$$\delta(t,t_0) = \frac{l^2}{96}\left(\left(1+k_{creep,l}\right)\psi(t_0)_{(\beta=0.5)end,l} + 10\left(1+k_{creep,m}\right)\psi(t_0)_{(\beta=0.5),m} + \left(1+k_{creep,r}\right)\psi(t_0)_{(\beta=0.5)end,r}\right) \tag{20}$$

where $k_{creep,m}$, $k_{creep,l}$, and $k_{creep,r}$, are the creep coefficients calculated using Eq. (4), at the mid-span section, at member's left end, and right end, respectively. Similarly, $\psi(t_0)_{(\beta=0.5),m}$, $\psi(t_0)_{(\beta=0.5)end,l}$ and $\psi(t_0)_{(\beta=0.5)end,r}$ are the initial curvatures, at mid-span, and at the two member's end, calculated using Eq. (6).

For a typical case of a simply supported beam, $\psi_{end,\mathrm{l}}$ and $\psi_{end,\mathrm{r}}$ equal 0 and the deflection including creep at time *t* from Eq. (20) leads to the following expression:

$$\delta(t,t_0) = \frac{10l^2}{96}\left(1+k_{creep,m}\right)\psi(t_0)_{(\beta=0.5),m} \tag{21}$$

Taking into account that the initial deflection is:

$$\delta(t_0)_{(\beta=0.5)} = \frac{10l^2}{96}\psi(t_0)_{(\beta=0.5),m} \tag{22}$$

and substituting Eq.(22) in Eq.(21), the deflection including creep can be approximated multiplying the initial deflection by the proposed coefficient $k_{creep}$:

$$\delta(t,t_0) = \left(1 + k_{creep,m}\right)\delta(t_0)_{(\beta=0.5)} \tag{23}$$

On the other side, long-term deflection due to uniform shrinkage, $\Delta\delta_{sh}(t,t_0)$, can be obtained using Mohr's second theorem leading to the following expression:

$$\Delta\delta_{sh}(t,t_0) = \Delta\psi_{sh}(t,t_0)k_s l^2 \tag{24}$$

where $k_s$ depends on the support conditions of the beam [29]:

$k_s = 0.50$ for cantilevers

$k_s = 0.13$ for simply supported beams

$k_s = 0.09$ for spans with one end continuous (multi spans)

$k_s = 0.08$ for spans with one end continuous (two spans)

$k_s = 0.07$ for spans with both ends continuous

Using Eq. (14) in Eq. (24), the long-term deflection due to shrinkage can be obtained as:

$$\Delta\delta_{sh}(t,t_0) = \frac{\varepsilon_{sh}(t,t_0)}{d}k_{sh}k_s l^2 \tag{25}$$

In the particular case of a simply supported beam, the long-term deflection due to shrinkage can be calculated by:

$$\Delta\delta_{sh}(t,t_0) = \frac{\varepsilon_{sh}(t,t_0)l^2}{8d}\left(1 + \sqrt{n\rho}\right) \tag{26}$$

## 3.3 Evaluation of total deflections of FRP RC members

Simplified procedures used for SRC structures are adopted in FRP RC codes and guidelines, with or without modification, as is the case of ACI 440.1R-06 [17] and CSA-S806-02 [18]. As indicated previously, these methods are very simple and straightforward although they do not explicitly account for the variation of material properties or environmental conditions.

On the other hand, more general procedures, such as that from CEB-FIP [11-13], specifically include different materials and values of creep and shrinkage. Although this method was deduced for SRC structures, it has been proved to be suitable for other reinforcing materials such as FRP [19,22].

In this section the aforementioned methods are introduced, and a study is performed to compare their predictions with those from the proposed method for a wide range of parameters.

### *3.3.1 Prediction models*

*ACI 440.1R-06*

According to ACI 440.1R-06 [17], the total deflection, including the effect of creep and shrinkage, $\delta_{T(ACI\,440)}$, of FRP RC members can be obtained from the initial deflection due to sustained load, $\delta_{(sus)}$:

$$\delta_{T(ACI\,440)} = (1 + 0.6\lambda)\delta_{(sus)} \tag{27}$$

where 0.6 is a reduction factor based on tests carried out by Brown and Bartholomew [15] and Brown [16], and $\lambda$ is the coefficient in ACI 318-08 that has been widely used for SRC structures [8,10,29]:

$$\lambda = \frac{\xi}{1+50\rho'} \tag{28}$$

where $\rho'$ is the compression reinforcement ratio and $\xi$ is the time-dependent factor for sustained loads, which includes the effects of creep and shrinkage.

If compression reinforcement is not considered $(\rho'=0)$, as stated for FRP RC structures, the parameter $\lambda$ reduces to $\xi$, and Eq. (27) can be written as:

$$\delta_{T(ACI\,440)} = (1+0.6\xi)\delta_{(sus)} \tag{29}$$

*CSA-S806-02*

According to CSA-S806-02 [18], the equation for total deflection of FRP RC structures is the same as for SRC members with no reduction:

$$\delta_{T(CSA)} = (1+\xi)\delta_{(sus)} \tag{30}$$

*CEB-FIP*

Based on the procedure presented in the CEB Manual on Cracking and Deformations [12], described and illustrated in Ghali et al. [13], total deflections, $\delta_{T(CEB-FIB)}$, can be obtained by interpolating between state 1 (uncracked transformed section) and state 2 (fully-cracked transformed section):

$$\delta_{T(CEB-FIB)} = 0.5\left(\frac{M_{cr}}{M}\right)^2 \delta_{T,1}(t,t_0) + \left(1-0.5\left(\frac{M_{cr}}{M}\right)^2\right)\delta_{T,2}(t,t_0) \tag{31}$$

where, the predicted total deflections for each state (1 and 2) can be obtained as the sum of the initial deflection, $\delta(t_0)_i$, the long-term deflection due to creep, $\Delta\delta(t,t_0)_{creep,i}$, and the long-term deflection due to shrinkage, $\Delta\delta(t,t_0)_{sh,i}$:

$$\delta_{T,i} = \delta(t_0)_i + \Delta\delta(t,t_0)_{creep,i} + \Delta\delta(t,t_0)_{sh,i} \tag{32}$$

where subscript *i* takes the value of 1 for the uncracked state and 2 for the fully-cracked state. The long-term deflections due to creep and shrinkage are obtained separately from the following expressions:

$$\Delta\delta(t,t_0)_{creep,i} = \delta(t_0)_i \varphi(t,t_0)\kappa_{\varphi,i} \tag{33}$$

$$\Delta\delta(t,t_0)_{sh,i} = \frac{\varepsilon_{sh}(t,t_0)}{d}\frac{l^2}{8d}\kappa_{sh,i} \tag{34}$$

being $\kappa_{\varphi,i}$ and $\kappa_{sh,i}$ the curvature coefficients related to creep and shrinkage, respectively:

$$\kappa_{\varphi,i} = \frac{I_{c,i}(t,t_0) + A_{c,i}y_{c,i}(t,t_0)\Delta y_i(t,t_0)}{\bar{I}_i(t,t_0)} \tag{35}$$

$$\kappa_{sh,i} = \frac{A_{c,i}y_{c,i}(t,t_0)d}{\bar{I}_i(t,t_0)} \tag{36}$$

where $A_{c,i}$ is the area of concrete considered effective (entire concrete area in state 1, but only area of compression zone in state 2), $I_{c,i}(t,t_0)$ is the moment of inertia of $A_{c,i}$ about an axis through the centroid of the age-adjusted transformed section, $y_{c,i}(t,t_0)$ is the centroid of $A_{c,i}$ measured downwards from the centroid of the age-adjusted transformed section, $\Delta y_i(t,t_0)$ is the y-coordinate of the centroid of the age-adjusted transformed section, measured downwards from the centroid of the transformed section at $t_0$, and $\bar{I}_i(t,t_0)$ is the moment of inertia of the age-adjusted transformed section about an axis through its centroid. A detailed explanation of the procedure and graphs for obtaining $\kappa_{\varphi,i}$ and $\kappa_{sh,i}$ can be found in Appendix F of [13].

The age-adjusted transformed section properties are calculated using the age-adjusted elastic modulus of concrete:

$$\overline{E_e}(t,t_0) = \frac{E_c}{1+\chi(t,t_0)\varphi(t,t_0)} \tag{37}$$

where $\chi(t,t_0)$ is the ageing coefficient.

Calculation of $\kappa_{\varphi,i}$ and $\kappa_{sh,i}$ is not immediate and design charts have been developed for practical applications [12,13].

### *3.3.2 Proposed method*

Deflections at time *t* can be obtained by adding that part of the deflection including creep and long-term deflection due to shrinkage, through the corresponding coefficients. Using the approach presented in Section 2.3, the total deflection can be computed as:

$$\delta_{T,proposed} = \delta(t_0)_{\beta=0.5}\left(1+k_{creep}\right)+\frac{\varepsilon_{sh}(t,t_0)l^2}{8d}k_{sh} \tag{38}$$

It is worth mentioning that, the proposed method (Eq. 38) explicitly account for the influence of environmental conditions and mechanical properties; moreover the contribution to long-term deflection of creep and shrinkage effects are accounted for separately.

### *3.3.3 Comparison with experimental data*

To properly model the long-term behaviour of RC members using the CEB-FIP and the proposed method, the mechanical properties of the materials as well as the environmental conditions are needed. In this section all the methodologies exposed in the previous section are compared with experimental long-term deflections of GFRP RC beams presented by Hall and Ghali [19], which reported the data needed for the analytical model (geometry, loads applied, materials properties, relative humidity in the laboratory, free shrinkage strain). The beams, with a cross section of 280x180mm and 3500mm in length (3200mm span), were reinforced with 3Ø15mm GFRP bars and subjected to sustained loading for approximately 8 months. Two levels of sustained flexural moment, $M$, were considered ($M/M_{cr}$=1.5, $M/M_{cr}$=3). The modulus of elasticity of concrete, $E_c$, was 21GPa, and the compressive concrete strength, $f_c$, was 31MPa. The modulus of elasticity of GFRP bars, $E_f$, was 42 GPa. The beams were subjected to short-term cyclical loading to represent service conditions before the application of a pair of concentrated loads. The temperature in the laboratory remained constant at 23±2ºC and the average relative humidity over the period of the tests was 24%. The creep coefficient was calculated with equations given by the CEB-FIB Model Code 1990 [11], while the free shrinkage was determined from the experimental cylindrical shrinkage specimens [19].

The obtained results are presented in Figure 3.2. It can be observed that ACI 440.1R-06 and CSA-S806-02 predictions overestimate the mid-span deflections for the two beams, mainly for the higher load level. However, a good agreement between experimental data and mid-span deflection prediction using the proposed method, Eq. (38), and the CEB-FIP procedure [12,13] has been obtained for both beams.

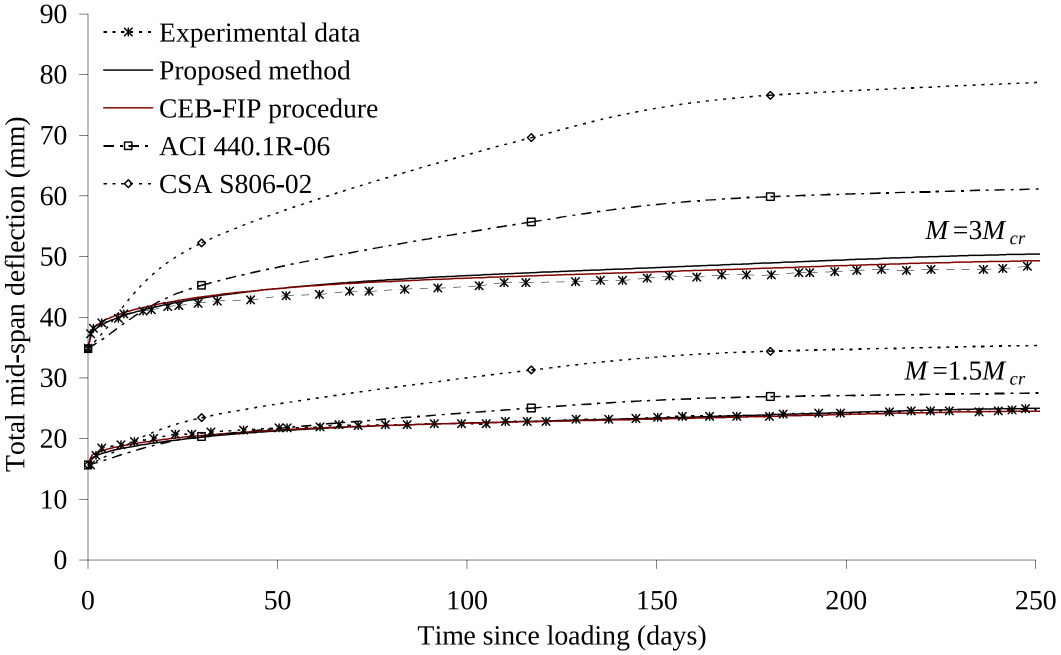

Figure 3.2. Comparison of experimental data with the predicted total mid-span deflection predictions using different methods.

### *3.3.4 Comparison of methodologies for deflection prediction*

Predictions of total deflection using the proposed method and those from ACI 440.1R-06, CSA-S806-02 and CEB-FIP procedures are analysed and compared by varying different parameters that can influence the results to highlight their influence on the different approaches. A comparison is made for a simply supported beam with rectangular section and uniformly distributed load. Four levels of applied load leading to maximum flexural moments of $1.5M_{cr}$, $2M_{cr}$, $3M_{cr}$ and $5M_{cr}$ have been used. Typical values of $d/h$=0.9, $f_c$=30MPa, reinforcement ratio $\rho$ ranging between 0 and 0.03, and $E_f$ ranging between 40 and 120 GPa are considered (which cover typical values for GFRP, AFRP, and CFRP). Three different values for free shrinkage strain, $\varepsilon_{sh}$ , equal to 200, 350 and 500με and for creep coefficient, $\varphi$, equal to 2 and 3 have been considered. A typical value of 0.8 has been taken for the aging coefficient $\chi(t,t_0)$ used in the formulation of CEB-FIP.

Although different approaches are available to compute instantaneous deflections [1-4] in this work the initial first-load deflection, $\delta(t_0)$ (which is taken as a reference) is calculated using Bischoff's approach for the equivalent moment of inertia, $I_e$ [4,30], since previous studies have shown its general applicability to FRP RC members as well as to SRC members:

$$I_e = \frac{I_2}{1-\left(1-\frac{I_2}{I_1}\right)\left(\frac{M_{cr}}{M}\right)^2} \tag{39}$$

Results obtained using the different methods are presented in Figures 3.3 and 3.4.

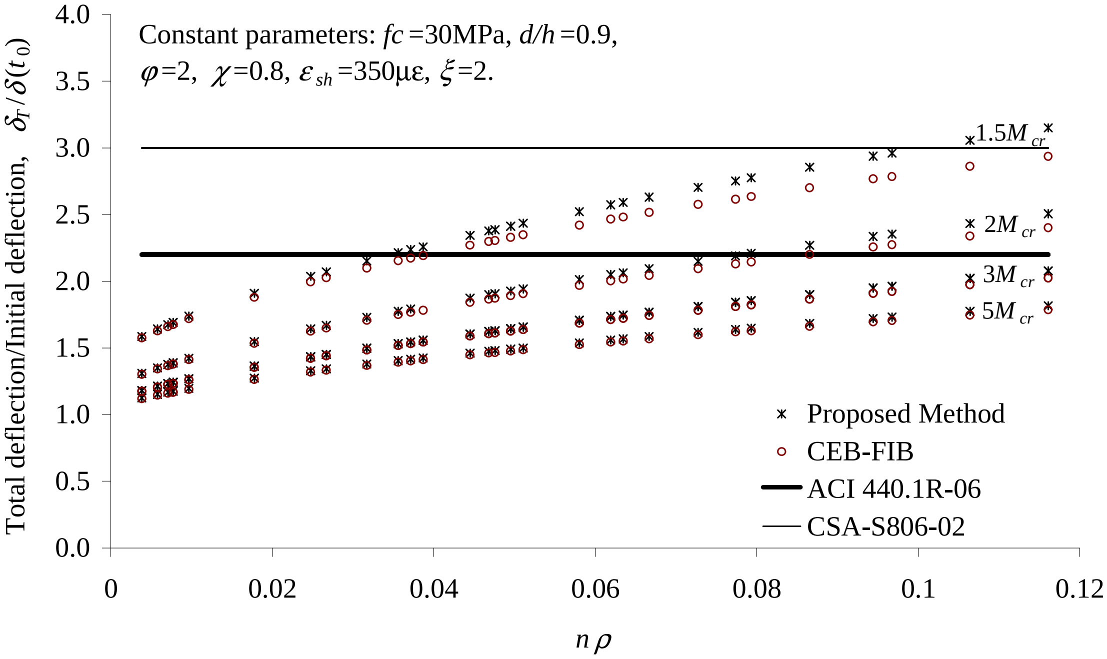

Figure 3.3 Effect of applied moment on the total-to-initial deflection prediction ratio, $\frac{\delta_T}{\delta(t_0)}$.

The influence of the applied moment, $M$, relative to the cracking moment, $M_{cr}$, versus $n\rho$ on the total-to-initial deflection prediction ratio, $\frac{\delta_T}{\delta(t_0)}$, is shown in Figure 3.3. It is observed that the CEB-FIP procedure and the proposed method (Eq. 38) present the same trend, with little differences between them, showing a clear dependence on the level of load. Moreover, it is shown that increasing $n\rho$ leads to higher total-to initial deflection prediction ratio due to the increase in the height of the compressive concrete block, which implies an increment of curvature caused by creep and shrinkage of concrete. On the other hand, it can be seen that the total-to-initial deflection prediction ratio is constant when using ACI 440.1R-06 and CSA-S806-02 methods, since their time-dependent factors do not depend either on sectional properties or values of creep and shrinkage of concrete. Depending on the reinforcement ratio, $\rho$, the moduli of elasticity of FRP reinforcement and concrete, $n$, the applied load $M/M_{cr}$, and the values of creep and shrinkage (time of loading, concrete grade, environmental conditions, sectional dimensions), results of deflection predictions can be very different depending on the influencing parameters.

(a)

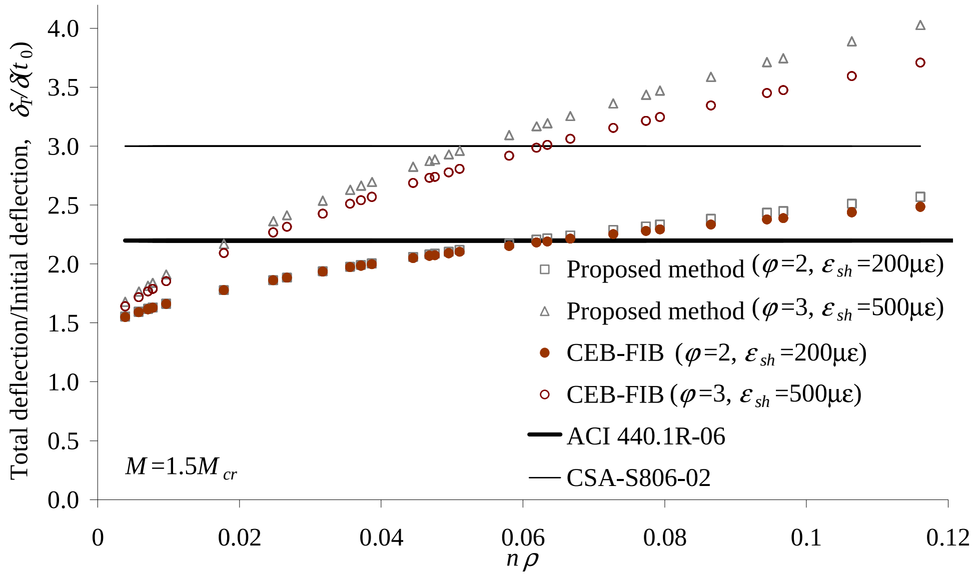

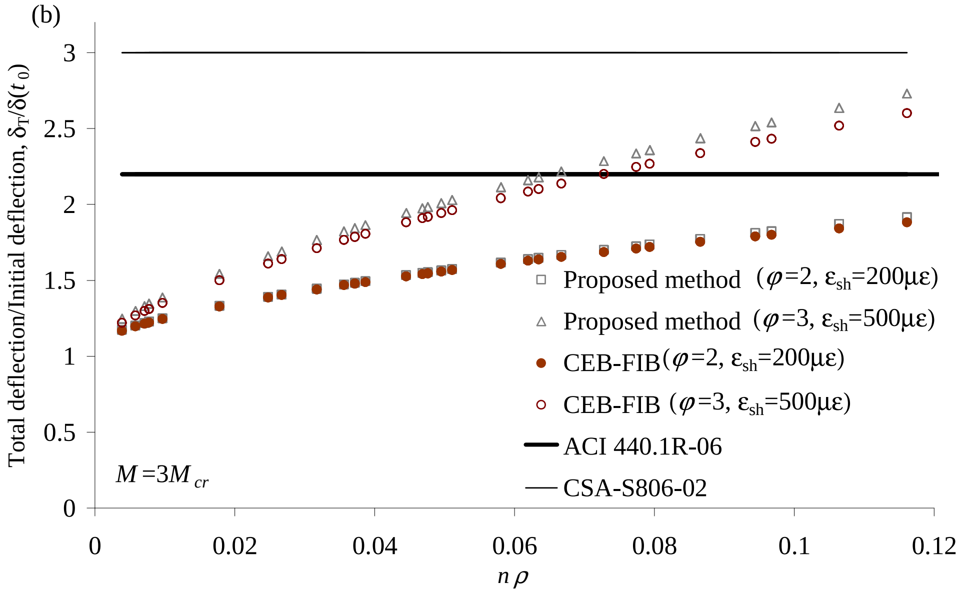

Figure 3.4. Effect of the free shrinkage strain and creep coefficient on the total-to-initial deflection prediction ratio $\dfrac{\delta_T}{\delta(t_0)}$. Applied moments: (a) M=1.5Mcr , (b) M=3Mcr.

A similar comparison is presented in Figure 3.4, where the influence of environmental conditions (affecting creep and shrinkage) is studied for applied moments equal to 1.5 $M_{cr}$ (Figure 3.4a) and 3$M_{cr}$ (Figure 3.4b). Using the CEB-FIP procedure and the proposed method, the total-to-initial deflection prediction ratio increases as the values of creep and shrinkage increase, as expected. Nevertheless, the ratio is constant when using ACI 440.1R-06 and CSA-S806-02 methods, showing substantial differences which depend on the values of the influencing parameters.

Ratios $\dfrac{\delta_T}{\delta(t_0)}$ obtained with these methods are compared in Tables 3.2 and 3.3 for $n\rho$ equal to 0.04 and 0.1. Values of creep coefficient equal to 2 and 3 have been taken, and the free shrinkage strain is 200 and 500 $\mu\varepsilon$. The applied moment is 1.5$M_{cr}$ in Table 3.2, and 3$M_{cr}$ in Table 3.3.

Total-to-initial deflection ratios are quantified for the analysed cases. Variation of $n\rho$ between the indicated values leads to changes of around 35% (1.5$M_{cr}$, Table 3.2 and 30% (3$M_{cr}$, Table 3.3) in deflection predictions for the highest values of creep and shrinkage considered. Similarly, variation of creep and shrinkage, keeping constant the value of $n\rho$, causes changes in deflection predictions of 50% (Table 3.2) and 30% (Table 3.3). For a typical case of a GFRP reinforced beam with $n\rho$=0.04, and applied moment of 3$M_{cr}$ (Table 3.3), the total-to-initial deflection ratio calculated with the proposed method and CEB-FIP vary from 1.46 to 1.74, and 1.46 to 1.80, respectively, when $\varphi$ and $\varepsilon_{sh}$ increase from 2 to 3, and 200 to 500$\mu\varepsilon$. On the contrary, the influence of these parameters is not reflected when using simplified coefficients of ACI and CSA.

Additionally, predictions from the different methods are compared through their relative values. The proposed method and CEB-FIP predictions fit quite well, with relative differences ranging from 0.92 to 1.00 for an applied moment of 1.5$M_{cr}$ (Table 3.2) and from 0.96 to 1.00 for 3$M_{cr}$ (Table 3.3). ACI and CSA procedures present considerable differences, mainly for the case of 3$M_{cr}$ (generally on the side of safety, although they depend on the values of creep and shrinkage) showing higher values for CSA, which do not incorporate a reduction factor. In general, these differences increase when $n\rho$ decreases.

| | | Proposed method | | CEB-FIP | | ACI | CSA | Relative differences | | | | | |
|---|---|---|---|---|---|---|---|---|---|---|---|---|---|
| $\varphi$ | $\varepsilon_{sh}$ ( $\mu\varepsilon$ ) | $n\rho$=0.04 (1) | $n\rho$=0.1 (2) | $n\rho$=0.04 (3) | $n\rho$=0.1 (4) | - (5) | - (6) | (3)/(1) | (4)/(2) | (5)/(1) | (5)/(2) | (6)/(1) | (6)/(2) |
| 2 | 200 | 2.00 | 2.45 | 2.00 | 2.39 | 2.20 | 3.00 | 1.00 | 0.98 | 1.10 | 0.90 | 1.50 | 1.22 |
| 2 | 500 | 2.51 | 3.47 | 2.39 | 3.18 | 2.20 | 3.00 | 0.95 | 0.92 | 0.88 | 0.63 | 1.20 | 0.86 |
| 3 | 200 | 2.20 | 2.73 | 2.17 | 2.66 | 2.20 | 3.00 | 0.99 | 0.97 | 1.00 | 0.81 | 1.36 | 1.10 |
| 3 | 500 | 2.70 | 3.74 | 2.57 | 3.48 | 2.20 | 3.00 | 0.95 | 0.93 | 0.81 | 0.59 | 1.11 | 0.80 |

Table 3.2. Comparison of the total-to-initial deflection prediction ratio, $\frac{\delta_T}{\delta(t_0)}$, for $M$=1.5$M_{cr}$. Constant parameters: $f_c$=30MPa, d/h=0.9, $\xi$ =2.

| | | Proposed method | | CEB-FIP | | ACI | CSA | Relative differences | | | | | |
|---|---|---|---|---|---|---|---|---|---|---|---|---|---|
| $\varphi$ | $\varepsilon_{sh}$ ($\mu\varepsilon$) | $n\rho$=0.04<br>(1) | $n\rho$=0.1<br>(2) | $n\rho$=0.04<br>(3) | $n\rho$=0.1<br>(4) | -<br>(5) | -<br>(6) | (3)/(1) | (4)/(2) | (5)/(1) | (5)/(2) | (6)/(1) | (6)/(2) |
| 2 | 200 | 1.46 | 1.77 | 1.46 | 1.75 | 2.20 | 3.00 | 1.00 | 0.99 | 1.51 | 1.24 | 2.05 | 1.69 |
| 2 | 500 | 1.62 | 2.16 | 1.62 | 2.09 | 2.20 | 3.00 | 1.00 | 0.97 | 1.36 | 1.02 | 1.85 | 1.39 |
| 3 | 200 | 1.62 | 2.01 | 1.58 | 1.95 | 2.20 | 3.00 | 0.98 | 0.97 | 1.36 | 1.09 | 1.85 | 1.49 |
| 3 | 500 | 1.80 | 2.39 | 1.74 | 2.30 | 2.20 | 3.00 | 0.97 | 0.96 | 1.22 | 0.92 | 1.67 | 1.26 |

Table 3.3. Comparison of the total-to-initial deflection prediction ratio, $\frac{\delta_T}{\delta(t_0)}$, for $M$=3$M_{cr}$. Constant parameters: $f_c$=30MPa, d/h=0.9, $\xi$ =2.

## 3.4 Conclusions

Simplified procedures to calculate long-tem deflections due to creep and shrinkage found in codes and guidelines for internally reinforced FRP RC structures such as ACI 440.1R-06 and CSA-S806-02 are simple and straightforward but do not account for variations in mechanical properties of materials and environmental conditions. This fact could be of major importance for FRP RC structures where mechanical reinforcement properties change when using different types of fibres. A rational alternative that maintains simplicity is proposed by using the multiplicative coefficients for creep and shrinkage deflections, $k_{creep}$ and $k_{sh}$, presented in this paper. Both coefficients have been derived from mathematical manipulation of equations based on general principles of structural mechanics.

The method has been compared to experimental results and to the well-known CEB-FIP, ACI 440.1R-06 and CSA-S806-02 procedures. It has been shown that the total-to-initial deflection prediction ratio using the proposed method and the CEB-FIP procedure, which incorporate the material properties and environmental conditions, strongly depends on the product of the modular ratio by the reinforcement ratio, and also on the values of creep and shrinkage of concrete. Higher values of $n\rho$ lead to higher values of the total-to-initial deflection prediction ratio. Similarly the ratio increases with increasing values of creep and shrinkage. This fact is not specifically reflected in the other two simplified procedures that use a multiplicative coefficient that depends only on time but is constant for all other parameters.

The presented method is simple and straightforward like those based on multiplicative coefficients, but it is able to account for the influence of environmental conditions and mechanical properties involved in the long-term deflections of FRP RC members.

## 3.5 Acknowledgements

The authors acknowledge the support provided by the Spanish Government (Ministerio de Educación y Ciencia), Project ref. BIA2007-60222. The first author thanks the Ministerio de Educación y Ciencia for Grant BES-2008-005740 and the mobility grant SEST1000I000920XV0.

## 3.6 Appendix. Generalized coefficient for long-term curvatures due to creep

According to Eurocode 2 [14], the initial curvature, $\psi(t_0)$, at a cracked section can be calculated by:

$$\psi(t_0) = \psi_1(t_0)\beta\left(\frac{M_{cr}}{M}\right)^2 + \psi_2(t_0)\left(1-\beta\left(\frac{M_{cr}}{M}\right)^2\right) \qquad \text{(A.3.1)}$$

$$\psi_1(t_0) = \frac{M}{E_c I_1}\ ,\ \psi_2(t_0) = \frac{M}{E_c I_2} \qquad \text{(A.3.2)}$$

where $\psi_1(t_0)$ and $\psi_2(t_0)$ are the curvatures for uncracked and fully-cracked transformed sections, respectively, $M$ is the applied moment at the section and $M_{cr}$ is the cracking moment. $\beta$ is the coefficient representing the influence of the duration of the loading and is equal to 1 for first loading and equal to 0.5 for sustained or cycling loading. $E_c$ is the modulus of elasticity of concrete at time $t_0$, and $I_1$ and $I_2$ are the moment of inertia for uncracked and fully-cracked transformed sections at time $t_0$, respectively.

For sustained loads, the curvature including creep, $\psi(t,t_0)$, at a cracked section can be calculated by:

$$\psi(t,t_0) = \psi_1(t,t_0)0.5\left(\frac{M_{cr}}{M}\right)^2 + \psi_2(t,t_0)\left(1-0.5\left(\frac{M_{cr}}{M}\right)^2\right) \qquad \text{(A.3.3)}$$

The curvatures including creep for uncracked $\psi_1(t,t_0)$ and fully-cracked transformed sections $\psi_2(t,t_0)$ read:

$$\psi_1(t,t_0)=\frac{M}{E_c(t,t_0)I_1(t,t_0)}\ ,\ \psi_2(t,t_0)=\frac{M}{E_c(t,t_0)I_2(t,t_0)} \tag{A.3.4}$$

$I_1(t,t_0)$ and $I_2(t,t_0)$ are the moments of inertia of the effective uncracked and a fully-cracked transformed sections, respectively, calculated using the effective modulus of elasticity of concrete, $E_c(t,t_0)$, which is obtained as:

$$E_c(t,t_0)=\frac{E_c}{1+\varphi(t,t_0)} \tag{A.3.5}$$

where $E_c$ is the elastic modulus of concrete at the time $t_0$, and $\varphi(t,t_0)$ is the creep coefficient.

For an uncracked section, an approximation of the curvature including creep at time *t*, can be obtained from the direct product of the creep coefficient and the initial curvature:

$$\psi_1(t,t_0)\approx\left(1+\varphi(t,t_0)\right)\psi_1(t_0) \tag{A.3.6}$$

For an uncracked rectangular section, the initial curvature can be approximated by:

$$\psi_1(t_0)\approx\frac{12M}{E_c bh^3} \tag{A.3.7}$$

where *b* is the section width and *h* is the height.

The sectional stiffness of a fully-cracked transformed section reads:

$$E_c(t,t_0)I_2(t,t_0)=E_f A_f\left(d-x(t,t_0)\right)\left(d-\frac{x(t,t_0)}{3}\right) \tag{A.3.8}$$

where $A_f$ is the area of tensile reinforcement, $d$ is the effective depth, $x(t, t_0)$ is the neutral axis depth of the effective transformed section, and $E_f$ is the modulus of elasticity of FRP reinforcement. Therefore, curvature including creep for a fully-cracked transformed section, $\psi_2(t,t_0)$, is:

$$\psi_2(t,t_0) = \frac{M}{E_f A_f \left(d - x(t,t_0)\right)\left(d - \frac{x(t,t_0)}{3}\right)} \tag{A.3.9}$$

In the absence of compressive reinforcement, the neutral axis depth for an effective fully-cracked transformed section at time $t$, can be written as:

$$x(t,t_0) = dn\rho\left(1+\varphi(t,t_0)\right)\left(-1+\sqrt{1+\frac{2}{n\rho\left(1+\varphi(t,t_0)\right)}}\right) \tag{A.3.10}$$

Assuming $d/h$=0.9, from Eq. (A.3.1) to Eq. (A.3.10), the ratio between curvature including creep and initial curvature, $\frac{\psi(t,t_0)}{\psi(t_0)}$, can be obtained from the following expression:

$$\frac{\psi(t,t_0)}{\psi(t_0)} = \frac{\left(\frac{0.5\left(\frac{M_{cr}}{M}\right)^2\left(1+\varphi\right)}{0.11d^3} + \frac{1-0.5\left(\frac{M_{cr}}{M}\right)^2}{dn\rho\left(d - dn\rho\left(1+\varphi\right)\left(-1+\sqrt{1+\frac{2}{n\rho\left(1+\varphi\right)}}\right)\right)\left(d - \frac{1}{3}dn\rho\left(1+\varphi\right)\left(-1+\sqrt{1+\frac{2}{n\rho\left(1+\varphi\right)}}\right)\right)}\right)}{\frac{\left(\frac{M_{cr}}{M}\right)^2}{0.11d^3} + \frac{1-\left(\frac{M_{cr}}{M}\right)^2}{dn\rho\left(d - dn\rho\left(-1+\sqrt{1+\frac{2}{n\rho}}\right)\right)\left(d - \frac{1}{3}dn\rho\left(-1+\sqrt{1+\frac{2}{n\rho}}\right)\right)}} \tag{A.3.11}$$

where $\varphi = \varphi(t, t_0)$ is the creep coefficient.

Assuming that the typical values for $n\rho$ can range from 0 to 0.12 and those for $\varphi$ from 1 to 3, the curvature ratio $\frac{\psi(t,t_0)}{\psi(t_0)}$ can be simplified using the Taylor series development of Eq. (A.3.11) about point ($n\rho$, $\varphi$) = (0, 2) as :

$$\frac{\psi(t,t_0)}{\psi(t_0)} \approx X\left(1 + 0.73\varphi\sqrt{n\rho}\right) \tag{A.3.12}$$

where, $0.73\varphi\sqrt{n\rho}$ is equal to $k_{creep}$, as it was defined in [25]. The parameter $X$ depends on the ratio $M/M_{cr}$, and its values for different applied moments are summarized in Table A.3.1.

| $M/M_{cr}$ | 1.5 | 2 | 3 | 5 |
|---|---|---|---|---|
| $X$ | 1.37 | 1.15 | 1.04 | 1.01 |

Table A.3.1. Values of $X$ for different $M/M_{cr}$.

It is noteworthy that the curvature ratio $\frac{\psi(t,t_0)}{\psi(t_0)}$ can be obtained from the proposed coefficient presented in [25] for a fully-cracked transformed section, $k_{creep}$, multiplied by the $X$ term that accounts for the tension-stiffening effect and the time-dependent loss of flexural stiffness.

Since $\varphi$ equals 0 when $t=t_0$, the curvature ratio in Eq. (A.3.12) equals $X$ at $t_0$. According to this assumption, and substituting $\varphi=0$ in Eq. (A.3.11) the parameter $X$ reads:

$$X=\frac{\psi_1(t_0)0.5\left(\frac{M_{cr}}{M}\right)^2+\psi_2(t_0)\left(1-0.5\left(\frac{M_{cr}}{M}\right)^2\right)}{\psi_1(t_0)\left(\frac{M_{cr}}{M}\right)^2+\psi_2(t_0)\left(1-\left(\frac{M_{cr}}{M}\right)^2\right)}=\frac{\psi(t_0)_{\beta=0.5}}{\psi(t_0)_{\beta=1}} \tag{A.3.13}$$

Therefore, using Eq. (A.3.12) in Eq. (A.3.13), the curvature including creep can be obtained from the following expression:

$$\psi(t,t_0)=\left(1+0.73\varphi\sqrt{n\rho}\right)\psi(t_0)_{\beta=0.5} \tag{A.3.14}$$

## 3.7 References

1.Masmoudi R., Thériault M., Benmokrane B. Flexural behavior of concrete beams reinforced with deformed fiber reinforced plastic reinforcing rods. ACI Structural Journal 1998;95(6):665-76.

2. Pecce M., Manfredi G., Cosenza E. Experimental response and code models of GFRP RC beams in bending. Journal of Composites for Construction 2000;4(4):182-90.

3. Yost JR, Gross SP, Dinehart D.W. Effective moment of inertia for GFRP reinforced concrete beams. ACI Structural Journal 2003;100(6):732-39.

4. Bischoff P.H. Reevaluation of Deflection Prediction for Concrete Beams Reinforced with Steel and Fiber Reinforced Polymer Bars. Journal of Structural Engineering, ASCE 2005;131(5):752-67.

5.. Gravina R.J, Smith S.T. Flexural behaviour of indeterminate concrete beams reinforced with FRP bars. Engineering Structures 2008;30(9):2370-80.

6. Issa M.S., Metwally I.M., Elzeiny S.M.. Influence of fibers on flexural behavior and ductility of concrete beams reinforced with GFRP rebars. Engineering Structures 2011;33(5):1754-1763.

7. Barris C., Torres Ll., Turon A., Baena M., Catalan A. An experimental study of the flexural behaviour of GFRP RC beams and comparison with prediction models. Composite Structures 2009;91(3):286-295.

8. American Concrete Institute Committee 318 ACI. Building code requirements for structural concrete and commentary (ACI 318-08). American Concrete Institute, Farmington Hills, Michigan, USA; 2008.

9. CSA Standard A23.3-04. Design of concrete structures. Canadian Standards Association, Mississauga, Ontario, Canada; 2004.

10. Branson D.E. Compression steel effect on long-time deflections. ACI Journal Proceedings 1971;68(8):555-59.

11. CEB- FIP 1990. Model code for concrete structures. Comité Euro-International du Béton. Féderation Internationale de la Précontrainte, Thomas Telford House, London, England; 1990.

12. Comité Euro-International du Béton (CEB). Manual on Cracking and Deformations.Bulletin d'Information 158-E; 1985.

13. Ghali A., Favre R., Elbadry M.. Concrete Structures: Stresses and Deformations. Third Edition. New York: Spon Press; 2002.

14. CEN 2004. Eurocode 2: Design of Concrete Structures. Part 1.1: General rules and rules for buildings (EN 1992-1-1:2004).Comité Européen de Normalisation, Brussels; 2004.

15. Brown V., Bartholomew C. Long-term deflections of GFRP-reinforced concrete beams. In: Firts International Conference on Composites in Infra-Structure. Tucson, Arizona, USA, 1996. p. 389-00.

16. Brown V., Sustained load deflections in GFRP-reinforced concrete beams. In: 3rd International RILEM Symposium on Non-Metallic (FRP) Reinforcement for Concrete Structures (FRPRCS-3). Sapporo, Japan, 1997. p. 495-02.

17. American Concrete Institute Committee 440 ACI. Guide for the design and construction of structural concrete reinforced with FRP bars (ACI 440.1R-06) American Concrete Institute, Farmington Hills, Michigan, USA; 2006.

18. CSA Standard CAN/CSA-S806-02. Design and construction of building components with fibre-reinforced polymers. Canadian Standards Association, Mississauga, Ontario, Canada; 2002.

19. Hall T., Ghali A. Long-term deflection prediction of concrete members reinforced with glass fibre reinforced polymer bars. Canadian Journal of Civil Engineering 2000;27(5):890-98.

20. Gross S.P., Yost Y.R., Crawford J.V.. Serviceability of high strength concrete beams with internal FRP reinforcement under sustained load. In: 3rd International Conference on FRP Composites in Civil Engineering (CICE 2006). Miami, Florida, USA; 2006.

21. Yousseff T., Benmokrane B., El-Salakawy E.  Deflection and strain variation of GFRP-reinforced concrete beams after one year of continuous loading.Proceedings of the 9th International Symposium on Fiber-Reinforced Polymer Reinforcement for Concrete Structures (FRPRCS-9), Sydney, Australia; 2009.

22. Arockiasamy M., Chidambaram S., Amer A., Shahawy M.. Time-dependent deformations of concrete beams reinforced with CFRP bars. Composites Part B: Engineering, 2000;31(6-7):577-92.

23. Laoubi K., El-Salakawy E., Benmokrane B.. Creep and durability of sand-coated glass FRP bars in concrete elements under freeze/thaw cycling and sustained loads. Cement and Concrete Composites, 2006;28(10):869-878.

24. Bazant Z.P.. Prediciton of concrete creep effects using Age-Adjusted Efective Modulus Method. American Concrete Institute Journal 1972; 69:212–17

25. Miàs C., Torres Ll., Turon A., Baena M., Barris C. A simplified method to obtain time-dependent curvatures and deflections of concrete members reinforced with FRP bars. Composite Structures 2010;92(8):1833-38.

26. Gilbert R.I. Time Effects in Concrete Structures. Amsterdam: Elsevier, 1988.

27. Cosenza E., P.G. Debernardi. Calculation of stresses, deformation and deflections of reinforced and prestressed concrte elements in service. Bulletin CEB 235, 1997; p. 105-41.

28. Gilbert R.I.. Shrinkage, Cracking and Deflection- The Serviceability of Concrete Structures. Structural Enginnering 2001;1(1):2-14.

29. ACI Committee 435. Control of deflections in concrete structures(ACI 435R-95). American Concrete Institute, Detroit, Michigan, USA; 1995.

30. Scanlon A., Bischoff P.H.. Shrinkage restraint and loading history effects on deflections of flexural members. ACI Structural Journal 2008;105(4):498-06.

# 4. Experimental study of immediate and time-dependent deflections of GFRP reinforced concrete beams

# Experimental study of immediate and time-dependent deflections of GFRP reinforced concrete beams

C. Miàs, Ll. Torres, A. Turon, C. Barris. Experimental study of immediate and time-dependent deflections of GFRP reinforced concrete beams. Composite Structures, 2012 (in Press, Accepted Manuscript).

**doi:** 10.1016/j.compstruct. 2012.08.052

## Summary

*Due to the mechanical properties of fibre reinforced polymer (FRP) bars, deflections often drive the design of FRP reinforced concrete (RC) flexural members. This has led to an increasing number of studies focused on the analysis of short-term deflections of FRP RC beams. However, investigations and experimental data focused on long-term deflections are scarce. The time-dependent deflection in RC beams is a function of member geometry, material properties and loading characteristics. Maximum service loads, as well as repeated loading, affect the deflections under sustained loads. This paper presents the results and discussion of an experimental programme concerning eight glass FRP RC beams tested at service load, and subsequently subjected to sustained loading for 250 days. Two reinforcement ratios and two levels of sustained load were considered. The experimental results revealed an effect of the loading-unloading processes and the reinforcement ratio on short and time-dependent deflections. No significant influence of the sustained load level was observed. Moreover, the theoretical predictions obtained with different models have been compared with the experimental results. The modified time-dependent factor presented in ACI 440.1R-06, together with the modified Bischoff's equation to compute the immediate deflections due to sustained load, gives the best agreement with experimental deflections.*

## 4.1 Introduction

Fibre reinforced polymer (FRP) bars have been proved to be an alternative to conventional internal reinforcement for reinforced concrete (RC) structures in corrosive environments or when effects of electromagnetic fields may be present. Although FRP bars have higher strength than conventional steel reinforcement their modulus of elasticity is lower. Consequently, for the same conditions of geometry, concrete and area of reinforcement, FRP RC flexural members are expected to undergo larger deformations than steel RC members. This has led to an increasing numbers of studies focused on the analysis of short-term deflections of FRP RC beams [1-10]. The lower the stiffness of the reinforcement, the lower is the neutral axis depth in cracked sections, resulting in a smaller concrete area in compression. As a result, the relative deformation increment associated with creep and shrinkage, and therefore the time-dependent deflection, is expected to be lower than for conventional steel RC members. The long-term increase in deflection is a function of member geometry, load characteristics (magnitude and duration of sustained load, and age of concrete at the time of loading), and material properties (elastic modulus of concrete and FRP reinforcement, creep and shrinkage of concrete) [11]. Therefore, properties of the FRP rebars have a significant influence on the long-term deflections of FRP RC beams [12]. Up to now, few published studies have examined the time-dependent deflection of FRP RC beams [12-20]. The reported results have generally concluded that total mid-span deflection versus time since loading of FRP and steel RC beams follow a similar trend. Likewise, the deflection increase, as a multiplier of the initial deflection, is significantly lower for FRP RC members than that observed for steel.

To compute long-term deflections, ACI 440.1R-06 [11] adopts the same methodology as for steel RC structures of ACI 318R-08 [21], but reducing the multiplying factor with the application of an empirical reduction coefficient of 0.6, based on experimental results for glass FRP (GFRP) RC beams carried out by Brown [13] and Brown and Bartholomew [14]. On the other hand, CSA-S806-02 [22] proposes a more conservative approach, adopting the same coefficients as for steel RC. Recent studies [18-20] show that current ACI 440.1R-06 and CSA-S806-02 predictions are conservative in the estimation of the deflection increase over time in GFRP and CFRP RC beams.

The aim of this paper is to present results of an experimental study of GFRP RC beams tested at service load, and subsequently subjected to sustained loading for 250 days. Two different amounts of GFRP reinforcement and two levels of sustained load were used to analyse the influence of these parameters on the increase of deflection due to creep and shrinkage. Both short-term and long-term deflections are presented and discussed. Experimental results are compared to predictions from guidelines for FRP RC structures, as ACI 440.1R-06 and CSA S806-02.

## 4.2 Test specimens and materials

### *4.2.1 Beams specifications*

A total of 8 RC beams were tested in flexure. All beams were 140mm in width and 190mm in depth. The length of the beams was 2450mm, with a span of 2200mm (Figure 4.1). The tensile reinforcement consisted of two GFRP bars of 12mm or 16mm diameter, giving two different reinforcement ratios. The shear-span was reinforced with steel stirrups (Ø8mm/80mm), and no stirrups were provided in the pure bending zone. The clear cover was 20mm.

The beams were designed as N_L*x*-G*yyz*, where L*x* denotes the level of sustained load (L1 and L2); *yy* the diameter of the GFRP bar (12mm or 16mm) and *z* the differences between twin beams. The identification and the geometric properties of the tested beams are summarized in Table 4.1.

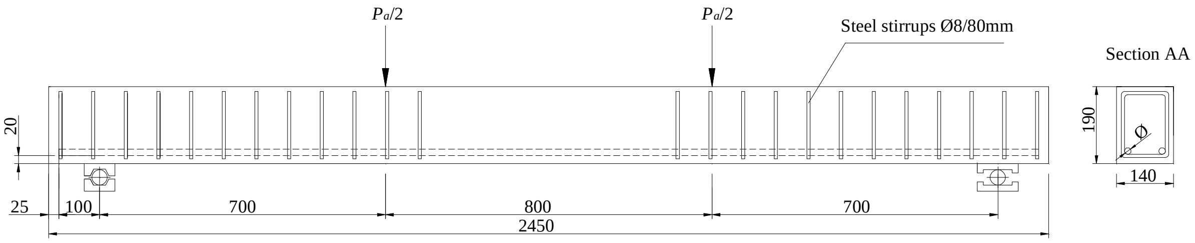
$P_a/2$
$P_a/2$
Steel stirrups Ø8/80mm
Section AA
20
190
Ø
140
25
100
700
800
700
2450

Figure 4.1. Geometric details of the tested beams.

| Identification beam | | Ø bar (mm) | $\rho$ (%) |
|---|---|---|---|
| Beams<br>**N_G12** | N_L1_G12a | 12 | 1.0 |
| | N_L1_G12b | 12 | 1.0 |
| | N_L2_G12a | 12 | 1.0 |
| | N_L2_G12b | 12 | 1.0 |
| Beams<br>**N_G16** | N_L1_G16a | 16 | 1.8 |
| | N_L1_G16b | 16 | 1.8 |
| | N_L2_G16a | 16 | 1.8 |
| | N_L2_G16b | 16 | 1.8 |

Table 4.1. Geometric properties of beams.

### *4.2.2 Material properties*

The concrete mix was designed for a target compressive strength of 30MPa with the following composition: 185 kg/m$^3$ of water, 880 kg/m$^3$ of fine aggregate, 875 kg/m$^3$ of coarse aggregate (maximum size: 12mm), 320 kg/m$^3$ of ordinary Portland cement and a 0.58 water/cement ratio. The experimental compressive strength, $f_c$, was 27.7MPa and the modulus of elasticity, $E_c$, was 25.7GPa. Both were determined from cylinder tests according to UNE 83.304-84 and ASTM C 469-10 standards respectively.

The GFRP bars used in these experiments were type E-CR GFRP ComBAR with a nominal modulus of elasticity of 60GPa. Nominal diameters of 12mm and 16mm were used.

The mean values of mechanical properties obtained from uniaxial tension tests, according ACI 440 3R-04 [23] are shown in Table 4.2.

| Diameter Ø (mm) | Modulus of elasticity $E_f$ (GPa) | Tensile strength $f_{fu}$ (MPa) |
|---|---|---|
| 12 | 64.5 | 1424 |
| 16 | 63.4 | 1327 |

Table 4.2. Mechanical properties of GFRP rebars.

### *4.2.3 Test set-up*

The simply supported beams, spanning 2200mm, were subjected to two concentrated loads at 700mm from the beam supports, as shown in (Figure 4.1).

The experimental program consisted of two phases. Firstly, the beams were tested in the instantaneous loading set-up shown in Figure 4.2a. A servo-controlled hydraulic jack with a capacity of 300kN was used together with a steel spreader beam to transmit the load to two rollers 800mm apart. The load was applied in displacement control mode at a displacement rate of 0.7mm/min until a maximum value, *P*, representative of service conditions, and then cycled twice between the maximum load and a minimum of 2kN. The maximum load, $P$, was calculated assuming a maximum bar strain equal to 2000με, which is in accordance with [24,25]. $P$ was equal to 14kN for the beams reinforced with 2Ø12 GFRP bars, and to 16kN for the beams reinforced with 2Ø16. Secondly, immediately after the short-term test, the beams were moved to load frames designed for the sustained loading, and loaded for a period of 250 days (Figure 4.2b). The sustained load, $P_{sus}$, was selected to obtain instantaneous concrete compressive stresses of $0.3f_c$ and $0.45f_c$ at the top fibre of the mid-span section. The magnitudes of the applied sustained loads are given in Table 4.3. For beam identification, $L1$ corresponds to beams tested with a load applied to obtain a compressive stress equal to $0.3f_c$, while $L2$ is used for a compressive stress equal to $0.45f_c$. It is worth mentioning that the maximum load $P$ is higher than the sustained $P_{sus}$, which would be the common situation in a real structure.

Three transducers were used to measure the deflection of the tested beams, one at mid-span, and the other two at 400mm from mid-span. These two transducers were replaced by dial gauges in long-term measurements.

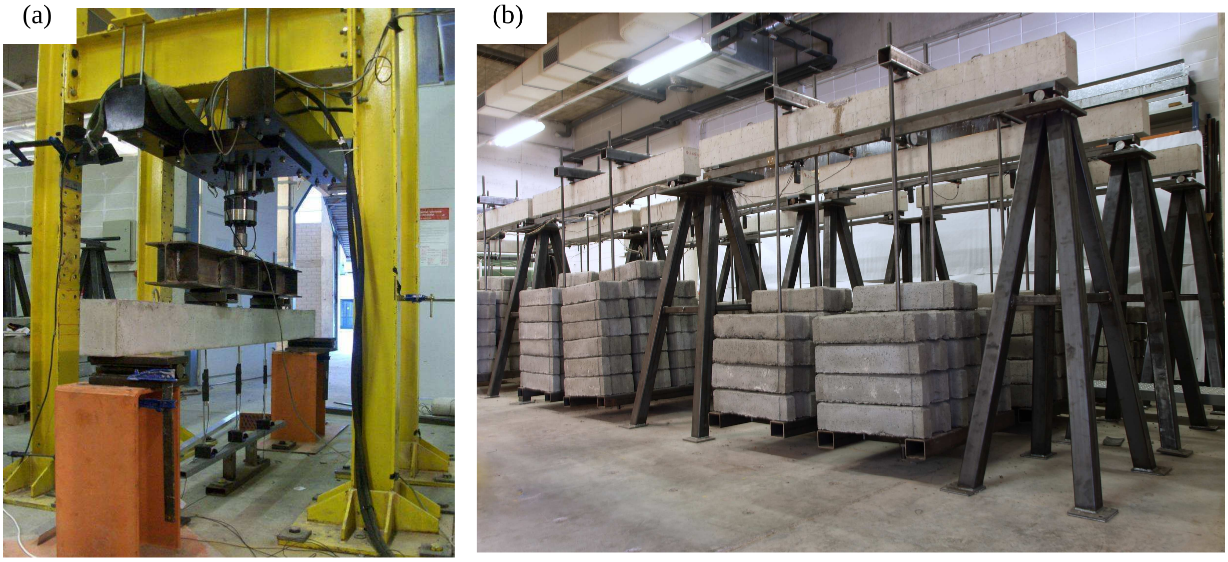

Figure 4.2. Experimental set-up (a) instantaneous loading tests (b) sustained loading test.

| N_L1_G12 | N_L2_G12 | N_L1_G16 | N_L2_G16 |
|---|---|---|---|
| 9 kN | 11 kN | 10 kN | 14 kN |

Table 4.3. Applied sustained load, $P_{sus}$.

The temperature and humidity of the lab were registered during the long-term tests, with the mean relative values equal to 22ºC and 55% respectively.

## 4.3 Test results and discussion

### *4.3.1 Short-term deflections*

The load-deflection curves obtained in the short-term test for the concrete beams reinforced with 2Ø12 GFRP and 2Ø16 GFRP bars are presented in Figure 4.3 and Figure 4.4, respectively. In all cases, an initial linear branch is observed, which corresponds to the stiffness of the uncracked beam. With further loading, progressive cracking occurred when the applied moment exceeded the cracking moment, causing a stiffness reduction. Therefore, the slope reduces progressively up to the maximum applied load, *P*. Then the beam was subjected to two cycles of unloading-reloading. During the two cycles the slope reduces significantly with respect to that of the initial elastic branch. Moreover, a permanent deformation is observed after the unloading takes place. This leads to higher mid-span deflections than those obtained in the monotonic branch, provided that the applied load is equal or lower than the applied maximum load, *P*.

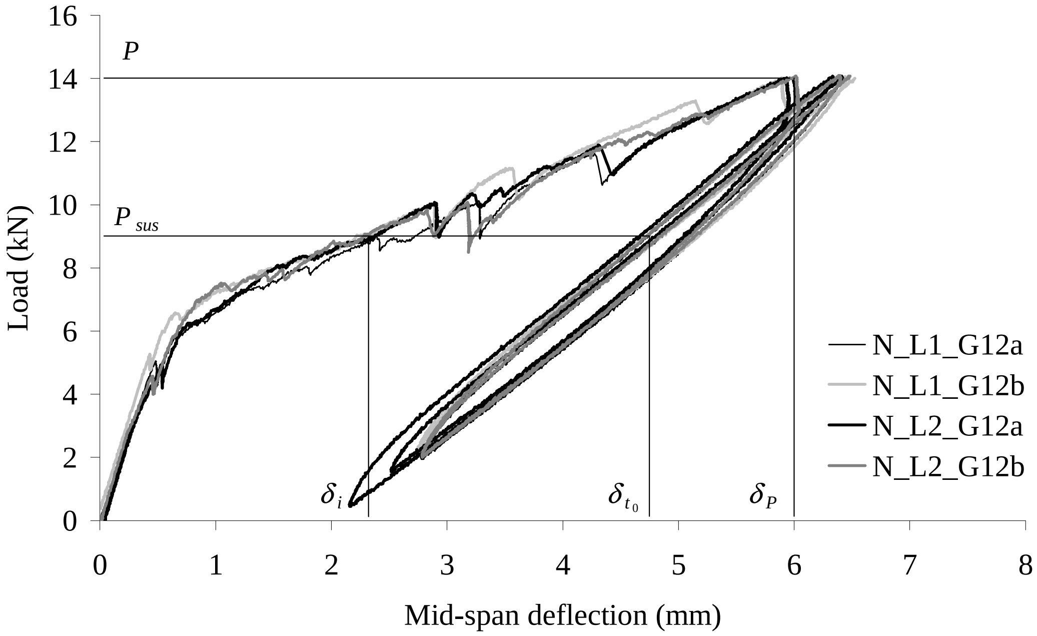

Figure 4.3. Load mid-span deflection curves for beams N_G12.

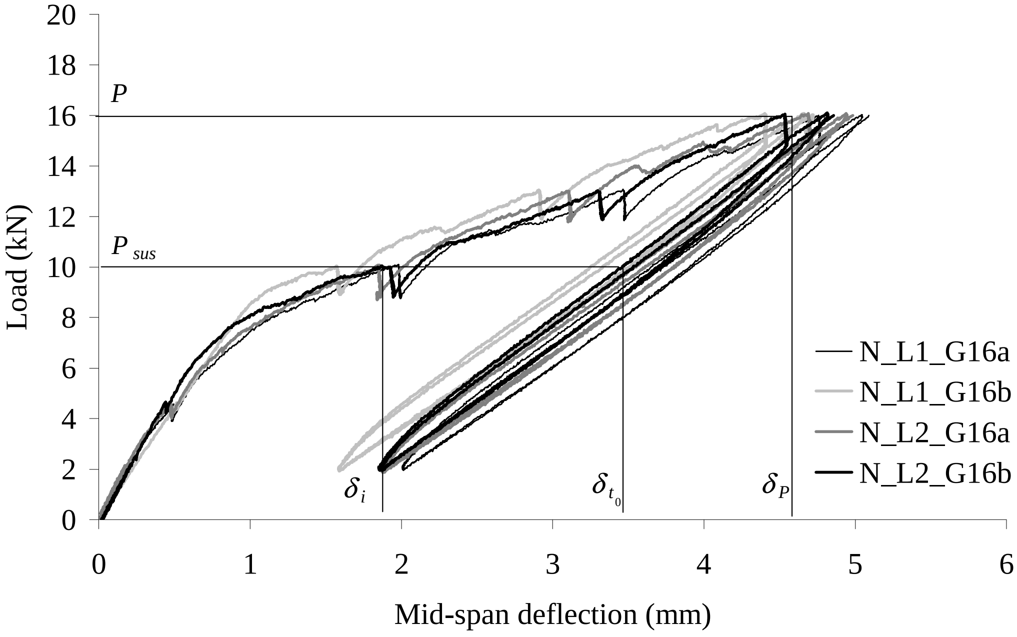

Figure 4.4. Load mid-span deflection curves for beams N_G16.

The different situations of loads and deflections corresponding to the applied maximum and sustained loads are indicated in Figures 4.3 and 4.4. Following the initial monotonic loading curve, $\delta_i$ corresponds to the experimental instantaneous deflections at $P_{sus}$, and $\delta_p$ corresponds to the experimental deflection at maximum load, $P$. The immediate deflection after cycling when $P_{sus}$ is subsequently applied is designated as $\delta_{t_0}$. For the sake of clarity in Figures 4.3 and 4.4, both deflections at $P_{sus}$ are only illustrated for an applied load corresponding to the level of load $L1$.

Deflection at maximum load, $P$

On average, the experimental deflections, $\delta_p$, at load $P$ are equal to 6.0 and 4.6, for beams N_G12 and N_G16 respectively. As observed in Figures 4.3 and 4.4, and as expected, beams with a lower reinforcement ratio present higher deflections due to lower stiffness. Therefore, although the applied maximum load is higher for beams reinforced with 2Ø16, the corresponding deflection is lower than the deflection on concrete beams reinforced with 2Ø12.

Deflection at  sustained load, $P_{sus}$

Experimental deflections corresponding to load $P_{sus}$ for every pair of twin beams are given in Table 4.4.

As can be observed, the experimental deflections after cycling, $\delta_{t_0,\exp}$, are higher than the initial instantaneous deflection for the same load, $\delta_{i,exp}$. This difference is more significant when the load is closer to the cracking one, $P_{cr}$. So, for level L1 of beams N_G12 ($P_{sus}/P_{cr}$ = 1.3) and N_G16 ($P_{sus}/P_{cr}$=1.4) the relationship between both deflections, $\delta_{t_0,\exp} / \delta_{i,\exp}$, is equal to 2.0 and 1.8 respectively. For level L2 of beams N_G12 ($P_{sus}/P_{cr}$ =1.6) and N_G16 ($P_{sus}/P_{cr}$ =1.8), the ratio $\delta_{t_0,\exp} / \delta_{i,\exp}$ is equal to 1.4 and 1.2 respectively.

| | N_L1_G12 | N_L2_G12 | N_L1_G16 | N_L2_G16 |
|---|---|---|---|---|
| Load, $P_{sus}$ (kN) | 9 | 11 | 10 | 14 |
| Instantaneous deflection, $\delta_{i,\,exp}$ (mm) | 2.3 | 3.9 | 1.9 | 3.7 |
| Immediate deflection after cycling, $\delta_{t_0,\exp}$ (mm) | 4.8 | 5.5 | 3.4 | 4.4 |
| $\delta_{t_0,\exp}$ / $\delta_{i,\,exp}$ | 2.0 | 1.4 | 1.8 | 1.2 |

Table 4.4. Experimental deflections at load $P_{sus}$.

### 4.3.2 Short-term deflection prediction

The short-term deflection of a simply supported beam subjected to four-point bending moment with two applied loads, $P_a/2$ , at a distance $a$ from the supports, can be obtained as:

$$\delta = \frac{P_a/2\; a}{24E_cI_e}\left(3L^2 - 4a^2\right) \tag{1}$$

where $I_e$ is the effective moment of inertia. To compute $I_e$ ACI 440.1R-06 [11] recommends applying a reduction factor, $\beta_d$ , to the moment of inertia obtained using Branson's equation for steel RC members:

$$I_{e,ACI\,440} = \left(\frac{M_{cr}}{M}\right)^3 \beta_d I_g + \left[1 + \left(\frac{M_{cr}}{M}\right)^3\right] I_{cr} \le I_g \tag{2}$$

where $M_{cr}$ is the cracking moment, $M$ is the applied moment, $I_g$ is the gross moment of inertia, $I_{cr}$ is the moment of inertia of the transformed cracked section and $\beta_d$ can be obtained as:

$$\beta_d = \frac{1}{5}\left(\frac{\rho_f}{\rho_{fb}}\right) \tag{3}$$

where $\rho_f$ is the reinforcement ratio and $\rho_{fb}$ is the balanced reinforcement ratio.

On the other hand, CSA S806-02 [22] proposes that the moment-curvature relation of FRP reinforced concrete members shall be assumed to be trilinear with the slope of the three segments being $E_cI_g$ , zero and $E_cI_{cr}$ (i.e. no tension-stiffening is considered). For the particular case of four-point bending, the instantaneous deflection can be calculated using the following equation:

$$\delta_{CSA} = \frac{{P_a}/{2}\, L^3}{24E_cI_{cr}}\left[3\left(\frac{a}{L}\right)-4\left(\frac{a}{L}\right)^3-8\left(1-\frac{I_{cr}}{I_g}\right)\left(\frac{L_g}{L}\right)^3\right] \tag{4}$$

where $L_g$ is the length of that part of the beam still uncracked.

An alternative formulation for the effective moment of inertia can be obtained from the expression proposed by Bischoff [5]:

$$I_{e,Bischoff} = \frac{I_{cr}}{1-\left(1-\frac{I_{cr}}{I_g}\right)\left(\frac{M_{cr}}{M}\right)^2} \tag{5}$$

This equation accounts for the tension-stiffening effect and has been shown to be applicable to FRP RC members [26].

In Table 4.5, the average values of experimental deflections, $\delta_{P,exp}$, corresponding to the maximum load, *P*, for N_G12 and N_G16 beams, are compared with ACI 440.1R-06 and CSA S806-02 recommendations together with Bischoff's equation.

| Experimental data | | | ACI 440.1R-06 | | CSA S806-02 | | Bischoff (Eq. 5) | |
|---|---|---|---|---|---|---|---|---|
| Beams | $P$ (kN) | $\delta_{P,exp}$ (mm) | $\delta_P$ (mm) | *exp/calc* | $\delta_P$ (mm) | *exp/calc* | $\delta_P$ (mm) | *exp/calc* |
| N_G12 | 14 | 6.0 | 4.7 | 1.28 | 8.5 | 0.71 | 6.7 | 0.90 |
| N_G16 | 16 | 4.6 | 4.8 | 0.96 | 6.2 | 0.74 | 5.3 | 0.87 |

Table 4.5. Comparison of deflections corresponding to load $P$.

As can be observed, for beams reinforced with 2Ø12 GFRP bars, the ratio between the experimental deflection at maximum load, $\delta_P$, and the ACI 440.1R-06 prediction is 1.28. Approximately the same value is found in [6], where a statistical analysis of predicted deflections at service conditions (considering a bar strain equal to 2000με), with a sample size of 67 GFRP RC beams was presented. However, for beams reinforced with 2Ø16 GFRP bars, the ratio between the experimental values and ACI predictions is 0.96. The ratio between the experimental deflections at maximum load, $\delta_P$, and the predictions using CSA and Bischoff approaches is equal to 0.7 and 0.9 respectively. In the above mentioned study [6], the mean ratio between the experimental deflection and CSA predictions for beams reinforced with GFRP was found to be 0.6, which indicates that CSA tends to overestimate the deflections at service loads.

From the previous results it can be observed that CSA overestimates deflections since their formulation does not take into account tension-stiffening, tending to be conservative; Bischoff approach gives reasonable predictions for all cases; and ACI 440 does not predict deflections with the same precision for the range of reinforcement ratios and loads used, with a tendency of better predictions for higher reinforcement ratios. Discussion about the empirical derivation of Branson’s equation for steel RC members, and subsequent empirically derived coefficients to improve precision of ACI 440 equation for low reinforcement stiffness can be found elsewhere [5].

The aforementioned methods have also been used to predict the instantaneous deflection, $\delta_i$, corresponding to the load $P_{sus}$ in the initial monotonic curve (Table 4.6). As can be observed, the ACI 440.1R-06 equation (Eq. 2) underestimates the instantaneous deflections of the tested beams, mainly in the case of N_G12 beams, where the ratio between the experimental and the predicted instantaneous deflection is equal to 1.74 for level L1, and 1.58 for level L2. For N_G16 beams this ratio is 1.12 and 1.07, for levels L1 and L2 respectively. On the other hand, the CSA equation (Eq. 4) overpredicts the instantaneous deflections in all beams. The overestimation is more significant in beams with an applied load corresponding to level L1, where the applied load is closer to the cracking moment, independently of the reinforcement ratio. On average, the ratio between the experimental and the CSA predicted instantaneous deflection ranges between 0.48 and 0.71. Bischoff's equation (Eq. 5) gives the best prediction for all beams, with an average ratio between the experimental and the predicted instantaneous deflection ranging between 0.84 and 0.96.

| Experimental data | | ACI 440.1R-06 | | CSA S806-02 | | Bischoff (Eq. 5) | |
|---|---|---|---|---|---|---|---|
| Beams | $\delta_{i,exp}$ (mm) | $\delta_{i,ACI}$ (mm) | $^{exp}/_{calc}$ | $\delta_{i,CSA}$ (mm) | $^{exp}/_{calc}$ | $\delta_{i,B..}$ (mm) | $^{exp}/_{calc}$ |
| N_L1_G12 | 2.3 | 1.3 | 1.74 | 4.8 | 0.48 | 2.4 | 0.96 |
| N_L2_G12 | 3.9 | 2.5 | 1.58 | 6.3 | 0.61 | 4.2 | 0.93 |
| N_L1_G16 | 1.9 | 1.7 | 1.12 | 3.6 | 0.52 | 2.3 | 0.84 |
| N_L2_G16 | 3.7 | 3.5 | 1.07 | 5.2 | 0.71 | 4.2 | 0.88 |

Table 4.6. Instantaneous deflections corresponding to load $P_{sus}$

In Table 4.7, the experimental immediate deflections after cycling, $\delta_{t_0,\exp}$, are compared with the corresponding predictions. The beams presented a cracking state (and a corresponding stiffness) according to the maximum attained load ($P$) before the application of the sustained load ($P_{sus}$). This fact has been taken into account in the calculation of the equivalent moment of inertia using the maximum applied moment in Eq. 2, for ACI predictions. Likewise, in Eq. 4 for CSA predictions, the parameter $L_g$ is considered to be constant and equal to the corresponding value at the maximum applied load.

Moreover, based on [27], predictions of immediate deflections after cycling, $\delta_{t_0}$, can be computed modifying the effective moment of inertia by including a $\beta$ coefficient with the value of 0.5 in Eq. 5:

$$I_e = \frac{I_{cr}}{1-\beta\left(1-\frac{I_{cr}}{I_g}\right)\left(\frac{M_{cr}}{M}\right)^2} \tag{6}$$

This $\beta$ factor accounts for the loss of stiffness that occurs from cracking under repeated loading or due to sustained loads.

| Experimental data | | ACI 440.1R-06 | | CSA S806-02 | | Bischoff (Eq. 6) | |
|---|---|---|---|---|---|---|---|
| Beams | $\delta_{t_0,\exp}$ (mm) | $\delta_{t_0,ACI}$ (mm) | *exp/calc* | $\delta_{t_0,CSA}$ (mm) | *exp/calc* | $\delta_{t_0,B.}$ (mm) | *exp/calc* |
| N_L1_G12 | 4.8 | 3.0 | 1.60 | 5.43 | 0.88 | 5.1 | 0.95 |
| N_L2_G12 | 5.5 | 3.7 | 1.49 | 6.64 | 0.83 | 6.2 | 0.89 |
| N_L1_G16 | 3.4 | 3.0 | 1.13 | 3.90 | 0.87 | 3.6 | 0.94 |
| N_L2_G16 | 4.4 | 4.0 | 1.09 | 5.26 | 0.84 | 4.9 | 0.90 |

Table 4.7. Immediate deflection corresponding to load $P_{sus}$ after cycling.

As it can be observed in Table 4.7, ACI 440.1R-06 underestimates the immediate deflections after cycling of the tested beams. On the other hand, CSA overpredicts the instantaneous deflections in all beams, being an average ratio between the experimental and the predicted immediate deflection equal to 0.85. Bischoff's equation with $\beta$ factor (Eq. 6) gives the best prediction for all beams, with an average ratio equal to 0.9.

### *4.3.3 Time-dependent deflections*

The total mid-span deflections versus time since loading, $\delta_T$ , of the two pairs of beams reinforced with 2Ø12GFRP and 2Ø16GFRP bars are presented in Figures 4.5a and 4.5b respectively. The total deflection includes the immediate deflection after cycles and the long-term deflection due to creep and shrinkage. Good repeatability between twin beams is observed. The curves for the 2Ø12 GFRP and 2Ø16 GFRP RC beams have similar shapes, regardless of the applied sustained load level. As can be seen in the steep slope at the beginning of the curves, the deflection increased considerably with time in the initial period. At 10 days since loading the total deflections increased around 65% of the total increase in all beams, while 90% of total increase was attained around 90 days after loading. The ratios between total deflections and immediate deflections are presented in Table 4.8. No significant influence of the applied level of sustained load is observed. From 10 to 250 days since loading, the ratios vary from 1.20 to 1.85, for beams reinforced with 2Ø12GFRP bars, and from 1.32 to 2.03 for beams reinforced with 2Ø16. On average, the ratios of N_G16 beams are around 11% higher than in N_G12 beams, which indicates an influence of the reinforcement ratio on the total deflections. This is due to the fact that higher reinforcement ratios lead to higher neutral axis depth (larger compressed area of concrete), causing higher creep deformations, and therefore higher time-dependent deflections.

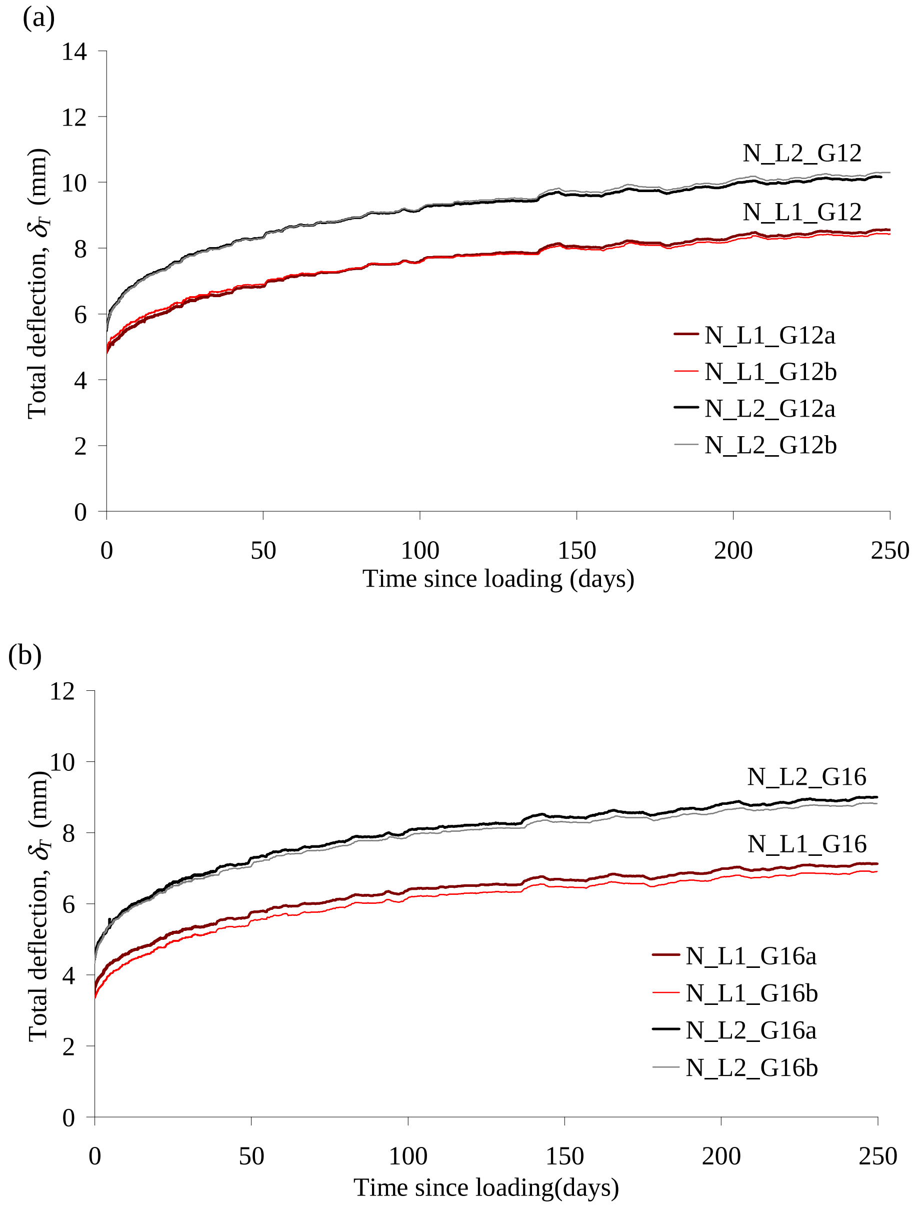

Figure 4.5. Total deflections for (a) beams reinforced with 2Ø12 GFRP bars

(b) beams reinforced with 2Ø16 GFRP.

| Time since loading (days) | N_L1_G12 | N_L2_G12 | N_L1_G16 | N_L2_G16 |
|---|---|---|---|---|
| 10 | 1.20 | 1.23 | 1.32 | 1.34 |
| 30 | 1.36 | 1.42 | 1.52 | 1.56 |
| 90 | 1.57 | 1.61 | 1.78 | 1.80 |
| 180 | 1.70 | 1.74 | 1.94 | 1.93 |
| 250 | 1.83 | 1.85 | 2.03 | 2.01 |

Table 4.8. Ratio between total deflection and immediate deflection.

### *4.3.4 Prediction of time-dependent deflections*

According to ACI 440.1R-06 [11], the total deflection of FRP RC members including the effect of creep and shrinkage, $\delta_{T(ACI\,440)}$, can be obtained from the initial deflection due to sustained load, $\delta_{(sus)}$, from:

$$\delta_{T(ACI\,440)} = (1 + 0.6\xi)\delta_{(sus)} \tag{7}$$

where 0.6 is a reduction factor based on tests carried out by Brown and Bartholomew [14] and Brown [13], and $\xi$ is the time-dependent factor for sustained loads, which is equal to 1.0, 1.2, 1.4 and 2.0 for 3, 6, 12 and 60 months, respectively (an approximate value of 0.7 has been assumed for 1 month, following the curve given in [22]).

CSA-S806-02 [22] proposes a more conservative approach and recommends the following equation with no reduction factor:

$$\delta_{T(CSA)} = (1+\xi)\delta_{(sus)} \tag{8}$$

Experimental data and total deflection predictions are compared in Figures 4.6 and 4.7. Due to the small difference between twin beams only experimental results of beams type –*a* have been plotted to improve the readability of the graphs.

The theoretical total deflections calculated using ACI 440.1R-06 (Eq. 7) and CSA-S806-002 (Eq. 8) recommendations have been determined from the deflection due to sustained load, $\delta_{(sus)}$, as: (1) experimental immediate deflection, $\delta_{t_0,\exp}$; (2) theoretical immediate deflection due to sustained load after cycling, $\delta_{t_0,ACI}$ (Eq. 1) or $\delta_{t_0,CSA}$ (Eq. 3); and (3) theoretical immediate deflection using Bischoff's equation, $\delta_{t_0,B.}$ (Eq. 6).

As can be observed in Figures 4.6 and 4.7, CSA S806-02 (Eq. 8) overestimates the total deflections, whatever immediate deflection is used. As observed in Table 4.9, the ratio between experimental results and CSA S806-02 predictions at 180 days since loading ranges between 0.75 and 0.88 when the experimental immediate deflection $\delta_{t_0,\exp}$ is used in Eq. 8. Using the theoretical immediate deflections from CSA, $\delta_{t_0,CSA}$ (Eq. 4), and Bischoff, $\delta_{t_0,B}$ (Eq. 6), the ratio varies from 0.66 to 0.75 and 0.73 and 0.81, respectively. This overestimation is probably due to the direct use in CSA S806-02 of the time-dependent factor originally calibrated for steel RC members. With the same type of concrete, dimensions, area of reinforcement and environmental conditions, the neutral axis depth for a beam reinforced with GFRP is lower than that of a beam reinforced with conventional steel, due to the difference in the elastic modulus. In terms of time-dependent behaviour, due to the lower compression area of concrete, the increase of the curvature associated with creep and shrinkage is lower.

Therefore, the long-term deflections in FRP reinforced concrete beams are expected to be lower than steel RC beams.

On the other hand, as can be observed in Figures 4.6 and 4.7, the total deflections are underestimated for all beams when using the theoretical immediate deflections from ACI, $\delta_{t_0,ACI}$, in Eq. 7, mainly for those reinforced with 2Ø12 GFRP bars. This is shown in Table 4.10, where the ratio between experimental and predicted total deflections (Eq. 2, Eq. 7) ranges between 1.53 and 1.56 for beams reinforced with 2Ø12 GFRP bars, and between 1.23 and 1.27 for beams reinforced with 2Ø16.

Multiplying the ACI time-dependent factor (Eq. 7) by the experimental immediate deflection, $\delta_{t_0,\exp}$, the ratio between the experimental and predicted total deflection varies from 0.96 to 1.03 for beams N_G12 and from 1.11 to 1.13 for beams N_G16. Similarly, using the predicted immediate deflections calculated with the modified Bischoff's equation, $\delta_{t_0,B}$ (Eq. 6), the ratio varies from 0.91 to 0.94 for beams N_G12 and from 1.02 to 1.04 for N_G16. The difference in ratios between beams reinforced with 2Ø12 GFRP bars and 2Ø16 can be attributed to the aforementioned influence of the reinforcement ratio on the depth of the compressed area of concrete. This effect has been mentioned in section 4.3.3, where an experimental total-to-immediate deflection ratio has been found to be 11% higher for beams N_G16 than for beams N_G12.

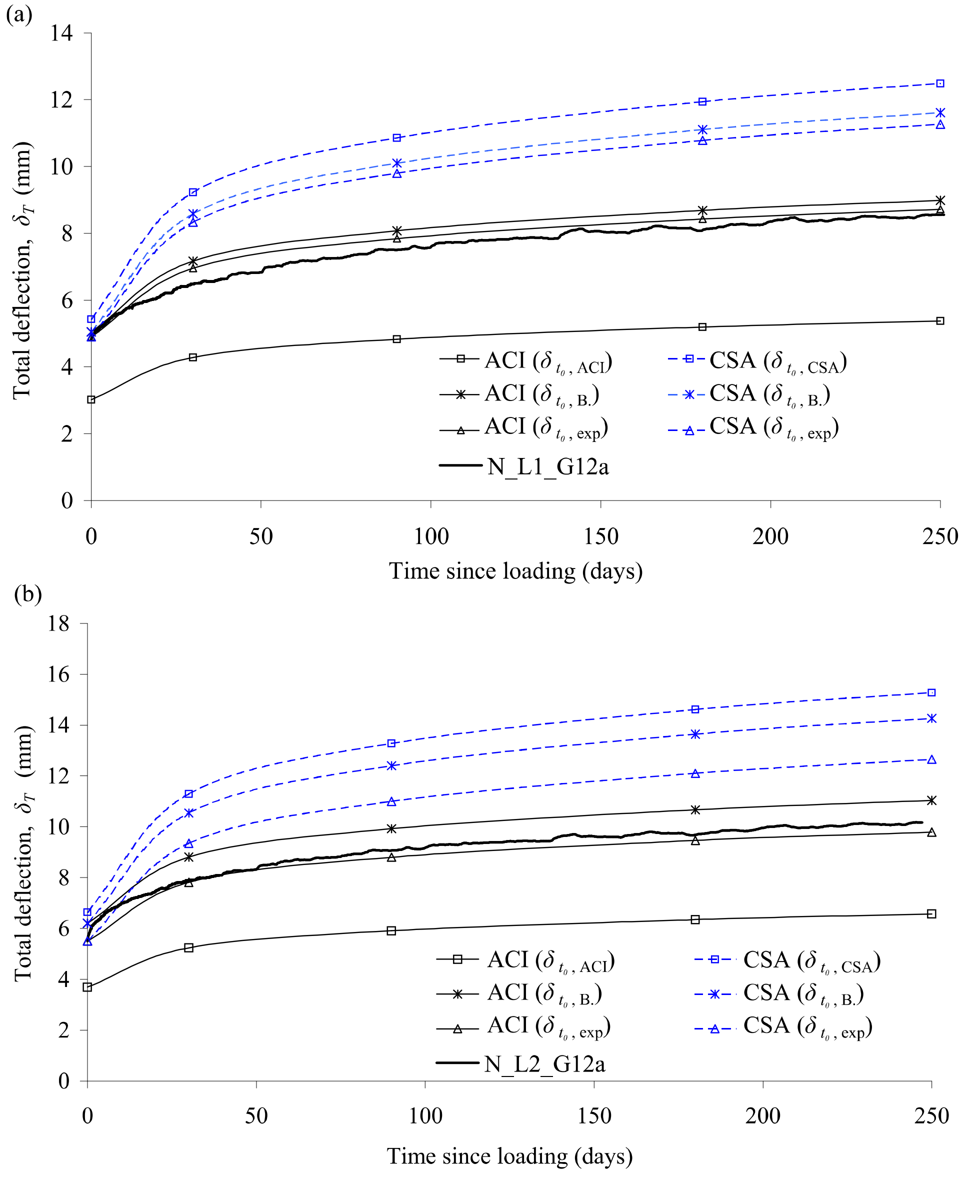

Figure 4.6.Total deflections for beams: (a) N_L1_G12a, (b) N_L2_G12a.

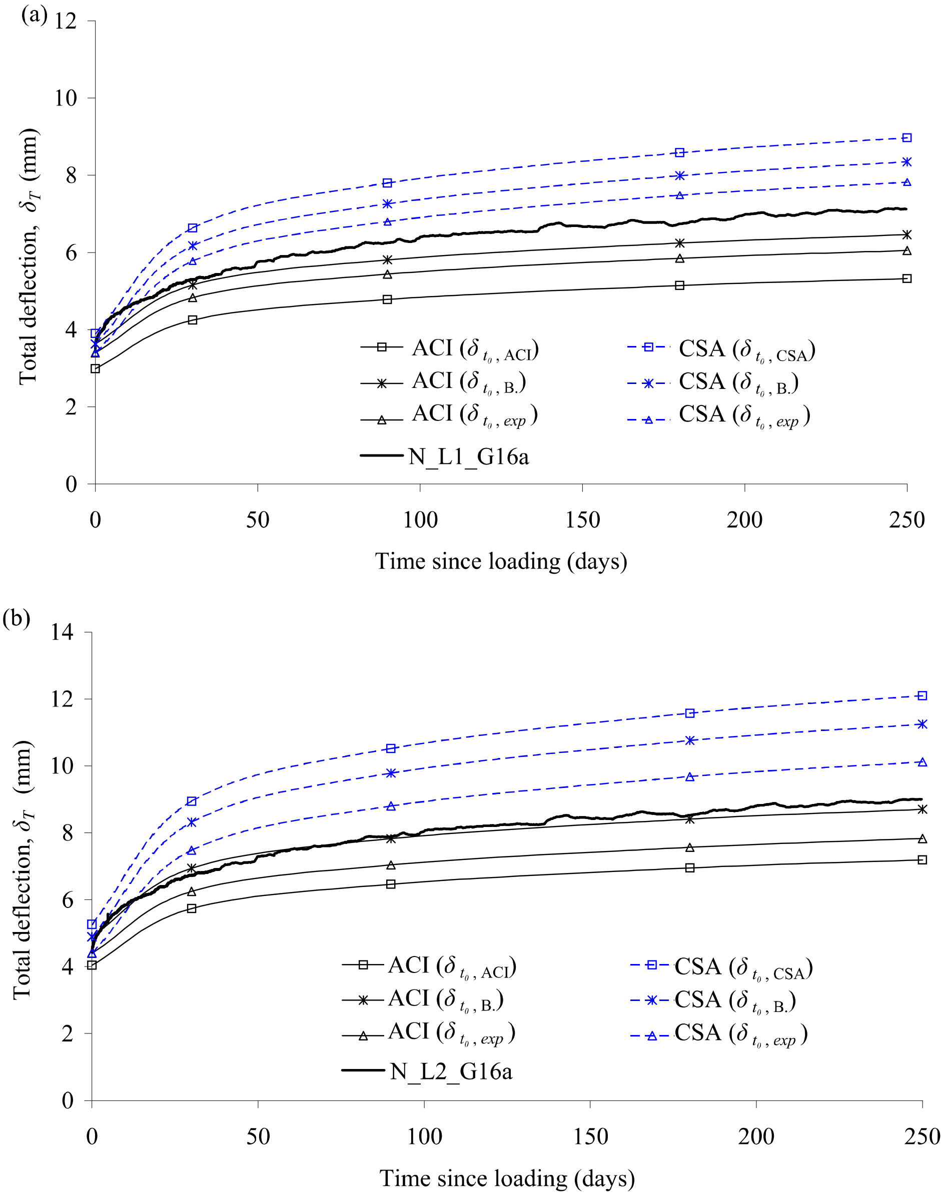

Figure 4.7. Total deflections for beams: (a) N_L1_G16a, (b) N_L2_G16a.

| Experimental data | | $\delta_{t_0,\exp}(1+\xi)$ | | $\delta_{t_0,CSA}(1+\xi)$ | | $\delta_{t_0,B.}(1+\xi)$ | |
|---|---|---|---|---|---|---|---|
| Beams | $\delta_T$ (mm) | $\delta_T^{(1)}$ (mm) | *exp/calc* | $\delta_T^{(2)}$ (mm) | *ex/calc* | $\delta_T^{(3)}$ (mm) | *exp/calc* |
| N_L1_G12 | 8.1 | 10.8 | 0.75 | 11.9 | 0.68 | 11.1 | 0.73 |
| N_L2_G12 | 9.7 | 12.1 | 0.80 | 14.6 | 0.66 | 13.6 | 0.71 |
| N_L1_G16 | 6.7 | 7.5 | 0.86 | 8.6 | 0.75 | 8.0 | 0.81 |
| N_L2_G16 | 8.5 | 9.7 | 0.88 | 11.6 | 0.74 | 10.8 | 0.79 |

Table 4.9. Comparison between total deflections and analytical predictions using CSA-S806-02 approach (Eq. (8)). Time since loading: 180 days.

| Experimental data | | $\delta_{t_0,\exp}(1+0.6\xi)$ | | $\delta_{t_0,ACI}(1+0.6\xi)$ | | $\delta_{t_0,B.}(1+0.6\xi)$ | |
|---|---|---|---|---|---|---|---|
| Beams | $\delta_T$ (mm) | $\delta_T^{(1)}$ (mm) | *exp/calc* | $\delta_T^{(2)}$ (mm) | *exp/calc* | $\delta_T^{(3)}$ (mm) | *exp/calc* |
| N_L1_G12 | 8.1 | 8.4 | 0.96 | 5.2 | 1.56 | 8.7 | 0.94 |
| N_L2_G12 | 9.7 | 9.5 | 1.03 | 6.3 | 1.53 | 10.7 | 0.91 |
| N_L1_G16 | 6.7 | 5.8 | 1.11 | 5.1 | 1.27 | 6.2 | 1.04 |
| N_L2_G16 | 8.5 | 7.6 | 1.13 | 6.9 | 1.23 | 8.4 | 1.02 |

Table 4.10. Comparison between total deflections and analytical predictions using ACI 440.1R-06 approach (Eq. (7)). Time since loading: 180 days.

## 4.4 Conclusions

Experimental results on 8 simply supported GFRP RC beams tested under sustained loading for a period of 250 days have been presented and discussed. The beams were initially subjected to a short-term loading representative of the service load, and subsequently a lower sustained load was applied. Two levels of sustained load and two different reinforcement ratios were studied.

Regarding the experimental results and their comparison with prediction models the following conclusions are drawn:

- The application of the sustained load, lower than the maximum, after a process of unloading and reloading, causes an “immediate” deflection after cycling larger than that corresponding to the same load in the initial monotonic loading.

- The immediate deflection after cycling presents values between 1.2 and 2 times larger than those of the initial monotonic loading, depending on the reinforcement ratio and the level of sustained load. The difference between both deflections is higher when the load is closer to the cracking one.

- Regarding the theoretical predictions, ACI 440.1R-06 underestimates the initial and immediate deflection after cycling, mainly for the beams reinforced with 2Ø12 GFRP bars, while CSA S806-02 overpredicts these deflections in all beams. Bischoff’s equation and its modification to compute deflections after repeated load gives better agreement with experimental data for all the beams.

- The time-dependent deflection increased considerably with time in the initial period. At 10 days since loading the total deflections increased around 60% of the total increase in beams reinforced with 2Ø12GFRP bars and about 50% for beams reinforced with 2Ø16GFRP bars, while 90% of total increase was attained around 90 days after loading.

- From 10 to 250 days since loading, the ratios vary from 1.20 to 1.85 for beams reinforced with 2Ø12GFRP bars, and from 1.32 to 2.03 for beams reinforced with 2Ø16 GFRP bars.

- No significant influence of the applied levels of sustained load was observed in the increase of total deflections.

- Beams reinforced with 2Ø16 GFRP bars presented a total-to-immediate deflection ratio around 11% higher than beams reinforced with 2Ø12GFRP bars, which indicates an influence of the reinforcement ratio on the total deflections.

- Regarding the theoretical predictions, the modified Bischoff's equation together with the modified time-dependent factor presented in ACI 440.1R-06 could reasonably predict the total deflections of concrete beams reinforced with GFRP. The use of the CSA S806-02 time-dependent factor overestimates the experimental results in all beams.

## 4.5 Acknowledgements

The authors acknowledge the support provided by the Spanish Government (Ministerio de Ciencia e Innovación), Project ref. BIA2010-20234-C03-02. The first author thanks the Ministerio de Educación y Ciencia for Grant BES-2008-005740. The authors also thank Schök Bauteile GMBH for supplying GFRP bars.

## 4.6 References

1. Masmoudi R, Thériault M, Benmokrane B. Flexural behavior of concrete beams reinforced with deformed fiber reinforced plastic reinforcing rods. ACI Structural Journal 1998; 95(6):665-76.

2. Pecce M, Manfredi G, Cosenza E. Experimental response and code models of GFRP RC beams in bending. Journal of Composites for Construction 2000; 4(4):182-90.

3. Yost JR, Gross SP, Dinehart DW. Effective moment of inertia for GFRP reinforced concrete beams. ACI Structural Journal 2003; 100(6):732-39.

4. Abdalla HA. Evaluation of deflection in concrete members reinforced with fibre reinforced polymer (FRP) bars. Composite Structures 2002; 56(1):63-71.

5. Bischoff PH. Reevaluation of Deflection Prediction for Concrete Beams Reinforced with Steel and Fiber Reinforced Polymer Bars. Journal of Structural Engineering, ASCE 2005; 131(5):752-67.

6. Mota C, Alminar S, Svecová D. Critical review of deflection formulas for FRP-RC members. Journal of Composites for Construction 2006; 10(3):183-94.

7. Rasheed HA, Nayal R, Melhem H. Response prediction of concrete beams reinforced with FRP bars. Composite Structures 2004; 65(2):193-04.

8. Barris C, Torres Ll, Turon A, Baena M, Catalan A. An experimental study of the flexural behaviour of GFRP RC beams and comparison with prediction models. Composite Structures 2009; 91(3):286-95.

9. Kara IF, Ashour AF. Flexural performance of FRP reinforced concrete beams. Composite Structures 2012; 94(5):1616-25.

10. Al-Sunna R, Pilakoutas K, Hajirasouliha I, Guadagnini M. Deflection behaviour of FRP reinforced concrete beams and slabs: An experimental investigation. Composites Part B: Engineering 2012; http://dx.doi.org/10.1016/j.compositesb.2012.03.007.

11. Barris C, Torres Ll, Baena M, Pilakoutas K, Guadagnini M. Serviceability limit state of FRP RC beams. Advances in Structural Engineering 2012;15(4):653-63.

12. American Concrete Institute Committee 440 ACI. Guide for the design and construction of structural concrete reinforced with FRP bars (ACI 440.1R-06). Farmington Hills (Michigan, USA): American Concrete Institute; 2006.

13. Joh O, Wang Z, Goto Y. Long-term deflection of fiber reinforced polymer concrete beams. Special Publication SP 188-51, Fourth International Symposium on Fiber Reinforced Polymer Reinforcement for Reinforced Concrete Structures 1999; pp. 577-90.

14. Brown V, Sustained load deflections in GFRP-reinforced concrete beams. 3rd International RILEM Symposium on Non-Metallic (FRP) Reinforcement for Concrete Structures (FRPRCS-3). Sapporo, Japan, 1997; pp. 495-02.

15. Brown V, Bartholomeu C, Long-term deflections of GFRP-reinforced concrete beams. First International Conference on Composites in Infra-Structure. Tucson, Arizona, USA, 1996; pp. 389-00.

16. Arockiasamy M, Chidambaram S, Amer A, Shahawy M. Time-dependent deformations of concrete beams reinforced with CFRP bars. Composites Part B: Engineering, 2000; 31(6-7):577-92.

17. Hall T, Ghali A. Long-term deflection prediction of concrete members reinforced with glass fibre reinforced polymer bars. Canadian Journal of Civil Engineering 2000; 27(5):890-98.

18. Gross SP, Yost JR, Kevgas G. Time-dependent behavior of normal and high strength concrete beams reinforced with GFRP bars under sustained loads. High Performance Materials in Bridges 2003; pp.451-62.

19. Gross SP, Yost JR, Crawford JV, Serviceability of high strength concrete beams with internal FRP reinforcement under sustained load. 3rd International Conference on FRP Composites in Civil Engineering (CICE 2006). Miami, Florida, USA; 2006.

20. Yousseff T, Benmokrane B, El-Salakawy E, Deflection and strain variation of GFRP-reinforced concrete beams after one year of continuous loading. Proceedings of the 9th international symposium on fiber-reinforced polymer reinforcement for concrete structures (FRPRCS-9). Sydney, Australia; 2009.

21. Laoubi K, El-Salakawy E, Benmokrane B. Creep and durability of sand-coated glass FRP bars in concrete elements under freeze/thaw cycling and sustained loads. Cement and Concrete Composites, 2006; 28(10):869-878.

22. American Concrete Institute Committee 318 ACI. Building code requirements for structural concrete and commentary (ACI 318-08). Farmington Hills (Michigan, USA): American Concrete Institute; 2008.

23. CSA Standard CAN/CSA-S806-02. Design and construction of building components with fibre-reinforced polymers. Canadian Standards Association, Mississauga, Canada; 2002.

24. American Concrete Institute Committee 440 ACI. ACI 440.3R-04. Guide test methods for fiber-reinforced polymers (FRPs) for reinforcing or strengthening concrete structures. Farmington Hills (Michigan, USA): American Concrete Institute; 2004.

25. Newhook J, Ghali A, Tadros G. Concrete flexural members reinforced with fiber reinforced polymer: Design for cracking and deformability. Canadian Journal of Civil Engineering 2002; 29(1):125-34.

26. ISIS Canada. Reinforcing concrete structures with fibre reinforced polymers- Design Manual No. 3. ISIS Canada Corporation, University of Manitoba, Manitoba, Canada; 2001.

27. Bischoff PH, Scanlon A. Effective moment of inertia for calculating deflections of concrete members containing steel and fiber reinforced polymer bars. ACI Structural Journal 2007; 104(1):68-75.

28. Scanlon A, Bischoff PH. Shrinkage restraint and loading history effects on deflections of flexural members. ACI Structural Journal 2008; 105(4):498-06.

# 5. Effect of material properties on long-term deflections of GFRP reinforced concrete members

C. Miàs, Ll. Torres, A. Turon, I. A. Sharaky. Effect of material properties on long-term deflections of GFRP reinforced concrete beams. *Submitted to* Construction and Building Materials Journal.

## Summary

*The influence of the compressive concrete strength and the reinforcement ratio on the long-term deflections GFRP reinforced concrete beams is analysed in this paper. A total of 20 beams cast with two different concrete strengths (30 and 50 MPa), and different reinforcement amounts of GFRP and steel were tested under short-term loading and then subjected to different levels of sustained loading for a period of time between 250 days and 700 days. The results obtained revealed the influence of the concrete and reinforcement properties on long-term deflections. Thus, the higher the reinforcement ratio and the lower the compressive strength were, the higher the total-to-instantaneous deflection ratio was.*

*The measured long-term deflections were compared to those calculated using available design equations for FRP RC structures, such as those from ACI 440.1R-06 and CSA-S806-02, as well as being compared to the CEB-FIP procedure. In addition, the experimental data were evaluated with a methodology proposed by the authors, based on multiplicative coefficients, obtained from a rational simplification of the Effective Modulus Method. Long-term deflections obtained with CEB-FIP and the proposed methodology were in good agreement with the experimental values. However, some differences were found when ACI 440.1R-06 or CSA-S806-02 procedures were applied.*

## 5.1 Introduction

Fibre reinforced polymer (FRP) bars have a wide range of applications as primary reinforcement in concrete structures subjected to corrosive environments [1-4]. These bars have a higher strength than conventional steel reinforcement, but they have a lower elastic modulus. Consequently, the relative deformation increment associated with creep and shrinkage in FRP reinforced concrete (RC) flexural members is lower than for conventional steel RC members since a smaller concrete area is subject to compression. Therefore, the material properties of FRP rods have a strong influence on the long-term deflections of FRP RC beams [5]. Experimental results, carried out by Brown and Bartholomew [6] and Brown [7], on glass fibre reinforced polymer (GFRP) RC beams reported a similar trend of long-term behaviour between steel and GFRP bars, indicating that the same fundamental approach [8,9] in predicting the long-term deflection can be used by simply adding a modification factor. Similar behaviour has been observed in long-term deflections of carbon fibre reinforced polymer (CFRP) RC beams as reported by Arockiasamy et al. [10]. From these experiments, Arockiasamy and co-authors proposed adding a modification factor specific for CFRP RC members. Based on [6,7], ACI 440.1R-06 [11] recommended, for typical applications, a modification factor of 0.6 to be applied to the ACI 380 time-dependent factor [8,9] . However, the Canadian standard CSA-S806-02 [12] proposes a more conservative approach by adopting the same coefficients as for steel. Recent experimental data published by Miàs et al. [13] showed that the CSA S806-02 approach over-predicted the total deflections of 8 concrete (target 30MPa) beams reinforced with different amounts of GFRP bars (2Ø12 and 2Ø16mm) and subjected to different levels of sustained load. This overestimation was due to the direct use in the CSA S806-02 [12] of the time-dependent factor originally calibrated for steel RC members. As aforementioned, due to the difference between the elastic modulus of steel and GFRP, with the same type of concrete, dimensions, and area of reinforcement, the neutral axis depth for a beam reinforced with GFRP is smaller than that of a beam reinforced with conventional steel. Moreover, in [13], experimental total deflections were also compared with ACI predictions. From the comparison, the authors concluded that using the modified time-dependent factor presented in ACI 440.1R-06, together with the modified Bischoff's equation [14,15] to compute the immediate deflections due to sustained load, give a good agreement with the experimental data. Gross et al. [16] considered the influence of concrete strength in the time-dependent deflections GFRP RC beams in an experimental campaign using 6 normal strength concrete beams and 6 high strength concrete beams reinforced with GFRP bars, which were tested under sustained loading for a period of 180 days. The authors compared the experimental time-dependent deflection multipliers with the ACI 440 time-dependent factor, being the ACI 440 factor lower than the experimental multiplier for normal concrete beams, and higher than the experimental multiplier for high strength concrete beams. On the other hand, experimental results carried out by Al-Salloum and Almusallam [17] and a parametric study carried out by the authors [18] show an influence of environmental conditions (which affect concrete creep and shrinkage) on long-term deflections of GFRP RC beams.

The long-term deflections in RC beams are, basically, due to creep and shrinkage of concrete. Creep and shrinkage values are dependent on environmental conditions, member geometry, load characteristics (age of concrete at the time of loading, magnitude and duration of sustained load) and material properties. To accurately predict the long-term behaviour of steel and FRP RC beams, all of these parameters must be taken into account. International codes and recommendations specific for steel RC structures, such as Eurocode 2 [21], CEB Design Manual on Cracking and Deformation [22], and ACI 435 [23] propose the use of general methodologies like the Effective Modulus Method (EMM) [19] or the Age-Adjusted Effective Modulus Method (AEMM) [20], in whose formulations all the parameters involved in the creep and shrinkage effects are considered. Experimental results on long-term deflections of GFRP RC beams, presented by Hall and Ghali [24], demonstrated that predictions based on the procedure proposed in the CEB Design Manual on Cracking Deformations [22] together with equations found in [25], both based on AEMM, give good agreement with experimental results. Similarly, prediction of long-term deflections using the AEMM procedure was also accurate for RC beams reinforced with CFRP [10].

This paper presents an experimental study on the influence of the compressive concrete strength and the reinforcement ratio on the long-term deflections of GFRP  and steel RC beams. Results of the experimental total deflections of 20 beams, divided into 2 groups of 10 beams with different concrete strength, and reinforced with different amounts of GFRP and steel are presented and discussed. The first set of beams was cast with a target compressive concrete strength of 30MPa. The beams were tested under short-term loading and then subjected to different levels of sustained loading for 250 days. Thereafter the beams of the second set with a target compressive concrete strength of 50MPa, were tested with the same procedure up to 700 days. The influence of the compressive concrete strength and the reinforcement ratio in the long-term behaviour is reflected in the experimental results. Part of the experimental results from the first set of beams were published and discussed in Miàs et al. [13], however for comparison purposes these results are used again in this paper.

The measured long-term deflections are compared to those calculated using formulations available for FRP RC structures such as ACI 440.1R-06 [11] and CSA-S806-02 [12], as well as with the CEB-FIP [22,26] procedure. In addition, the experimental data are evaluated with the methodology proposed by Miàs et al. [27] and Torres et al.[18] , based on multiplicative coefficients, obtained from a rational simplification of the *Effective Modulus Method* [19,21].

## 5.2 Experimental test program

### *5.2.1 Beams specifications*

The beams were cast into two series, each with different target concrete strengths (30 and 50MPa). For each series, a total of 8 concrete beams of 140x190x2450 mm (Figure 5.1) and with a clear cover equal to 20mm were reinforced with two different amounts of GFRP bars (2Ø12 or 2Ø16) placed at the tension side (bottom). Additionally, for comparison purposes, 2 beams were reinforced with 2Ø10 steel bars, thus having a similar stiffness to beams reinforced with 2Ø16 GFRP. The shear-span was reinforced with steel stirrups (Ø8/80mm). No stirrups were provided in the pure bending zone.

The beams were designated as *A*_L*x*-*Jyyz*, where *A* denotes the concrete cast (N=target of 30MPa, H=target of 50MPa), *x* the level of sustained load (L1, L2); *J* the material of the reinforcement (G=GFRP, S=steel) and *yy*, the diameter of the bar (10, 12, 16 mm). Additionally, *z* differentiates between twin beams.

The geometry, features, and designation of the beams are shown in Figure 5.1 and Table 5.1.

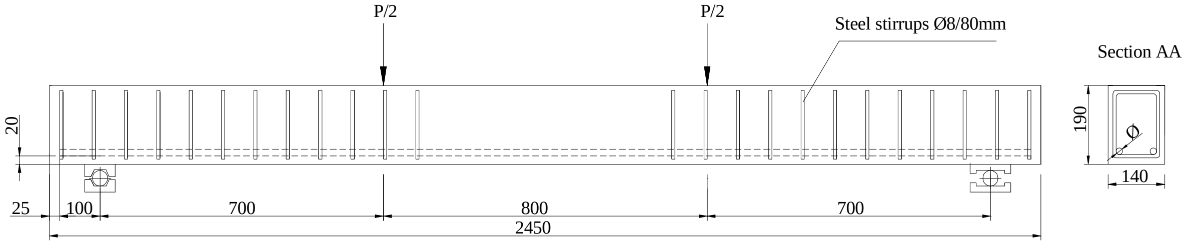

Figure 5.1. Geometric details of the tested beams

| | **Beam designation** | **Rebar material** | **Ø bar (mm)** | ***Reinforcement ratio, ρ* (%)** | **Target $f_c$ (MPa)** |
|---|---|---|---|---|---|
| **N_beams** | **N_L1-G12a** | GFRP | 12 | 1.0 | 30 |
| | **N_L1-G12b** | GFRP | 12 | 1.0 | 30 |
| | **N_L2-G12a** | GFRP | 12 | 1.0 | 30 |
| | **N_L2-G12b** | GFRP | 12 | 1.0 | 30 |
| | **N_L1-G16a** | GFRP | 16 | 1.8 | 30 |
| | **N_L1-G16b** | GFRP | 16 | 1.8 | 30 |
| | **N_L2_G16a** | GFRP | 16 | 1.8 | 30 |
| | **N_L2_G16b** | GFRP | 16 | 1.8 | 30 |
| | **N_L1_S10** | steel | 10 | 0.7 | 30 |
| | **N_L2_S10** | steel | 10 | 0.7 | 30 |
| **H_beams** | **H_L1-G12a** | GFRP | 12 | 1.0 | 50 |
| | **H_L1-G12b** | GFRP | 12 | 1.0 | 50 |
| | **H_L2-G12a** | GFRP | 12 | 1.0 | 50 |
| | **H_L2-G12b** | GFRP | 12 | 1.0 | 50 |
| | **H_L1-G16a** | GFRP | 16 | 1.8 | 50 |
| | **H_L1-G16b** | GFRP | 16 | 1.8 | 50 |
| | **H_L2_G16a** | GFRP | 16 | 1.8 | 50 |
| | **H_L2_G16b** | GFRP | 16 | 1.8 | 50 |
| | **H_L1_S10** | steel | 10 | 0.7 | 50 |
| | **H_L2_S10** | steel | 10 | 0.7 | 50 |

Table 5.1. Beams designation

### *5.2.2 Material properties*

***Concrete***

Two casts, with two different target compressive strengths (30 and 50MPa), were poured for the 2 different series of tests. The concrete was provided by a local ready-mix supplier with a maximum aggregate size of 12mm. The proportions of the concrete mix for the two concretes are summarized in Table 5.2.

| **Component** | **Units** | **C1** | **C2** |
|---|---|---|---|
| water | kg/m$^3$ | 185 | 160 |
| cement (CEM II/A-V 42.5R) | kg/m$^3$ | 320 | 430 |
| w/c ratio | | 0.58 | 0.37 |
| fine aggregate | kg/m$^3$ | 880 | 820 |
| coarse aggregate | kg/m$^3$ | 875 | 875 |
| superplasticizer Sikament 90P | % cement weight | - | 0.6 |
| superplasticizer Sika Viscocrete 5920 | % cement weight | - | 1 |
| **target compressive strength** | **MPa** | **30** | **50** |

Table 5.2. Composition of concrete

The beams were cast together with 8 cylinders (Ø=150mm, h=300mm) used to determine the mechanical properties of the concrete at 30 days, and 4 cylindrical specimens (Ø=150mm, h=450mm) used to determine the corresponding creep coefficient and free shrinkage strain. Details of the cylinders used in these tests are shown in Figures 5.2.a and 5.2.b

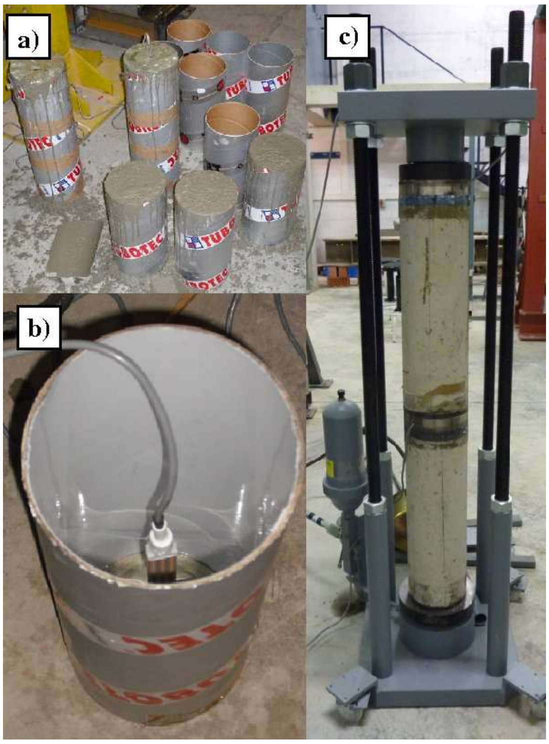

Figure 5.2. (a) Cylindrical moulds (b) cylindrical mould for the creep coefficient determining with embedded strain gauge (c) set-up for creep tests on cylinders

### *Characterization of concrete at time of beams loading*

The experimental compressive strength, $f_c$, and the modulus of elasticity, $E_c$, were determined from cylinder tests at 30 days after casting, corresponding to time $t_0$, at which the sustained loads were applied to beams and specimens used in the determination of the creep coefficient Concrete mechanical properties are summarized in Table 5.3.

| **Concrete mix** | **Target (MPa)** | **$E_c$ (GPa)** | **$f_c$ (MPa)** |
|---|---|---|---|
| **C1** | 30 | 25.7 | 27.7 |
| **C2** | 50 | 29.0 | 56 |

Table 5.3. Concrete mechanical properties

*Characterization of time-dependent properties of concrete*

In order to determine the creep coefficient according to ASTM C512-02, 2 concrete cylinders (Ø=150mm, L=450mm) with embedded strain gauges were stacked in a loading frame (Figure 5.2c) with a constant pressure equal to 10MPa and 15MPa, for concrete C1 and C2, respectively. The cylinders were loaded at the same time as the beams. Additional specimens were left unloaded and were also instrumented to determine free shrinkage strain.

The experimental values of creep and shrinkage strain are presented in section 5.3.1.

***Rebars***

The GFRP bars used in these experiments were type E-CR GFRP ComBAR with 75% glass content in volume. Nominal diameters of 12mm and 16mm were used.

The mean values of mechanical properties obtained from uniaxial tension tests, following ACI 440 3R-04 [28] recommendations, are shown in Table 5.4.

| Diameter | Modulus of elasticity, $E_f$, (GPa) | Rupture tensile strength, $f_{fu}$ , (MPa) |
|---|---|---|
| 12 | 64.5 (60) | 1424 (1000) |
| 16 | 63.4 (60) | 1327 (1000) |

Table 5.4. Mechanical properties of GFRP rebars. Values provided by manufacturer in brackets

The steel bars were B 500S type, with a modulus of elasticity equal to 200GPa, yield strength equal to 500 MPa and tensile strength equal to 550MPa.

### 5.2.3 Experimental set-up

The tests were prepared and carried out in two series. In each set of tests, 10 simply supported beams (N_beams or H_beams) spanning 2200mm were subjected to two concentrated loads for a period of time. The beams were tested up to service load and then subsequently to two short-term cyclical loadings, prior to being subjected to a representative sustained load.

### ***Short-term set-up***

The beams were tested in a structural steel loading frame. A servo-controlled hydraulic jack with a capacity of 300kN was used together with a steel spreader beam to transmit the load to two rollers located at 700mm from the beam supports (Figure 5.1). The load was applied in displacement control mode at a displacement rate of 0.7mm/min until a maximum value, *P* (summarized in Tables 5.5 and 5.6), and then cycled twice between the maximum load and a minimum of 2kN. The maximum load was designed to obtain a maximum bar strain equal to 2000με, representing the beam service conditions in accordance with [29,30].

### ***Sustained load set-up***

Immediately after the short-term test, the beams were moved to the corresponding sustained loading frames (Figure 5.3). The sustained loads were applied by attaching two piles of concrete blocks 800mm apart, and at 700mm from the beam supports (as in the short-term set up).

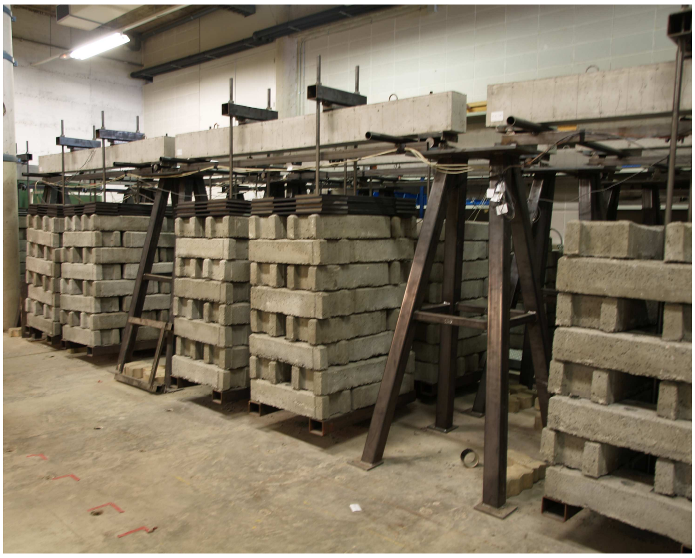

Figure 5.3. Set-up for long-term tests

The sustained load, $P_{sus}$, was designed to obtain instantaneous maximum concrete compressive stresses of around $0.3f_c$ and $0.45f_c$ at mid-span. The magnitudes of the sustained loads applied in N_Beams and H_Beams are given in Table 5.5 and Table 5.6, respectively. For the beam identification, $L1$ corresponds to beams tested with a load applied to obtain a compressive stress equal to $0.3f_c$, while $L2$ for a compressive stress equal to $0.45f_c$.

| **N_beams** | **N_L1_G12** | **N_L2_G12** | **N_L1_G16** | **N_L2_G16** | **N_L1_S10** | **N_L2_S10** |
|---|---|---|---|---|---|---|
| **Load, P, (kN)** | 14 | 14 | 16 | 16 | 16 | 16 |
| **Load, $P_{sus}$,(kN)** | 9 | 11 | 10 | 14 | 10 | 14 |

Table 5.5. – Maximum instantaneous loads, $P$, and sustained loads, $P_{sus}$, applied on N_beams series

| **H_beams** | **H_L1_G12** | **H_L2_G12** | **H_L1_G16** | **H_L2_G16** | **H_L1_S10** | **H_L2_S10** |
|---|---|---|---|---|---|---|
| **Load, $P$, (kN)** | 23 | 23 | 28 | 28 | 28 | 28 |
| **Load, $P_{sus}$,(kN)** | 13.5 | 19 | 17 | 22 | 17 | 22 |

Table 5.6. Maximum instantaneous loads, $P$, and sustained loads, $P_{sus}$, applied on H_beams

The registered temperature and relative humidity in the laboratory during the sustained loading tests were 22±2.8ºC and 55±12.3% for the first series of tests (N_beams) and 20±3.2ºC and 54±11.2%, for the second series. Recorded values are presented in Figures 5.4 and 5.5.

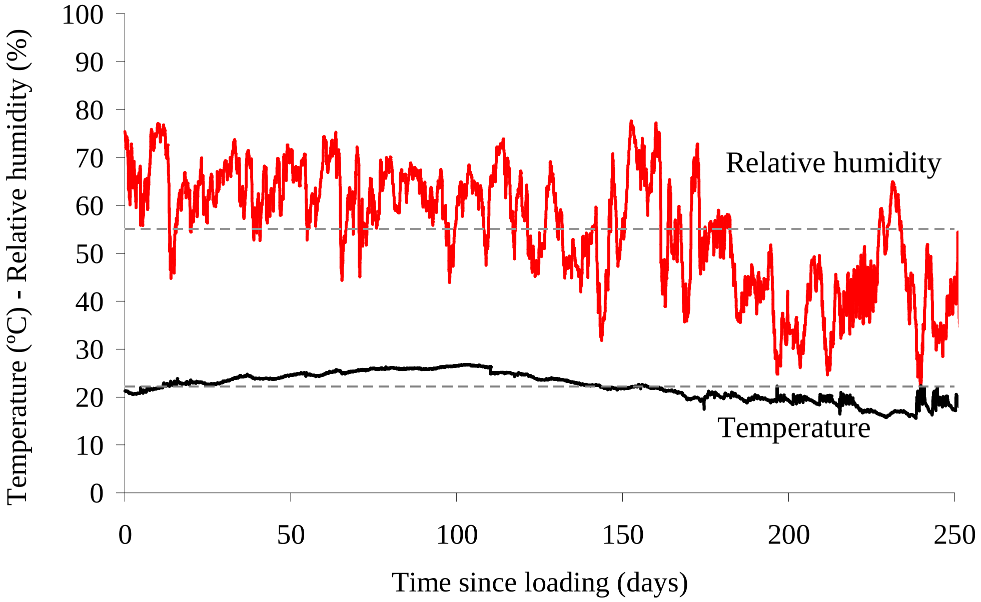

Figure 5.4. Temperature and relative humidity registered in the laboratory during N_beams tests

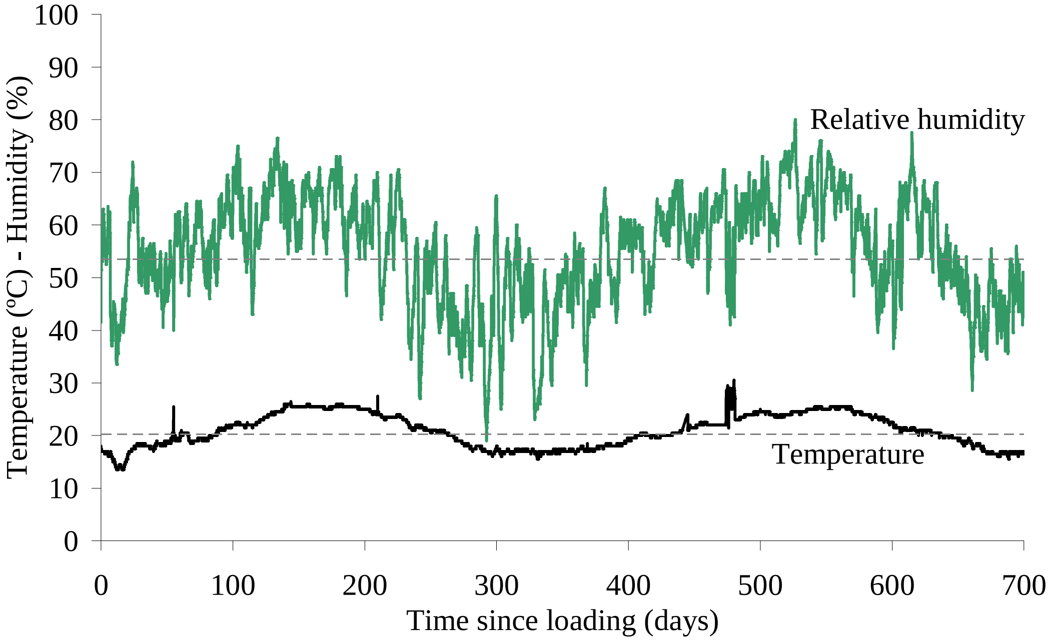

Figure 5.5. Temperature and relative humidity registered in the laboratory during H_beams tests

## 5.3 Experimental results

### *5.3.1 Time-dependent effects of concrete*

Shrinkage strains, $\varepsilon_{sh}(t,t_0)$, were continuously measured from 30 days after casting, corresponding to time $t_0$, when sustained loads were applied to beams and cylinders for creep tests. The evolution of the experimental shrinkage strains of the two series of concrete, C1 (30MPa) and C2 (50MPa), are shown in Figures 5.6 and 5.7, respectively.

The average values of experimental free shrinkage strain for both concretes are tabulated in Table 5.7. As can be observed, from 10 to 250 days, the shrinkage strain increased from 80 με to 386 με for concrete C1 (30MPa), and from 65 με to 358 με, for concrete C2 (50MPa), showing the influence of the concrete strength. On average, at 250 days, the shrinkage strain of concrete C1 (30MPa) was 10% greater than the shrinkage strain of concrete C2 (50MPa). At 700 days, the shrinkage strain of concrete C2 increased up to 404 με, 13% higher than that at 250 days.

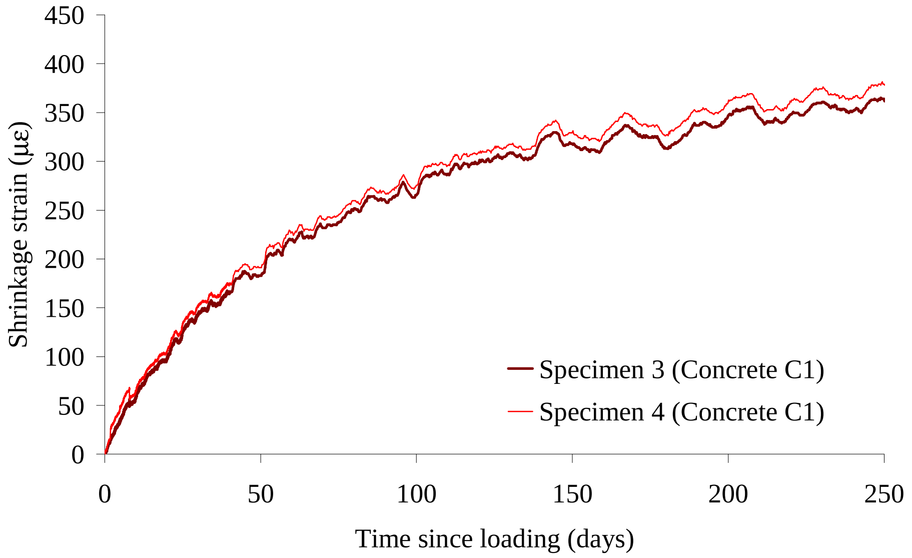

Figure 5.6. Experimental free shrinkage strain – Concrete of N_beams series

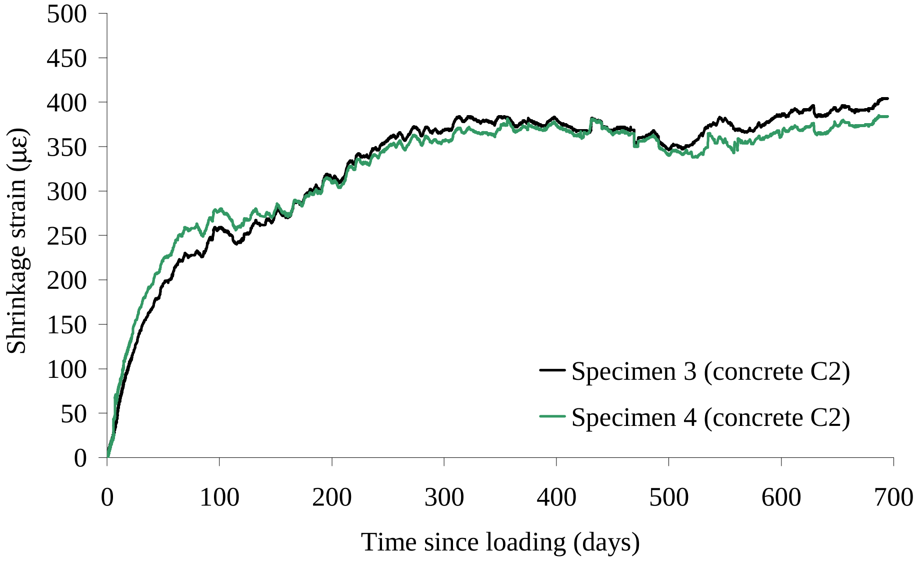

Figure 5.7. Experimental free shrinkage strain – Concrete of H_beams series

The evolution with time of the experimental creep coefficients obtained from the strain measurements of the cylinders of concrete C1 and C2, placed on the loading frame, is presented in Figures 5.8 and 5.9, respectively. The experimental creep coefficient is calculated from the ratio between the total creep strain and the instantaneous strain. The total creep strain $\varepsilon_t(t_0)$ is obtained by subtracting the shrinkage strain, $\varepsilon_{sh}(t,t_0)$, from the total strain $\varepsilon_t(t,t_0)$. Good agreement between the two cylinders used in each set of tests (C1 and C2) is observed. As is noticed in the steep slope of Figures 5.8 and 5.9, at the beginning of the tests (approximately up to 10 days since loading), the creep effect increases considerably with time and thereafter tends to increase slowly. Particularly for specimens C2, from 300 days since loading, the slope tends to increase more slowly to become almost constant. The average values of experimental creep coefficient for both concretes are indicated in Table 5.7. At 10 days since loading, the creep coefficient is 1.1 for specimens of concrete C1, and 0.75, for concrete C2. From 30 to 250 days since loading, the creep coefficient increases from 1.56

to 2.65 for concrete C1 and 1.11 to 1.87 for concrete C2. At 360 days, the creep coefficient for concrete C2 is 1.96, and increasing up to 2.10 at 700 days.

Comparing the experimental values of the two concretes, an influence of the concrete strength is observed in the creep coefficient [31], being the creep coefficient of C1 around 1.4 times greater than that of C2.

It is worth mentioning that the small jump of the values at time 170 days after loading, reflected in Figure 5.8, and the different jumps in Figure 5.9 are not the effect of the environmental conditions, but rather the application of small increments of load in the creep loading frame, to maintain constant the stress on the specimens.

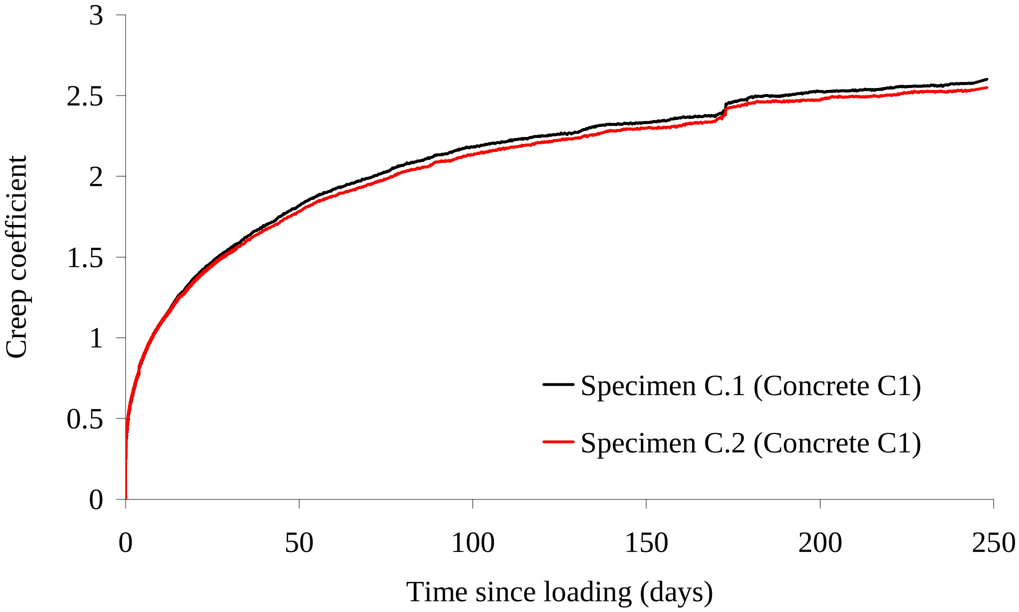

Figure 5.8. Experimental creep coefficient – Concrete of N_beams series

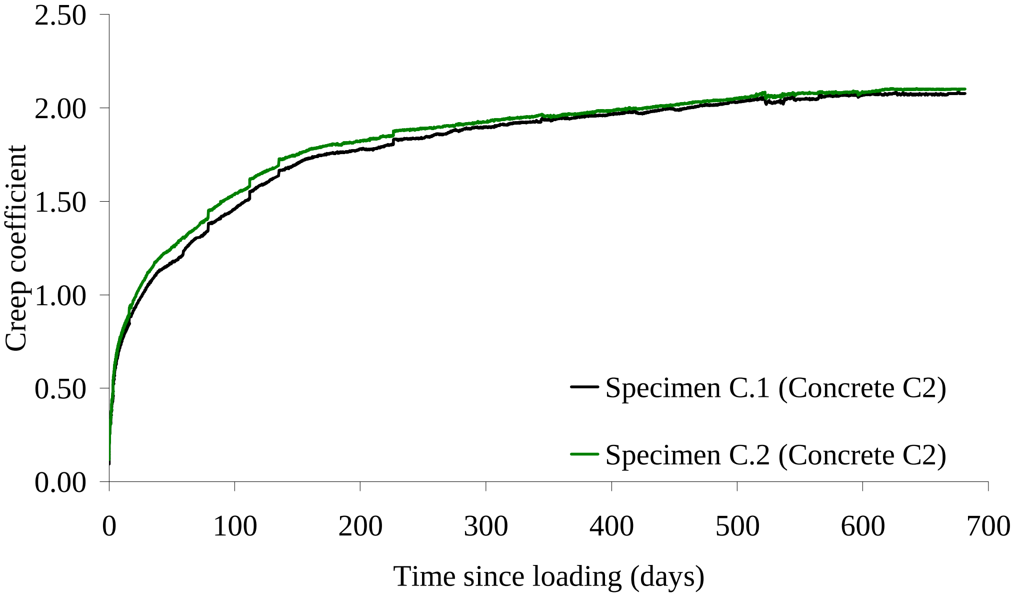

Figure 5.9. Experimental creep coefficient – Concrete of H_beams series

| Concrete | Time (days) | Creep coefficient | Shrinkage strain (με) |
|---|---|---|---|
| **C1** | 10 | 1.10 | 80 |
| **C1** | 30 | 1.56 | 155 |
| **C1** | 90 | 2.14 | 272 |
| **C1** | 180 | 2.49 | 334 |
| **C1** | 250 | 2.65 | 386 |
| **C2** | 10 | 0.75 | 65 |
| **C2** | 30 | 1.10 | 171 |
| **C2** | 90 | 1.50 | 262 |
| **C2** | 180 | 1.80 | 300 |
| **C2** | 250 | 1.87 | 358 |
| **C2** | 360 | 1.96 | 373 |
| **C2** | 500 | 2.05 | 351 |
| **C2** | 700 | 2.10 | 404 |

Table 5.7. Experimental time-dependent concrete properties (average values).

### *5.3.2 Experimental time-dependent deflections*

Experimental total deflections versus time since loading for N_beams are presented in Figure 5.10. The total deflection includes the immediate deflection and the long-term deflection due to creep and shrinkage. As it can be observed, the curves of GFRP (Figures 5.10a and 5.10b) and steel (Figure 5.10c) RC beams have a similar trend. The results show that the creep and shrinkage effect were higher in the initial period, while tending to decrease over time. At 10 days since loading the total deflections increased between 55% and 65% of the total increase in all beams, while 90% of total increase was attained around 90 days after loading. The total-to-immediate deflections ratio varies from 1.20, 1.23, 1.32 and 1.34 (at 10 days since loading) to 1.57, 1.61, 1.78, 1.80 (at 90 days since loading) respectively, for the pair of beams N_L1_G12, N_L2_G12, N_L1_G16 and N_L2_G16 (Table 6-8). At 250 days since loading, the ratio total-to-immediate deflection is equal to 1.83 and 1.85 for beams N_L1_G12 and N_L2_G12, and equal to 2.03 and 2.01 for beams N_L1_G16 and N_L2_G16, showing an influence of the reinforcement ratio in the total-to-immediate deflection ratios. The higher the reinforcement ratio, the larger the neutral axis depth, and therefore, a larger compressive concrete block, causing larger creep and shrinkage effects is expected. The neutral axis depth not only depends on the reinforcement ratio, but also on the modular ratio, $n$, which is the ratio between the elastic modulus of the reinforcement ($E_{FRP}$ or $E_{steel}$) and the elastic modulus of the concrete ($E_c$). For beams with similar conditions of geometry, concrete and reinforcement ratio, the neutral axis depth for FRP RC beams is smaller than that of steel RC beams and therefore, the time-dependent deflections are expected to be lower. However, if the reinforcement has the same stiffness, i.e., if $n_{\mathrm{FRP}}\cdot\rho_{\mathrm{FRP}}= n_{\mathrm{steel}}\cdot\rho_{\mathrm{steel}}$, the neutral axis depth is the same and therefore the increase of the deflection due to creep and shrinkage is equivalent. This is observed in Table 6-8, where the increase of the deflections, at 250 days, is around 2 times the immediate deflection for beams reinforced with 2Ø16 GRP bars and 2Ø10 steel bars, which have been selected to have a similar stiffness. No influence of the level of the sustained load is observed.

The same trend is observed in H_Beams (Figure 5.11). Since the beams were subjected to a sustained load for a longer period (up to 700days), a more stabilized curve is observed. Similarly to N_beams, an influence of the reinforcement ratio can be noticed in the total-to-immediate deflection ratio, which is, at 700 days, equal to 1.40, 1.41 for the pair of beams H_L1_G12 and H_L2_G12, respectively, and equal to 1.50, 1.51 for the pair of beams H_L1_G16, H_L2_G16, respectively (Table 5.9). Approximately the same ratio is observed for beams reinforced with 2 Ø 16 bars and 2 Ø 10 steel RC, being the total deflection around 1.5 times the immediate deflections.

The total-to-immediate deflection ratios of H_beams are around 25% lower than in N_beams at the same time since loading. This is because the experimental values of creep and shrinkage strain for N_beams (concrete C1) are higher than those for H_Beams (concrete C2) and consequently, higher long-term deflections for N_beams are expected. This indicates that the increase in long-term deflection not only depends on reinforcement ratio, but also on the concrete strength.

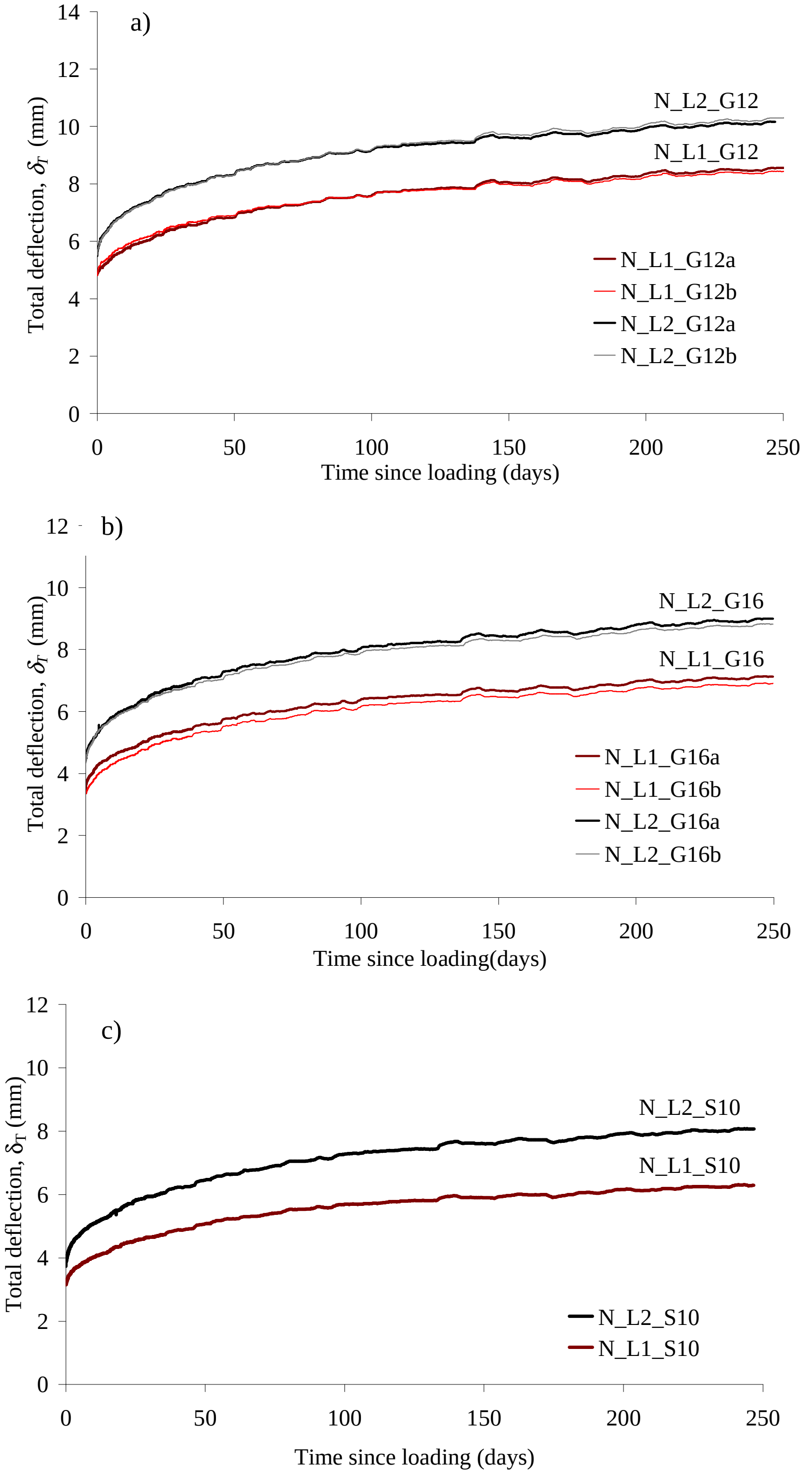

Figure 5.10. Total deflections for N_beams reinforced with (a) 2Ø12 GFRP, (b) 2Ø16 GFRP, (c) 2Ø10 steel bars

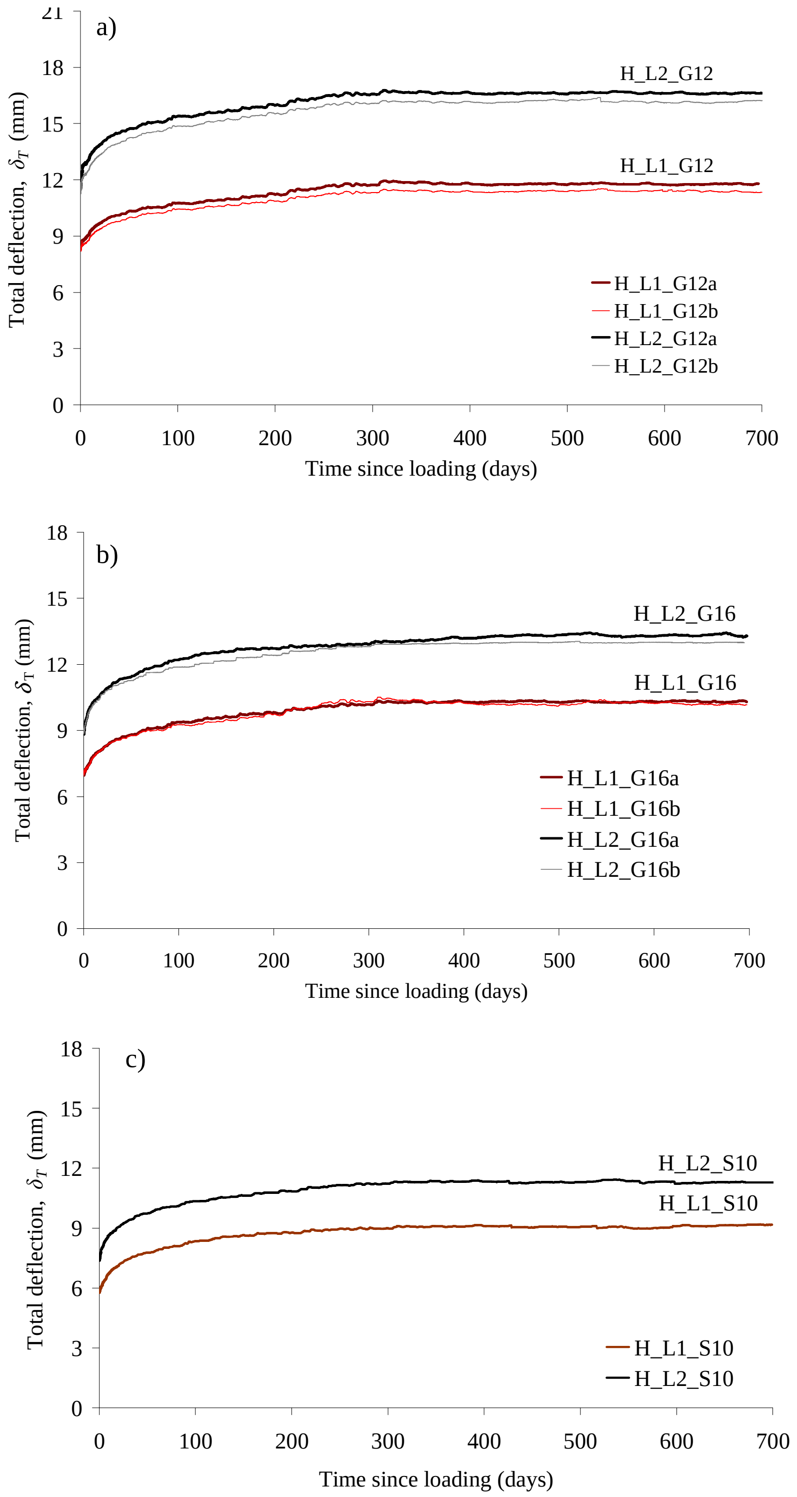

Figure 5.11. Total deflections for H_beams reinforced with (a) 2Ø12 GFRP, (b) 2Ø16 GFRP, (c) 2Ø10 steel bars

| Time(days) | N_L1_G12 | N_L2_G12 | N_L1_G16 | N_L2_G16 | N_L1_S10 | N_L2_S10 |
|---|---|---|---|---|---|---|
| **10** | 1.20 | 1.23 | 1.32 | 1.34 | 1.27 | 1.36 |
| **30** | 1.36 | 1.42 | 1.52 | 1.56 | 1.47 | 1.58 |
| **90** | 1.57 | 1.61 | 1.78 | 1.80 | 1.78 | 1.92 |
| **180** | 1.70 | 1.74 | 1.94 | 1.93 | 1.90 | 2.06 |
| **250** | 1.83 | 1.85 | 2.03 | 2.01 | 1.99 | 2.15 |

Table 5.8. Ratio between the total and immediate deflection for N_beams

| Time(days) | H_L1_G12 | H_L2_G12 | H_L1_G16 | H_L2_G16 | H_L1_S10 | H_L2_S10 |
|---|---|---|---|---|---|---|
| **10** | 1.07 | 1.13 | 1.16 | 1.22 | 1.17 | 1.18 |
| **30** | 1.19 | 1.21 | 1.23 | 1.25 | 1.29 | 1.28 |
| **90** | 1.27 | 1.29 | 1.32 | 1.38 | 1.43 | 1.40 |
| **180** | 1.33 | 1.35 | 1.41 | 1.44 | 1.51 | 1.46 |
| **250** | 1.39 | 1.40 | 1.47 | 1.46 | 1.54 | 1.52 |
| **360** | 1.41 | 1.41 | 1.49 | 1.47 | 1.55 | 1.51 |
| **500** | 1.40 | 1.41 | 1.50 | 1.52 | 1.55 | 1.51 |
| **700** | 1.40 | 1.41 | 1.50 | 1.51 | 1.56 | 1.52 |

Table 5.9. Ratio between the total and immediate deflection for H_beams

## 5.4 Comparison with analytical models

The experimental total deflections versus time since loading are compared with analytical predictions using the procedures proposed in ACI 440.1R-04 [11] and CSA-S806-02 [12] for FRP RC members. The experimental data are also compared with predictions obtained from the CEB-FIP [22,25] methodology, whose suitability for the prediction of FRP RC time-dependent deflections of FRP RC beams has been proven in recent studies [10,24]. Moreover, a comparison is made using a proposed methodology, recently presented by the authors [18,27], and which is based on multiplicative coefficients to predict time-dependent deflections of FRP RC members. The aforementioned procedures are detailed in the Appendix.

Since the sustained load was applied after two loading cycles, and ACI and CSA procedures do not specifically account for this situation, the short-term deflection has been calculated using Bischoff's approach (Eq. A.5.6 in the Appendix) with $\beta$=0.5 [13-15].

The experimental total deflection versus time of N_beams reinforced with GFRP bars is presented and compared to the corresponding predictions in Figure 5.12. As can be observed, the CEB-FIP procedure and the proposed methodology give good agreement with the experimental data for different reinforcement ratios and sustained load levels. At 250 days since loading, the average ratios between the theoretical values and the experimental total deflections are 0.95 and 0.97 respectively (Table 5.10). It is worth mentioning that the creep coefficient and free shrinkage strain, used in the CEB-FIP and the proposed method, are determined from the characterization of the time-dependent properties of concrete presented in section 5.3.1.

The ACI 440.1R-06 equation gives good agreement with the experimental data for N_beams reinforced with 2Ø16 (Figures 5.12c and 5.12d), as it is seen in Table 5.10, where the ratio between the ACI predictions and the experimental data is, on average, equal to 0.96. For the beams reinforced with 2Ø12 FRP bars, this ratio is equal to 1.07. This is because the ACI time-dependent factor has the same value, and independent of the reinforcement ratio. Therefore, if the ACI predictions match well with the total deflections curve of N_G16, it is expected that, due to the lower reinforcement ratio of beams N_G12, the ACI will over-predict the total deflections, as it can be observed in Figure 5.12a and Figure 5.12b. On the other hand, the CSA S806-02 equation overestimates the deflections in all N_beams. On average, CSA S806-02 prediction is 1.32 times the experimental total deflection (Table 5.10). This overestimation can be explained by the fact that the CSA time-dependent factor is based, without any modification, on the steel RC formulation. Since FRP has a lower elastic modulus than steel, the increase of total deflections over time is lower, and therefore, the CSA equation is always expected to be conservative in its predictions of long-term deflections due to creep and shrinkage.

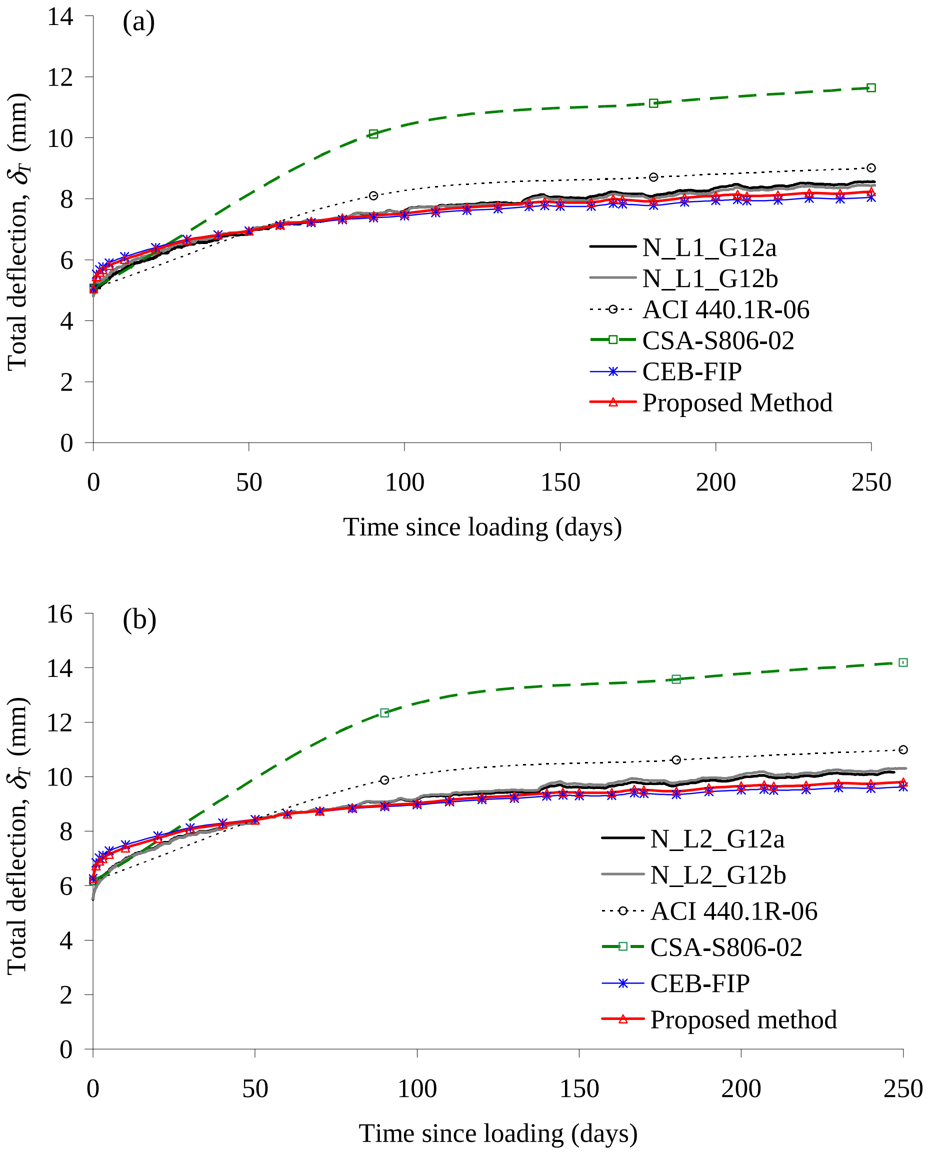
(a)
Total deflection, $\delta_T$ (mm)
0
2
4
6
8
10
12
14
0
50
100
150
200
250
Time since loading (days)
N_L1_G12a
N_L1_G12b
ACI 440.1R-06
CSA-S806-02
CEB-FIP
Proposed Method
(b)
Total deflection, $\delta_T$ (mm)
0
2
4
6
8
10
12
14
16
0
50
100
150
200
250
Time since loading (days)
N_L2_G12a
N_L2_G12b
ACI 440.1R-06
CSA-S806-02
CEB-FIP
Proposed method

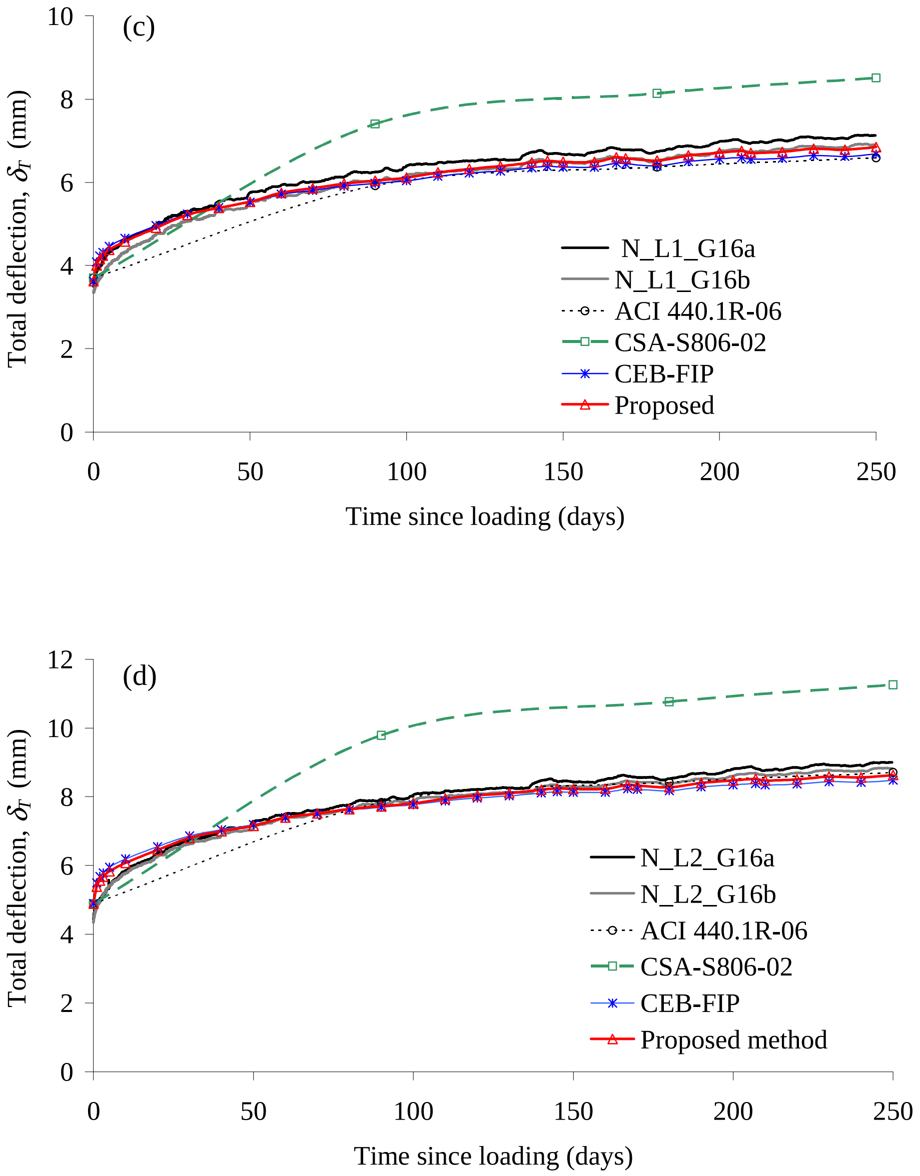

Figure 5.12. Total deflections versus time since loading for beams (a) N_L1_G12 (b) N_L2_G12 (c) N_L1_G16 and (d) N_L2_G16 beams

| **N_beams** | $\delta_{prop}/\delta_{\exp}$ | $\delta_{CEB-FIB}/\delta_{\exp}$ | $\delta_{ACI}/\delta_{\exp}$ | $\delta_{CSA}/\delta_{\exp}$ |
|---|---|---|---|---|
| **N_L1_G12** | 0.97 | 0.95 | 1.06 | 1.37 |
| **N_L2_G12** | 0.97 | 0.95 | 1.08 | 1.40 |
| **N_L1_G16** | 0.98 | 0.95 | 0.94 | 1.22 |
| **N_L2_G16** | 0.98 | 0.96 | 0.99 | 1.28 |
| **Mean** | **0.97** | **0.95** | **1.02** | **1.32** |

Table 5.10. Ratio between theoretical and experimental total deflection at 250 days since loading (N_beams).

The experimental total deflection versus time of H_beams reinforced with GFRP bars is presented and compared to the corresponding predictions in Figure 5.13. As can be observed, similarly to the case of N_beams, the CEB-FIP and the proposed method predictions fit quite well with the experimental results, with ratios between the theoretical and the experimental deflection, at 700 days since loading, equal to 0.95 and 0.97 (Table 5.11), respectively.

The ACI 440.1R-06 method overestimates the experimental values in all cases. At 700 days, the ACI 440.1R-06 predicts a total deflection 1.33 times the experimental deflection. Again, if the ACI predictions match quite well to experimental deflections in N_beams, mainly in beams reinforced with 2Ø16, then it can be expected that it will not be as adequate for predicting total deflections in H_beams, since the variation of the creep coefficient and the free shrinkage strain in concrete are not taken into account in the ACI time-dependent factor. As was also shown for N_beams, the ratio between ACI predictions and experimental deflections depends on the reinforcement ratio being higher for beams reinforced with 2Ø12. The CSA-S806-02 method overestimates by 1.78 times in average the experimental values

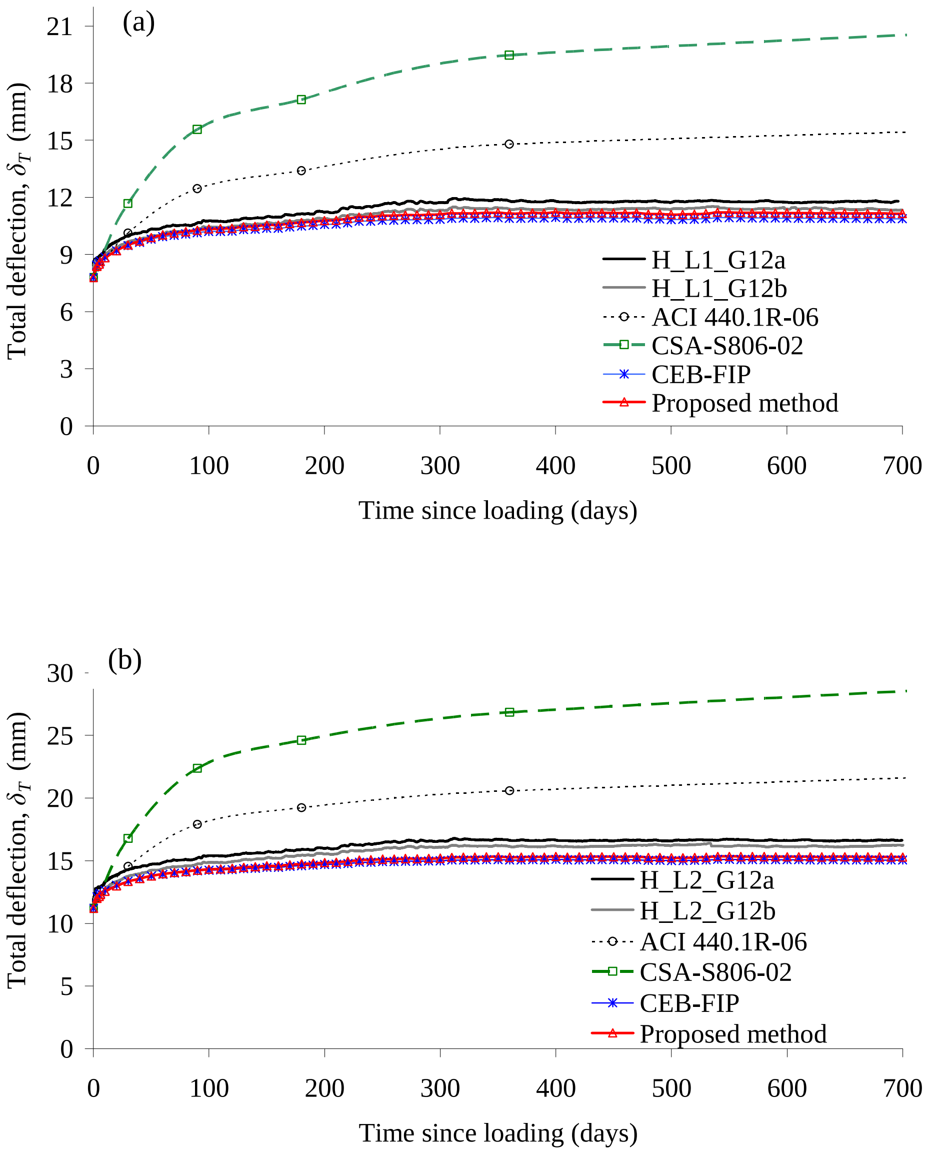
(a)
Total deflection, $\delta_T$ (mm)
0
3
6
9
12
15
18
21
0
100
200
300
400
500
600
700
Time since loading (days)
H_L1_G12a
H_L1_G12b
ACI 440.1R-06
CSA-S806-02
CEB-FIP
Proposed method
(b)
Total deflection, $\delta_T$ (mm)
0
5
10
15
20
25
30
0
100
200
300
400
500
600
700
Time since loading (days)
H_L2_G12a
H_L2_G12b
ACI 440.1R-06
CSA-S806-02
CEB-FIP
Proposed method

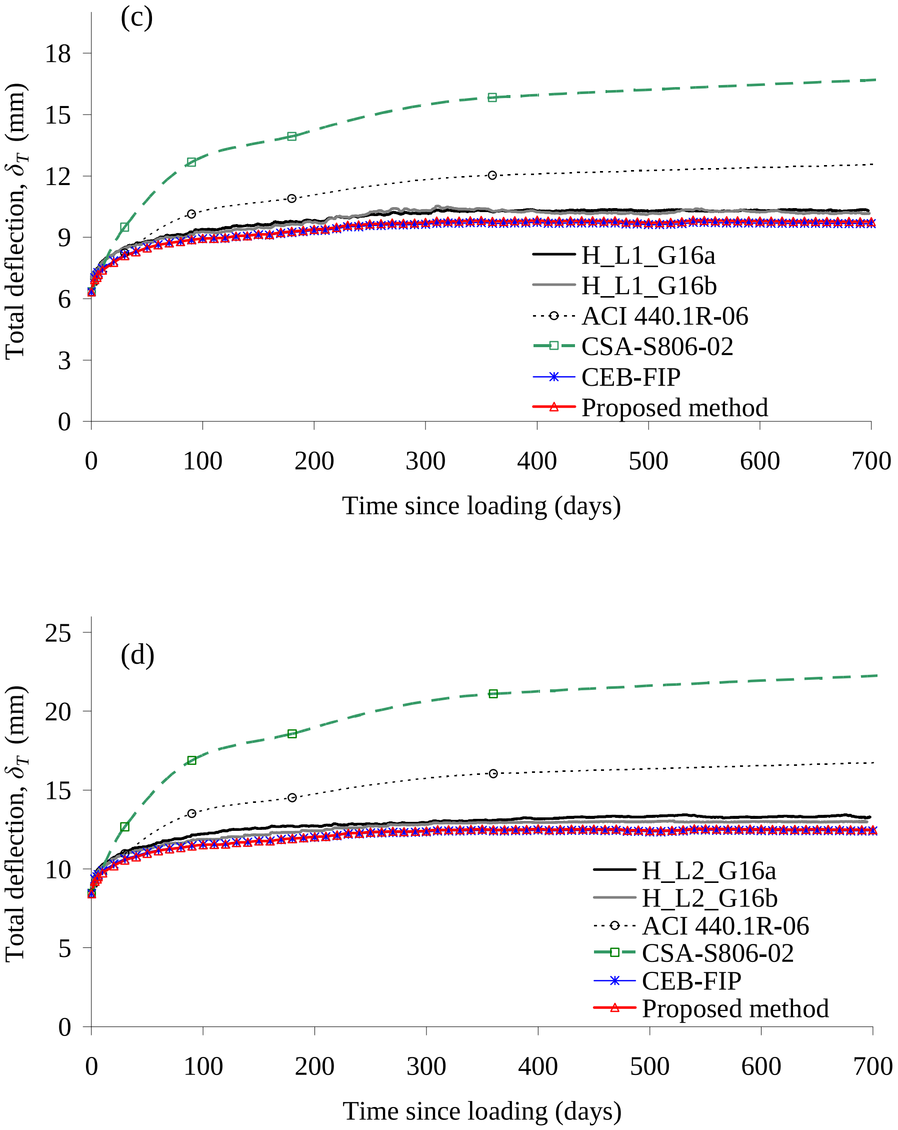

Figure 5.13. Total deflections versus time since loading for beams (a) H_L1_G12 beams and (b) H_L2_G12 beams (c) H_L1_G16 beams and (d) H_L2_G16 beams

| H_beams | $\delta_{prop}/\delta_{\exp}$ | $\delta_{CEB-FIB}/\delta_{\exp}$ | $\delta_{ACI}/\delta_{\exp}$ | $\delta_{CSA}/\delta_{\exp}$ |
|---|---|---|---|---|
| **H_L1_G12** | 0.97 | 0.95 | 1.37 | 1.83 |
| **H_L2_G12** | 0.94 | 0.93 | 1.38 | 1.84 |
| **H_L1_G16** | 0.96 | 0.95 | 1.26 | 1.68 |
| **H_L2_G16** | 0.96 | 0.96 | 1.32 | 1.76 |
| **Mean** | 0.96 | 0.95 | 1.33 | 1.78 |

Table 5.11. Ratio between theoretical and experimental total deflection at 700 days since loading (H_beams).

It is worth noting that the CEB-FIP [22,25] procedure and the proposed methodology [18,27] accurately predict the long-term deflections, since these methods account for the influence of the geometry, materials and environmental conditions, included in the creep coefficient and free shrinkage strain. On the other hand, the methods based on time-dependent factor (ACI 440.1R-06 [11], CSA-S 806-02 [12]), lead to conservative but inaccurate results

## 5.5 Conclusions

Experimental long-term deflections of 20 concrete beams with two different concrete strengths, reinforced with different amounts of GFRP and steel bars, and subjected to different levels of sustained load have been analysed. The study has been completed with the comparison of experimental results using available procedures found in the literature such as: ACI 440.1R-06, CSA- S806-02, CEB-FIP, together with a straightforward methodology proposed by the authors. Based on the results of this study, the following conclusions can be drawn:

- An influence of the reinforcement ratio in the total-to-immediate deflection ratios is observed in the GFRP RC beams. Moreover similar total-to-immediate deflection ratios are obtained for beams reinforced with 2Ø16 bars and 2Ø10 steel RC, since they have similar stiffness. No influence of the level of sustained load is observed.
- Higher total-to-immediate deflection ratios are observed in the beams with lower concrete strength (N_beams), since their experimental values of creep and shrinkage strain (concrete C1) are higher than those of beams with higher concrete strength (H_ beams, concrete C2.). This indicates that the increase in long-term deflection not only depends on the reinforcement ratio, but also on the concrete properties.
- The comparison of total-to-instantaneous deflection ratios of the two set of tests shows that the higher the reinforcement ratio and the lower the compressive strength are, the higher the total-to-instantaneous deflection ratio is.
- As regards the analytical predictions, the ACI 440.1R-06 approach gives good agreement with experimental results in all beams with lower concrete strength (N_beams), however, the method overestimates the deflections of the beams with higher concrete strength (H_ beams). The CSA S806.02 method over-predicts the deflections of all the GFRP RC tested beams. On the other hand, the CEB-FIP and the proposed methodology accurately predict the total deflections for all GFRP RC tested beams, since these two methodologies are able to account for the influence of environmental conditions and mechanical properties involved in the long-term deflections of FRP RC members.

## 5.6 Acknowledgements

The authors acknowledge the support provided by the Spanish Government (Ministerio de Ciencia e Innovación), Project ref. BIA2010-20234-C03-02. The first author thanks the Ministerio deEducación y Ciencia for Grant BES-2008-005740. The authors also thank the support of Schök Bauteile GMBH for the supply of GFRP bars.

## 5.7 Appendix

*ACI 440.1R-06*

According to ACI 440.1R-06 [11], the total deflection, including the effect of creep and shrinkage, $\delta_{T(ACI\,440)}$, can be obtained by multiplying the immediate deflection caused by sustained load, $\delta_{t_0}$, by the factor, λ:

$$\delta_{T(ACI\,440)} = (1 + 0.6\lambda)\delta_{t_0} \tag{A.5.1}$$

$$\lambda = \frac{\xi}{1 + 50\rho'} \tag{A.5.2}$$

where $\rho'$ is the compression reinforcement ratio and $\xi$ is the time-dependent factor for sustained loads, which includes the effects of creep and shrinkage and equals 1.0, 1.2 and 1.4 for 3, 6 and 12 months, respectively. For 5 years or more: $\xi$ =2.

*CSA-S806-02*

According to CSA-S806-02 [12], total deflection for flexural members is obtained by applying the time-dependent factor *S*, which takes the same values as ξ.

$$\delta_{T(CSA)} = (1 + S)\delta_{t_0} \tag{A.5.3}$$

### *Proposed methodology*

Recent studies conducted by the authors [18,27] proposed a straightforward methodology to predict long-term deflections due to creep and shrinkage based on rational multiplicative coefficients deduced from the principles of the *Effective Modulus Method* (Eurocode 2). For a simply supported beam the total deflection can be obtained from the immediate deflection and the multiplicative coefficients $k_{creep}$ and $k_{sh}$:

$$\delta_{T,proposed} = \delta_{t_0}\left(1 + k_{creep}\right) + \frac{\varepsilon_{sh}(t,t_0)l^2}{8d}k_{sh} \tag{A.5.4}$$

where $\varepsilon_{sh}$ is the free shrinkage strain and d is the effective depth. $k_{creep}$ and $k_{sh}$ can be obtained as follows :

$$k_{creep} = 0.73\varphi\sqrt{n\rho_f} \qquad k_{sh} = 1 + \sqrt{n\rho_f} \tag{A.5.5}$$

where $\varphi$ is the creep coefficient, $n$ is the ratio between modulus of elasticity of FRP, $E_f$, and the modulus of elasticity of concrete, $E_c$, and $\rho_f$ is the FRP tensile reinforcement ratio.

It is worth mentioning that, the proposed method (Eq. A.5.4-5) explicitly accounts for the influence of environmental conditions and mechanical properties; moreover the contribution to long-term deflection of creep and shrinkage effects is accounted for separately.

The immediate deflection due to sustained load, $\delta_{t_0}$, used in Eq. A.5.1, A.5.3-4, can be computed from Bischoff's equation [14,32] , modifying the effective moment of inertia, $I_e$, by including a $\beta$ coefficient with the value of 0.5[15] :

$$I_e = \frac{I_{cr}}{1 - \beta\left(\frac{M_{cr}}{M}\right)^2\left(1 - \frac{I_{cr}}{I_g}\right)} \tag{A.5.6}$$

where $M_{cr}$ is the cracking moment, $M$ is the applied moment, $I_g$ is the gross moment of inertia, $I_{cr}$ is the moment of inertia of the transformed cracked section.

### *CEB-FIP*

Based on the procedure presented in the CEB Manual on Cracking and Deformations [22], described and illustrated in Ghali et al. [25], total deflections, $\delta_{T(CEB-FIB)}$, can be obtained by interpolating between state 1 (uncracked transformed section) and state 2 (fully-cracked transformed section):

$$\delta_{T(CEB-FIB)} = 0.5\left(\frac{M_{cr}}{M}\right)^2 \delta_{T,1}(t,t_0) + \left(1 - 0.5\left(\frac{M_{cr}}{M}\right)^2\right)\delta_{T,2}(t,t_0) \tag{A.5.6}$$

where, the predicted total deflections for each state (1 and 2) can be obtained as the sum of the initial deflection, $\delta(t_0)_i$, the long-term deflection due to creep, $\Delta\delta(t,t_0)_{creep,i}$, and the long-term deflection due to shrinkage, $\Delta\delta(t,t_0)_{sh,i}$:

$$\delta_{T,i} = \delta(t_0)_i + \Delta\delta(t,t_0)_{creep,i} + \Delta\delta(t,t_0)_{sh,i} \tag{A.5.7}$$

where subscript *i* takes the value of 1 for the uncracked state and 2 for the fully-cracked state. The long-term deflections due to creep and shrinkage are obtained separately from the following expressions:

$$\Delta\delta(t,t_0)_{creep,i} = \delta(t_0)_i \varphi(t,t_0)\kappa_{\varphi,i} \tag{A.5.8}$$

$$\Delta\delta(t,t_0)_{sh,i} = \frac{\varepsilon_{sh}(t,t_0)}{d}\frac{l^2}{8d}\kappa_{sh,i} \tag{A.5.9}$$

being $\kappa_{\varphi,i}$ and $\kappa_{sh,i}$ the curvature coefficients related to creep and shrinkage, respectively:

$$\kappa_{\varphi,i} = \frac{I_{c,i}(t,t_0) + A_{c,i}y_{c,i}(t,t_0)\Delta y_i(t,t_0)}{\bar{I}_i(t,t_0)} \tag{A.5.10}$$

$$\kappa_{sh,i} = \frac{A_{c,i}y_{c,i}(t,t_0)d}{\bar{I}_i(t,t_0)} \tag{A.5.11}$$

where $A_{c,i}$ is the area of concrete considered effective (entire concrete area in state 1, but only area of compression zone in state 2), $I_{c,i}(t,t_0)$ is the moment of inertia of $A_{c,i}$ about an axis through the centroid of the age-adjusted transformed section, $y_{c,i}(t,t_0)$ is the centroid of $A_{c,i}$ measured downwards from the centroid of the age-adjusted transformed section, $\Delta y_i(t,t_0)$ is the y-coordinate of the centroid of the age-adjusted transformed section, measured downwards from the centroid of the transformed section at $t_0$, and $\bar{I}_i(t,t_0)$ is the moment of inertia of the age-adjusted transformed section about an axis through its centroid. A detailed explanation of the procedure and graphs for obtaining $\kappa_{\varphi,i}$ and $\kappa_{sh,i}$ can be found in Appendix F of [25].

The age-adjusted transformed section properties are calculated using the age-adjusted elastic modulus of concrete:

$$\bar{E}_e(t,t_0) = \frac{E_c}{1+\chi(t,t_0)\varphi(t,t_0)} \tag{A.5.12}$$

where $\chi(t,t_0)$ is the ageing coefficient.

Calculation of $\kappa_{\varphi,i}$ and $\kappa_{sh,i}$ is not immediate and design charts have been developed for practical applications [22,25].

## 5.8 References

1. Nanni A (Ed). Fiber Reinforced Plastic (FRP) Reinforcement for Concrete Structures: Properties and Aplications. Elsevier,Amsterdam; 1993.

2. GangaRao HVS, Taly N, Vijay PV. Reinforced Concrete Design with FRP Composites. Taylor & Francis Group, London; 2006.

3. Berg AC, Bank LC, Oliva MG, Russell JS. Construction and cost analysis of an FRP reinforced concrete bridge deck. Construction and Building Materials 2006; 20(8):515-26.

4. Hollaway LC. A review of the present and future utilisation of FRP composites in the civil infrastructure with reference to their important in-service properties. Construction and Building Materials 2010; 24(12):2419-45.

5. Joh O, Wang Z, Goto Y. Long-term deflection of fiber reinforced polymer concrete beams. Special Publication SP 188-51, Fourth International Symposium on Fiber Reinforced Polymer Reinforcement for Reinforced Concrete Structures, 1999; pp.577-90.

6. Brown V, Bartholomeu C, Long-term deflections of GFRP-reinforced concrete beams. First International Conference on Composites in Infra-Structure. Tucson, Arizona, USA, 1996; pp. 389-00.

7. Brown V, Sustained load deflections in GFRP-reinforced concrete beams. 3rd International RILEM Symposium on Non-Metallic (FRP) Reinforcement for Concrete Structures (FRPRCS-3). Sapporo, Japan, 1997; pp. 495-02.

8. American Concrete Institute Committee 318 ACI. Building code requirements for structural concrete and commentary (ACI 318-08). Farmington Hills (Michigan, USA): American Concrete Institute; 2008..

9. Branson DE. Compression steel effect on long-time deflections. ACI Journal Proceedings 1971; 68(8):555-59.

10. Arockiasamy M, Chidambaram S, Amer A, Shahawy M. Time-dependent deformations of concrete beams reinforced with CFRP bars. Composites Part B: Engineering, 2000; 31(6-7):577-92.

11. American Concrete Institute Committee 440 ACI. Guide for the design and construction of structural concrete reinforced with FRP bars (ACI 440.1R-06). Farmington Hills (Michigan, USA): American Concrete Institute; 2006.

12. CSA Standard CAN/CSA-S806-02. Design and construction of building components with fibre-reinforced polymers. Canadian Standards Association, Mississauga, Canada; 2002.

13. Miàs C, Torres L, Turon A, Barris C. Experimental study of immediate and time-dependent deflections of GFRP reinforced concrete beams. (Under revision) Submitted to Journal of Composite Structures.

14. Bischoff PH. Reevaluation of Deflection Prediction for Concrete Beams Reinforced with Steel and Fiber Reinforced Polymer Bars. Journal of Structural Engineering, ASCE 2005;131(5):752-67.

15. Scanlon A, Bischoff PH. Shrinkage restraint and loading history effects on deflections of flexural members. ACI Structural Journal 2008; 105(4):498-06.

16. Gross SP, Yost JR, Kevgas G. Time-dependent behavior of normal and high strength concrete beams reinforced with GFRP bars under sustained loads. High Performance Materials in Bridges 2003; pp.451-62.

17. Al-Salloum YA, Almusallam TH. Creep effect on the behavior of concrete beams reinforced with GFRP bars subjected to different environments. Constrution and Building Materials 2007; 21(7):1510-19.

18. Torres Ll., Miàs C, Turon A, Baena M. A rational method to predict long-term deflections of FRP reinforced concrete members. Engineering Structures 2012; 40:230-39.

19. Gilbert RI, Gianluca R. Time-dependent behaviour of concrete structures. Spon Press, Taylor & Francis Group, London; 2011.

20. Bazant ZP. Prediciton of concrete creep effects using Age-Adjusted Efective Modulus Method. ACI Journal 1972; 69, 212–17..

21. CEN 2004. Eurocode 2: Design of Concrete Structures. Part 1.1: General rules and rules for buildings (EN 1992-1-1:2004). Comité Européen de Normalisation, Brussels, 2004.

22. Comité Euro-International du Béton (CEB). CEB Design Manual on Cracking and Deformations.Bulletin d'Information 158-E;1985.

23. ACI Committee 435. Control of deflections in concrete structures (ACI 435R- 95). Detroit (Michigan, USA): American Concrete Institute; 1995.

24. Hall T, Ghali A. Long-term deflection prediction of concrete members reinforced with glass fibre reinforced polymer bars. Canadian Journal of Civil Engineering 2000; 27(5):890-98.

25. Ghali A, Favre R, Elbadry M. Concrete Structures: Stresses and Deformations. Third Edition. Spon Press ,New York; 2002.

26. CEB- FIP 1990. Model code for concrete structures. Comité Euro-International du Béton. Féderation Internationale de la Précontrainte, Thomas Telford House, London England; 1990.

27. Miàs C, Torres L, Turon A, Baena M, Barris C. A simplified method to obtain time-dependent curvatures and deflections of concrete members reinforced with FRP bars. Composite Structures 2010; 92(8):1833-38.

28. American Concrete Institute Committee 440 ACI. ACI 440.3R-04. Guide test methods for fiber-reinforced polymers (FRPs) for reinforcing or strengthening concrete structures. American Concrete Institute (ACI),Farmington Hills, Michigan, USA; 2004

29. Newhook J, Ghali A, Tadros G. Concrete flexural members reinforced with fiber reinforced polymer: Design for cracking and deformability. Canadian Journal of Civil Engineering 2002; 29(1):125-34

30. ISIS Canada. Reinforcing concrete structures with fibre reinforced polymers Design Manual No. 3. ISIS Canada Corporation, University of Manitoba, Manitoba, Canada; 2001.

31. Neville AM. Properties of Concrete, Fourth Edition, Longman Group Limited, Harlow, England:, 1995.

32. Bischoff PH, Scanlon A. Effective moment of inertia for calculating deflections of concrete members containing steel and fiber reinforced polymer bars. ACI Structural Journal 2007; 104(1):68-75.

# 6. Design methodology for long-term deflections

## 6.1 Calculation of long-term deflections

This section summarizes the methodology developed in this work to predict long-term deflections due to creep and shrinkage, based on rational multiplicative coefficients deduced from the principles of the *Effective Modulus Method*. This methodology is simple and straightforward, and, it accounts for mechanical properties and environmental conditions. The presented methodology is suitable to be incorporated in a design guideline.

Long-term deflection of one-way simply supported member due to the combined effects of creep and shrinkage is calculated from the immediate deflection, $\delta_{t_0}$, and the multiplicative coefficients $k_{creep}$ and $k_{sh}$ [1,2]:

$$\delta_{T,proposed} = \delta_{t_0}\left(1 + k_{creep}\right) + \frac{\varepsilon_{sh}(t,t_0)l^2}{8d}k_{sh} \tag{1}$$

where $\varepsilon_{sh}$ is the free shrinkage strain

$d$ is the effective depth

$l$ is the length of the member.

$k_{creep}$ and $k_{sh}$ can be obtained as follows :

$$k_{creep} = 0.73\varphi\sqrt{n\rho_f} \qquad k_{sh} = 1 + \sqrt{n\rho_f} \tag{2}$$

where $\varphi$ is the creep coefficient

$n$ is the modular ratio

$\rho_f$ is the FRP tensile reinforcement ratio

The immediate deflection due to sustained load, $\delta_{t_0}$, used in Eq. 1, can be computed as:

$$\delta_{t_0} = \frac{kM_{sus}l^2}{E_c I_e} \tag{3}$$

where $M_{sus}$ is the sustained moment,

$E_c$ is the elastic modulus of concrete

$I_e$ is the equivalent moment of inertia

$k$ is a factor that depends on support fixity and loading conditions (:

$= \frac{5}{48}$ for simply supported beam under uniform load )

The methodology requires using an effective moment of inertia $I_e$. Bischoff and Scanlon's equation [3, 4] is proposed, since it has been proven to be sufficiently accurate for calculation of deflections of FRP RC members:

$$I_e = \frac{I_{cr}}{1 - \beta\left(\frac{M_{cr}}{M_a}\right)^2\left(1 - \frac{I_{cr}}{I_g}\right)} \tag{4}$$

where β is coefficient taking into account the influence of the duration of the load

= 0.5 for sustained loads

$M_{cr}$ is the cracking moment

$M_a$ is the maximum applied moment

$I_g$ is the gross moment of inertia

$I_{cr}$ is the moment of inertia of the transformed cracked section.

## 6.2 Examples

Consider a simply supported beam tested in flexure. The beam of 200x250mm with effective depth equal to 225mm and span length of 4000mm is reinforced with 3Ø16 FRP bars placed at the tension side. The elastic modulus of concrete, $E_c$, is equal to 29 GPa, and the tensile strength of concrete, $f_{ct}$, is equal to 3.3MPa. A uniform load $q$ is applied at time $t_0$.

Calculate the deflection at mid-span, including effects of creep and shrinkage at time $t$. Considerer creep coefficient, $\varphi(t,t_0)$, equal to 2, and shrinkage strain, $\varepsilon_{sh}(t,t_0)$, equal to 300με.

Three cases are presented:

a) A uniform sustained load of 5kN/m is considered.
Reinforcement: GFRP ($E_f$=60GPa)

b) A uniform sustained load of 5kN/m is considered.
Reinforcement: CFRP ($E_f$ =120GPa)

c) At time $t_0$, the uniform sustained load of 5kN/m is applied immediately after the application of an instantaneous load equal to 6kN/m.
Reinforcement: GFRP ($E_f$=60GPa)

a) A uniform sustained load of 5kN/m is considered. Reinforcement: GFRP

$b$=200 mm $E_f$=60GPa

$h$= 250mm $E_c$=29GPA

$d$=225 mm $f_{ct}$=3.3MPa

$l$=4000mm $\varphi(t,t_0)$=2

$A_f$= 603.18mm $\varepsilon_{sh}(t,t_0)$=300 με

$q_{sus}$=5kN/m

*Sectional analysis at time $t_0$*

| | |
|---|---|
| $n_f = \frac{E_f}{E_f}$ | $n_f = \frac{60\cdot 10^3}{29\cdot 10^3} = 2.4$ |
| $\rho_f = \frac{A_f}{bd}$ | $\rho_f = \frac{603.18}{200\cdot 225} = 0.013$ |
| $x = dn\rho_f\left(-1+\sqrt{\left(1+\frac{2}{n\rho_f}\right)}\right)$ | $x = 225\cdot 2.4\cdot 0.013\left(-1+\sqrt{\left(1+\frac{2}{2.4\cdot 0.013}\right)}\right) = 50.29mm$ |
| $I_g = \frac{1}{12}bh^3$ | $I_g = \frac{1}{12}200\cdot 250^3 = 2.60\cdot 10^8\, mm^4$ |
| $I_{cr} = nA_f(d-x)(d-x/3)$ | $I_{cr} = 2.4\cdot 603.18(225-50.29)(225-50.29/3) = 5.27\cdot 10^7\, mm^4$ |

*Sustained Moment and Cracking Moment*

| | |
|---|---|
| $M_{sus} = \frac{ql^2}{8}$ | $M_{sus} = \frac{5\cdot 4000^2}{8} = 10^7\, Nmm$ |
| $M_{cr} = \frac{f_{ct}I_g}{h/2}$ | $M_{cr} = \frac{3.3\cdot 2.60\cdot 10^8}{250/2} = 6.88\cdot 10^6\, Nmm$ |

### *Equivalent moment of Inertia and immediate deflection*

| | |
|---|---|
| $I_e = \dfrac{I_{cr}}{1-\beta\left(\dfrac{M_{cr}}{M_{sus}}\right)^2\left(1-\dfrac{I_{cr}}{I_g}\right)}$ | $I_e = \dfrac{5.27\cdot 10^7}{1-0.5\left(\dfrac{6.88\cdot 10^6}{10^7}\right)^2\left(1-\dfrac{5.27\cdot 10^7}{2.60\cdot 10^8}\right)} = 6.49\cdot 10^7\, mm^4$ |
| $\delta_{t_0} = \dfrac{5M_{sus}l^2}{48E_cI_e}$ | $\delta_{t_0} = \dfrac{5\cdot 10^7\cdot 4000^2}{48\cdot 29000\cdot 6.49\cdot 10^7} = 10.27mm$ |

### *Multiplicative coefficients*

| | |
|---|---|
| $k_{creep} = 0.73\varphi\sqrt{n\rho_f}$ | $k_{creep} = 0.73\cdot 2\sqrt{2.4\cdot 0.013} = 0.26$ |
| $k_{sh} = 1+\sqrt{n\rho_f}$ | $k_{sh} = 1+\sqrt{2.4\cdot 0.013} = 1.18$ |

### *Deflection at time t*

| |
|---|
| $\delta_{T,proposed} = \delta_{t_0}\left(1+k_{creep}\right)+\dfrac{\varepsilon_{sh}(t,t_0)l^2}{8d}k_{sh}$ |
| $\delta_{T,proposed} = 10.27\left(1+0.26\right)+\dfrac{300\cdot 10^{-6}4000^2}{8\cdot 225}1.18 = 16.11mm$ |

b) A uniform sustained load of 5kN/m is considered. Reinforcement: CFRP

$b$=200 mm $E_f$=120GPa

$h$= 250mm $Ec$=29GPA

$d$=225 mm $f_{ct}$=3.3MPa

$l$=4000mm $\varphi(t,t_0)$=2

$A_f$= 603.18mm $\varepsilon_{sh}(t,t_0)$=300 με

$q_{sus}$=5kN/m

*Sectional analysis at time $t_0$*

| | |
|---|---|
| $n_f = \frac{E_f}{E_f}$ | $n_f = \frac{120 \cdot 10^3}{29 \cdot 10^3} = 4.8$ |
| $\rho_f = \frac{A_f}{bd}$ | $\rho_f = \frac{603.18}{200 \cdot 225} = 0.013$ |
| $x = dn\rho_f \left( -1 + \sqrt{\left(1 + \frac{2}{n\rho_f}\right)} \right)$ | $x = 225 \cdot 4.8 \cdot 0.013 \left( -1 + \sqrt{\left(1 + \frac{2}{4.8 \cdot 0.013}\right)} \right) = 67.52mm$ |
| $I_g = \frac{1}{12} bh^3$ | $I_g = \frac{1}{12} 200 \cdot 250^3 = 2.60 \cdot 10^8 mm^4$ |
| $I_{cr} = nA_f (d-x)(d-x/3)$ | $I_{cr} = 2.4 \cdot 603.18(225-67.52)(225-67.52/3) = 9.23 \cdot 10^7 mm^4$ |

*Sustained Moment and Cracking Moment*

| | |
|---|---|
| $M_{sus} = \frac{ql^2}{8}$ | $M_{sus} = \frac{5 \cdot 4000^2}{8} = 10^7 Nmm$ |
| $M_{cr} = \frac{f_{ct} I_g}{h/2}$ | $M_{cr} = \frac{3.3 \cdot 2.60 \cdot 10^8}{250/2} = 6.88 \cdot 10^6 Nmm$ |

*Equivalent moment of Inertia and immediate deflection*

| | |
|---|---|
| $I_e = \dfrac{I_{cr}}{1-\beta\left(\dfrac{M_{cr}}{M_{sus}}\right)^2\left(1-\dfrac{I_{cr}}{I_g}\right)}$ | $I_e = \dfrac{9.23{\cdot}10^7}{1-0.5\left(\dfrac{6.88{\cdot}10^6}{10^7}\right)^2\left(1-\dfrac{9.23{\cdot}10^7}{2.60{\cdot}10^8}\right)} = 1.09{\cdot}10^8\,mm^4$ |
| $\delta_{t_0} = \dfrac{5M_{sus}l^2}{48E_cI_e}$ | $\delta_{t_0} = \dfrac{5{\cdot}10^7\cdot4000^2}{48\cdot29000\cdot9.23{\cdot}10^7} = 6.12mm$ |

*Multiplicative coefficients*

| | |
|---|---|
| $k_{creep} = 0.73\varphi\sqrt{n\rho_f}$ | $k_{creep} = 0.73\cdot2\sqrt{4.8\cdot0.013} = 0.37$ |
| $k_{sh} = 1+\sqrt{n\rho_f}$ | $k_{sh} = 1+\sqrt{4.8\cdot0.013} = 1.25$ |

*Deflection at time t*

| |
|---|
| $\delta_{T,proposed} = \delta_{t_0}\left(1+k_{creep}\right)+\dfrac{\varepsilon_{sh}(t,t_0)l^2}{8d}k_{sh}$ |
| $\delta_{T,proposed} = 6.12\left(1+0.37\right)+\dfrac{300{\cdot}10^{-6}4000^2}{8\cdot225}1.25 = 11.73mm$ |

c) At time $t_0$, the uniform sustained load of 5kN/m is applied immediately after the application of an instantaneous load equal to 6kN/m. Reinforcement: GFRP.

| | |
|---|---|
| $b$=200 mm | $E_f$=60GPa |
| $h$= 250mm | $E_c$=29GPA |
| $d$=225 mm | $f_{ct}$=3.3MPa |
| $l$=4000mm | $\varphi(t,t_0)$=2 |
| $A_f$= 603.18mm | $\varepsilon_{sh}(t,t_0)$=300 με |
| $q_{sus}$=5kN/m | $q_a$=6kN/m |

*Sectional analysis at time $t_0$*

| | |
|---|---|
| $n_f = \frac{E_f}{E_f}$ | $n_f = \frac{60 \cdot 10^3}{29 \cdot 10^3} = 2.4$ |
| $\rho_f = \frac{A_f}{bd}$ | $\rho_f = \frac{603.18}{200 \cdot 225} = 0.013$ |
| $x = dn\rho_f \left( -1 + \sqrt{\left( 1 + \frac{2}{n\rho_f} \right)} \right)$ | $x = 225 \cdot 2.4 \cdot 0.013 \left( -1 + \sqrt{\left( 1 + \frac{2}{2.4 \cdot 0.013} \right)} \right) = 50.29 mm$ |
| $I_g = \frac{1}{12} bh^3$ | $I_g = \frac{1}{12} 200 \cdot 250^3 = 2.60 \cdot 10^8 mm^4$ |
| $I_{cr} = nA_f (d - x)(d - x/3)$ | $I_{cr} = 2.4 \cdot 603.18(225 - 50.29)(225 - 50.29/3) = 5.27 \cdot 10^7 mm^4$ |

*Maximum applied Moment, Sustained Moment and Cracking Moment*

| | |
|---|---|
| $M_a = \frac{ql^2}{8}$ | $M_a = \frac{6 \cdot 4000^2}{8} = 1.2 \cdot 10^7 Nmm$ |
| $M_{sus} = \frac{ql^2}{8}$ | $M_{sus} = \frac{5 \cdot 4000^2}{8} = 10^7 Nmm$ |
| $M_{cr} = \frac{f_{ct} I_g}{h/2}$ | $M_{cr} = \frac{3.3 \cdot 2.60 \cdot 10^8}{250/2} = 6.88 \cdot 10^6 Nmm$ |

*Equivalent moment of Inertia due to maximum load applied and immediate deflection due to sustained load.*

| | |
|---|---|
| $I_e = \dfrac{I_{cr}}{1-\beta\left(\dfrac{M_{cr}}{M_a}\right)^2\left(1-\dfrac{I_{cr}}{I_g}\right)}$ | $I_e = \dfrac{5.27\cdot 10^7}{1-0.5\left(\dfrac{6.88\cdot 10^6}{1.2\cdot 10^7}\right)^2\left(1-\dfrac{5.27\cdot 10^7}{2.60\cdot 10^8}\right)} = 6.06\cdot 10^7\, mm^4$ |
| $\delta_{t_0} = \dfrac{5M_{sus}l^2}{48E_cI_e}$ | $\delta_{t_0} = \dfrac{5\cdot 10^7\cdot 4000^2}{48\cdot 29000\cdot 6.06\cdot 10^7} = 11.00mm$ |

*Multiplicative coefficients*

| | |
|---|---|
| $k_{creep} = 0.73\varphi\sqrt{n\rho_f}$ | $k_{creep} = 0.73\cdot 2\sqrt{2.4\cdot 0.013} = 0.26$ |
| $k_{sh} = 1+\sqrt{n\rho_f}$ | $k_{sh} = 1+\sqrt{2.4\cdot 0.013} = 1.18$ |

*Deflection at time t*

| |
|---|
| $\delta_{T,proposed} = \delta_{t_0}\left(1+k_{creep}\right)+\dfrac{\varepsilon_{sh}(t,t_0)l^2}{8d}k_{sh}$ |
| $\delta_{T,proposed} = 11.00\left(1+0.26\right)+\dfrac{300\cdot 10^{-6}4000^2}{8\cdot 225}1.18 = 17.02mm$ |

## 6.3 References

1. Miàs C, Torres L, Turon A, Baena M, Barris C. A simplified method to obtain time-dependent curvatures and deflections of concrete members reinforced with FRP bars. Composite Structures 2010; 92(8):1833-38.

2. Torres Ll., Miàs C, Turon A, Baena M. A rational method to predict long-term deflections of FRP reinforced concrete members. Engineering Structures 2012; 40:230-39.

3. Bischoff PH. Reevaluation of Deflection Prediction for Concrete Beams Reinforced with Steel and Fiber Reinforced Polymer Bars. Journal of Structural Engineering, ASCE 2005;131(5):752-67.

4. Scanlon A, Bischoff PH. Shrinkage restraint and loading history effects on deflections of flexural members. ACI Structural Journal 2008; 105(4):498-06.

# 7. Conclusions

## 7.1 Summary

Fibre reinforced polymer (FRP) bars have emerged as an alternative to steel reinforcement in corrosive environment or where there is a possible interference form magnetic fields. FRP bars present different mechanical properties than those of steel, such as higher tensile strength, lower modulus of elasticity, and linear behaviour up to failure. The combination of high strength and low modulus has a direct effect on the flexural behaviour of FRP RC members, generally leading to higher deformability. Therefore, serviceability criteria may govern the design of FRP RC concrete beams. Investigations on the flexural behaviour of concrete members reinforced with FRP bars have been mainly concentrated on short-term behaviour, and therefore experimental data of long-term deflections are scarce. In the present work, the long-term behaviour of FRP RC beams has been investigated both analytically and experimentally.

Firstly, a rational methodology that maintains simplicity has been proposed by using the multiplicative coefficients, $k_{creep}$ and $k_{sh}$, derived from mathematical manipulation of equations based on general principles of the *Effective Modulus Method*. In the first phase of the work, this methodology has been compared to experimental results and available procedures found in the literature to check its suitability.

Secondly, an experimental program has been carried out to study the main variables involved in long-term deflections of FRP RC beams. Different reinforcement ratios, concrete strengths and sustained load levels have been considered. For comparison purposes steel reinforcement has also been used. The material short-term properties, like compressive concrete strength and modulus of elasticity of concrete and FRP bars, and the long-term properties, like creep coefficient and shrinkage strain, have been obtained from parallel experimental tests. The experimental immediate and long-term deflections have been reported and discussed. Furthermore they have been compared to some of the most representative prediction models.

Finally, the experimental results have been compared to predictions obtained from the simplified proposed methodology presented in this work.

## 7.2 Concluding Remarks

The most relevant conclusions from the analytical studies performed in Chapters 2 and 3 can be summarized as follows:

- The proposed multiplicative coefficients, $k_{creep}$ and $k_{sh}$, to predict long-term curvatures and deflections due to creep and shrinkage depend on modular ratio, $n$, reinforcement ratio, $\rho$, creep coefficient and shrinkage strain. Therefore both explicitly account for the influence of environmental conditions and mechanical properties.
- Higher values of the product $n\rho$ lead to higher values of total-to-initial deflection prediction ratio, due to the increase in the depth of the compressive concrete block, which implies an increment of curvatures caused by creep and shrinkage of concrete.
- Total-to-initial deflection prediction ratio increases with the increase of values of creep and shrinkage.

The most relevant conclusions from the experimental programme presented in Chapters 4 and 5 can be summarized as follows:

- An influence of the reinforcement ratio in the total-to-immediate deflection ratios is observed in the GFRP RC beams.
- Similar total-to-immediate deflection ratios are obtained between beams of similar stiffness (reinforced with 2Ø16 bars and with 2Ø10 steel RC).
- Higher total-to-immediate deflection ratios are observed in the beams with lower concrete strength, since their experimental values of creep and shrinkage strain are higher than those of beams with higher concrete strength. This indicates that the

increase in long-term deflection not only depends on reinforcement ratio, but also on the concrete properties, as shown in Chapters 2 and 3.

- The comparison of total-to-instantaneous deflection ratios between beams with different concrete strength and reinforcement ratio shows that the higher the reinforcement ratio and the lower the compressive strength are, the higher the total-to-immediate deflection ratio is.
- ACI 440.1R-06 approach gives good agreement with experimental results of the beams with the lower concrete strength; however, the method overestimates the deflections of the beams with the higher concrete strength. This is because ACI time-dependent factor does not take into account variation in creep and shrinkage when using different concretes. In addition its time-dependent coefficient only depends on time since loading and does not depend on the mechanical properties of the reinforcement, which affects the long-term behaviour as shown in analytical results (Chapter 2 and 3) and experimental data. The CSA S806.02 method over-predicts the deflections of all the GFRP RC tested beams, since it uses the same procedure as for steel RC, without any modification to account for differences between GFRP and steel bars.
- The CEB-FIP procedure accurately predicts the total deflections for all GFRP RC tested beams, since this formulation is able to account for the influence of environmental conditions and mechanical properties involved in the long-term deflections of FRP RC members.
- The proposed methodology accurately predicts the total deflections of the GFRP RC tested beams. It is worth noting that the present methodology is simple and straightforward like those based on multiplicative coefficients (ACI 440.1R-06 and CSA S806-02), but it is able to account for the influence of environmental conditions and mechanical properties.

## 7.3 Future Work

Based on the results of this research and the conducted literature review, the following points are proposed as future work:

- The effect of the long-term loading on the tensile strength of FRP bars and on the capacity of structural elements should be considered to properly estimate the reliability of structures subject to significant permanent loads during their life.
- An analytical study of the effect of loading history on long-term deflections, supported by experiments, should be performed to check the generalization of the proposed methodology.
- A specific study on the long-term structural response of hyperstatic FRP RC beams under sustained loads should be carried out. The main parameters affecting deformations (geometry, compressive and tensile reinforcement ratios, material characteristics, level of sustained load level) should be taken into consideration.
- Further experimental work is needed regarding the long-term behaviour of FRP reinforced concrete beams under environmental adversities such as freeze-taw cycles at elevated temperatures.
- A detailed study on crack width of FRP RC elements under sustained load, both analytical and experimental, should be performed to check the current expressions and to suggest modifications.
- A detailed numerical study using finite element method should be performed to study the long-term effects far from service loads. Bond-slip laws for different FRP bars, jointly with nonlinear material modelling of materials and time-dependent analysis shall be considered.
- The extension of the methodology for the case of steel reinforced concrete with compressive reinforcement should be studied. A parametric study and further experimental tests should be carried out for its validation.

Universitat de Girona
Escola Politècnica Superior
Dept. d’Enginyeria Mecànica i de la Construcció Industrial

AMADE
ANALYSIS AND ADVANCED MATERIALS
FOR STRUCTURAL DESIGN